

Issue 3

2018 | Volume 14

The Journal on Advanced Studies in Theoretical and Experimental Physics,
including Related Themes from Mathematics

PROGRESS IN PHYSICS



“All scientists shall have the right to present their scientific research results, in whole or in part, at relevant scientific conferences, and to publish the same in printed scientific journals, electronic archives, and any other media.” — Declaration of Academic Freedom, Article 8

ISSN 1555-5534

PROGRESS IN PHYSICS

A quarterly issue scientific journal, registered with the Library of Congress (DC, USA). This journal is peer reviewed and included in the abstracting and indexing coverage of: Mathematical Reviews and MathSciNet (AMS, USA), DOAJ of Lund University (Sweden), Scientific Commons of the University of St. Gallen (Switzerland), Open-J-Gate (India), Referativnyi Zhurnal VINITI (Russia), etc.

Electronic version of this journal:
<http://www.ptep-online.com>

Advisory Board

Dmitri Rabounski,
Editor-in-Chief, Founder
Florentin Smarandache,
Associate Editor, Founder
Larissa Borissova,
Associate Editor, Founder

Editorial Board

Pierre Millette
millette@ptep-online.com
Andreas Ries
ries@ptep-online.com
Gunn Quznetsov
quznetsov@ptep-online.com
Felix Scholkmann
scholkmann@ptep-online.com
Ebenezer Chifu
chifu@ptep-online.com

Postal Address

Department of Mathematics and Science,
University of New Mexico,
705 Gurley Ave., Gallup, NM 87301, USA

Copyright © *Progress in Physics*, 2018

All rights reserved. The authors of the articles do hereby grant *Progress in Physics* non-exclusive, worldwide, royalty-free license to publish and distribute the articles in accordance with the Budapest Open Initiative: this means that electronic copying, distribution and printing of both full-size version of the journal and the individual papers published therein for non-commercial, academic or individual use can be made by any user without permission or charge. The authors of the articles published in *Progress in Physics* retain their rights to use this journal as a whole or any part of it in any other publications and in any way they see fit. Any part of *Progress in Physics* howsoever used in other publications must include an appropriate citation of this journal.

This journal is powered by \LaTeX

A variety of books can be downloaded free from the Digital Library of Science:
<http://fs.gallup.unm.edu/ScienceLibrary.htm>

ISSN: 1555-5534 (print)
ISSN: 1555-5615 (online)

Standard Address Number: 297-5092
Printed in the United States of America

July 2018

Vol. 14, Issue 3

CONTENTS

Tselnik F. Cosmological Cold Dark Matter and Dark Energy Match Icosahedron Symmetry	109
Daywitt W. C. The Planck Vacuum Physics Behind the Huygens Principle and the Propagator Theory for the Schrödinger Electron	111
Potter F. Predicting Total Angular Momentum in TRAPPIST-1 and Many Other Multi-planetary Systems Using Quantum Celestial Mechanics	115
Millette P. A. On the Classical Scaling of Quantum Entanglement	121
Mashkin M. N. Matter in a Space of a Fractional Dimension. A Cosmological System of Spaces and Evolution of the Universe	131
Mashkin M. N. Calculation of the Density of Vacuum Matter, the Speed of Time and the Space Dimension	135
Andersen T. C. Fully Classical Quantum Gravity	138
Robitaille P.-M. Kirchhoff's Law of Thermal Emission: Blackbody and Cavity Radiation Reconsidered	141
Wackler C. M. Outline of a Kinematic Light Experiment	152
Mashkin M. N. Fractional Degrees of Freedom in Statistics	159
Sarasúa L. Seeliger's Gravitational Paradox and the Infinite Universe	165
Feeney A. M. Utilizing Future-Viewing Instruments	169
Robitaille P.-M. Thermodynamics and the Virial Theorem, Gravitational Collapse and the Virial Theorem: Insight from the Laws of Thermodynamics	179

Information for Authors

Progress in Physics has been created for rapid publications on advanced studies in theoretical and experimental physics, including related themes from mathematics and astronomy. All submitted papers should be professional, in good English, containing a brief review of a problem and obtained results.

All submissions should be designed in L^AT_EX format using *Progress in Physics* template. This template can be downloaded from *Progress in Physics* home page <http://www.ptep-online.com>

Preliminary, authors may submit papers in PDF format. If the paper is accepted, authors can manage L^AT_EX typing. Do not send MS Word documents, please: we do not use this software, so unable to read this file format. Incorrectly formatted papers (i.e. not L^AT_EX with the template) will not be accepted for publication. Those authors who are unable to prepare their submissions in L^AT_EX format can apply to a third-party payable service for LaTeX typing. Our personnel work voluntarily. Authors must assist by conforming to this policy, to make the publication process as easy and fast as possible.

Abstract and the necessary information about author(s) should be included into the papers. To submit a paper, mail the file(s) to the Editor-in-Chief.

All submitted papers should be as brief as possible. Short articles are preferable. Large papers can also be considered. Letters related to the publications in the journal or to the events among the science community can be applied to the section *Letters to Progress in Physics*.

All that has been accepted for the online issue of *Progress in Physics* is printed in the paper version of the journal. To order printed issues, contact the Editors.

Authors retain their rights to use their papers published in *Progress in Physics* as a whole or any part of it in any other publications and in any way they see fit. This copyright agreement shall remain valid even if the authors transfer copyright of their published papers to another party.

Electronic copies of all papers published in *Progress in Physics* are available for free download, copying, and re-distribution, according to the copyright agreement printed on the titlepage of each issue of the journal. This copyright agreement follows the *Budapest Open Initiative* and the *Creative Commons Attribution-Noncommercial-No Derivative Works 2.5 License* declaring that electronic copies of such books and journals should always be accessed for reading, download, and copying for any person, and free of charge.

Consideration and review process does not require any payment from the side of the submitters. Nevertheless the authors of accepted papers are requested to pay the page charges. *Progress in Physics* is a non-profit/academic journal: money collected from the authors cover the cost of printing and distribution of the annual volumes of the journal along the major academic/university libraries of the world. (Look for the current author fee in the online version of *Progress in Physics*.)

LETTERS TO PROGRESS IN PHYSICS

Cosmological Cold Dark Matter and Dark Energy Match Icosahedron Symmetry

Felix Tselnik

E-mail: tselnik@bgu.ac.il

A charge analogous though different from the usual electric charge is introduced with the same kind of gauge but applied to the icosahedron. This “cosmocharge” might be a source of the accelerating expansion of universe in cosmology (Dark Energy).

In a unimetric approach [1], *contact* is the prime concept defined by the point-like — yes/no — condition, and all predictions in a Contact Problem are made by means of counting top-velocity signal oscillations numbers between *bodies* moving along their trajectories. In so doing, we need no intermediaries like rulers, clocks, or reference frames that could introduce all of their own or hide something. Therefore only direct motion-to-motion measurements should be used. Then even the concept of body is introduced solely as something, for which Contact Problem makes sense.

Suggesting free motion to be rectilinear and uniform, we ascribe acceleration to external forces. However, as mentioned by Einstein, this picture leads to a vicious circle, since the absence of forces itself is verified just by this kind of motion. There is nothing intrinsic for an individual straight line. Moreover, how can we be sure in practice that rulers are straight and clocks click uniformly? And are such features of these auxiliary devices actually necessary for Contact Problem predictions? Can integration required to construct the trajectory in a field be carried out without approximation with such segments?

Metric-less approach makes it possible to dispense with these artificial schemes. Rather than consider particular lines, we could first work with classes of lines provided with some particular rules for mutual intersections and then develop full space-time geometry out of these. To this end, let us define first a special class of trajectories with the following property: Any two of these either do not intersect, or intersect in a single point. We *define* free trajectories as members of this class. Assuming their intersections to mark contacts, we can consider Contact Problem *for this class only*, implying its further application to the full Contact Problem with external forces. For this to be possible, general trajectories, which can have multiple contacts as mutual, so also with free trajectories, must satisfy some conditions:

- i. They contact some of free trajectories at each points;
- ii. At each point a next point exists, such that a free trajectory connecting these two points has no other contacts with this general trajectory. As shown in [1], we can define parallel trajectories and predict contacts using them by means of counting top-signal oscillations ratios.

The reaction of the body’s motion on external influences depends on its *charge* pertained to a particular *field*. Any Contact Problem can be specified by means of oscillations numbers and their ratios, provided the standard of charge can be transported to all points of a trajectory in question. It is just the availability of this procedure that provides the list of relevant fields as compatible with it. To this end, some particular arrangements of test trajectories — *spheres* — are used. Sphere is defined as a finite or infinite set of trajectories having common contact (the sphere center) with some definite ratios of (infinite) oscillations numbers in order to introduce a measure for operations such as field determining integration. Some kinds of spheres — *regular stars*, the trajectories of which are distributed according to the vertices of the Platonic solids, provide a basis for the electric charge gauge by means of detecting the related symmetries of their motions toward the star center solely under their interaction.

In particular, the cube symmetry defines the charge gauge for the electroweak interaction. Considering the trajectories of the two cube comprising tetrahedrons, one of which consists of four electrons and another of four positrons, we can develop a full gauge framework for these interactions, yet additionally requiring the existence of neutrinos (with the resulting parity violation) [2]. In the same sense the dodecahedron star, comprising besides the cube also the 12-vertices set of “roofs”, ascribed to the quarks, adds the strong interaction in accord with this additional symmetry. The set of roof trajectories might have a center on their own, provided the strong potential squarely increases (over a limited range) to form a strictly fine star. Their electromagnetic interaction with the cube sub-star of this dodecahedron (necessary to fix their position with respect to the cube) prevents the latter from being a strictly fine star. For this perturbation to fall within the range of the weak interaction, the quark masses must be accordingly small. The dodecahedron symmetry exhausts the list of interactions that could be ultimately registered with our electricity-based devices.

Of the five Platonic solids, only the cube and the icosahedron allow for arrangements of trajectories that can form strictly fine regular stars even for charged particles, provided these have equal masses and absolute values for oppositely charged particles (neither tetrahedron, nor octahedron can

form these). Since the icosahedron cannot be included in the richest with sub-stars dodecahedron, its possible charges have nothing in common with electric or other charges of the dodecahedron. Hence, this charge cannot be detected with our customary devices.

Like the roofs of the dodecahedron, the set of 12 trajectories of the icosahedron corresponding to its 12 vertices can be decomposed into 3 reciprocally orthogonal rectangles (however, having a particular — “golden” — ratio of their sides’ lengths for the star to be regular). Again, in each rectangle all these trajectories belong to test-bodies for the charge gauge, having equal masses and absolute values of some charge with opposite signs on their side vertices. Then mutual compensation of these charges lets these 3 rectangles be quite independent of each other due to compensation of effects of one charged rectangle on another.

Just as the usual electric charge in our ordinary situations creates a field that, in turn, is detectable due to charged bodies motion, this “cosmocharge” Q , though being not detectable with our conventional devices, still might be found in observations of far galaxies or their clusters [3]. If, analogously to baryon matter-antimatter asymmetry, one sign of cosmocharge has some larger density than its opposite one, then so created “cosmofield” will let our universe expand with acceleration now ascribed to the Dark Energy. Similarly to the rectangles of the strong interacting sub-star in the dodecahedron, the rectangles of the icosahedron can possess strictly fine center only for a force with a potential squarely increasing with distance. Consisting of opposite charges, such a “cosmoplasma” might fluctuate to have observable anisotropy in the universe expansion acceleration.

For basic electromagnetic interaction for the charge gauge in the dodecahedron, we had to restrict the strong interaction region to prevent adverse influence of 12 vertices subset on the cube symmetry. There is no need in this confinement now, since the charge of only one force is to be gauged. Hence the increasing field can exist over the whole universe keeping asymptotic freedom in our short range environment, while being effective far away.

Having no sub-symmetries in the icosahedron star, the cosmofield cannot involve other than strong-like interactions. However, its rectangles might have different values of Q and masses M , provided Q^2M are the same for all of them to form a regular icosahedron star. So, stable “cosmoatoms” might exist as combined of bodies with different Q ’s and M ’s to avoid annihilation.

Now, in general relativity, scalar action includes an artificially inserted baryon term, contributing to the momentum-energy tensor in the Einstein equation and basing only on a covariance argument. This source of space-time curvature looks natural for our local environment. Moreover, we can specify space-time scalar curvature as a violation of transitivity in the finite local oscillations numbers for sets of curved lines that are still regarded “parallel” in terms of our oscilla-

tions numbers. So defined, curvature should replace the scalar in the least action principle for Contact Problem. We then reverse the very definition of matter. Just as in Contact Problem a concept of body was introduced due to its participation in Contact Problem scheme, the concept of *matter* in cosmology is just a visualization of the observed curvature of space-time. Unlike baryon case of general relativity, there is no independent of curvature definition of matter now. Actually, no Cold Dark Matter, whether or not detectable, might exist there at all. Merely the empty space-time of the real universe is actually curved, while we ascribe the measured curvature to some imaginary Cold Dark Matter as its source in analogy to the Newton law.

Submitted on April 8, 2018

References

1. Tselnik F. Irony of the Method. *Progress in Physics*, 2016, v.12, issue 2, see p.95 in the paper.
2. Tselnik F. *Progress in Physics*, 2015, v.11, issue 1, 50.
3. Tselnik F. *Communications in Nonlinear Science and Numerical Simulation*, 2007, v.12, 1427.

The Planck Vacuum Physics Behind the Huygens Principle and the Propagator Theory for the Schrödinger Electron

William C. Daywitt

National Institute for Standards and Technology (retired), Boulder, Colorado, USA
E-mail: wcdawitt@me.com

This paper reviews a small portion of the quantum-electrodynamic propagator model as viewed from the Planck vacuum (PV) theory. The nonrelativistic calculations suggest that the degenerate collection of Planck-particle cores (that pervade the invisible, negative-energy vacuum state) is responsible for the Huygens principle, the propagator theory, and the Feynman diagrams.

1 Introduction

The theoretical foundation [1–3] of the PV theory rests upon the unification of the Einstein, Newton, and Coulomb superforces:

$$\frac{c^4}{G} \left(= \frac{m_* c^2}{r_*} \right) = \frac{m_*^2 G}{r_*^2} = \frac{e_*^2}{r_*^2} \quad (1)$$

where the ratio c^4/G is the curvature superforce that appears in the Einstein field equations. G is Newton's gravitational constant, c is the speed of light, m_* and r_* are the Planck mass and length respectively [4, p. 1234], and e_* is the massless bare charge. The fine structure constant is given by the ratio $\alpha = e^2/e_*^2$, where $(-e)$ is the observed electronic charge.

The two particle/PV coupling forces

$$F_c(r) = \frac{e_*^2}{r^2} - \frac{mc^2}{r} \quad \text{and} \quad F_*(r) = \frac{e_*^2}{r^2} - \frac{m_* c^2}{r} \quad (2)$$

the electron core $(-e_*, m)$ and the Planck-particle core $(-e_*, m_*)$ exert on the PV state, along with their coupling constants

$$F_c(r_c) = 0 \quad \text{and} \quad F_*(r_*) = 0 \quad (3)$$

and the resulting Compton radii

$$r_c = \frac{e_*^2}{mc^2} \quad \text{and} \quad r_* = \frac{e_*^2}{m_* c^2} \quad (4)$$

lead to the important string of Compton relations

$$r_c mc^2 = r_* m_* c^2 = e_*^2 \quad (= c\hbar) \quad (5)$$

for the electron and Planck-particle cores, where \hbar is the reduced Planck constant. The electron and Planck-particle masses are m and m_* respectively. To reiterate, the equations in (2) represent the forces the free electron and Planck-particle cores exert on the PV space, a space that is itself pervaded by a degenerate collection of Planck-particle cores [5].

The Planck constant is a secondary constant whose structure can take different forms, e.g.

$$\hbar [\text{erg sec}] = r_c mc = r_* m_* c = \left(\frac{e_*^2}{r_*} \right) t_* = m_* c^2 t_* \quad (6)$$

that are employed throughout the following text, where t_* ($= r_*/c$) is the Planck time [4, p. 1234].

Furthermore, the energy and momentum operators expressed as

$$\widehat{E} = i\hbar \frac{\partial}{\partial t} = i(m_* c^2) t_* \frac{\partial}{\partial t} = i(m_* c^2) r_* \frac{\partial}{c\partial t} \quad (7)$$

and

$$c\widehat{\mathbf{p}} = -i c \hbar \nabla = -i(m_* c^2) r_* \nabla = -i(mc^2) r_c \nabla \quad (8)$$

will be used freely in what follows.

Section 2 re-examines the Schrödinger equation in light of the PV theory, the calculations concluding that the pervaded vacuum state is the source of the scattering in the propagator theory. Section 3 presents a nonrelativistic look at the Huygens principle and the propagator theory for the electron core.

2 Schrödinger equation

The inhomogeneous Schrödinger equation, where $H = H_0 + V$ is the Hamiltonian operator, can be expressed as

$$\left(i\hbar \frac{\partial}{\partial t} - H \right) \psi(\mathbf{x}, t) = 0. \quad (9)$$

The free-space Hamiltonian is H_0 and V is some position and time-dependent potential that is assumed to slowly vanish in the remote past ($t \rightarrow -\infty$) and in the remote future ($t \rightarrow +\infty$). In free space $V = 0$ and (9) becomes

$$\left(i\hbar \frac{\partial}{\partial t} - H_0 \right) \phi(\mathbf{x}, t) = 0. \quad (10)$$

For $t' > t$, the formal solution to (9) or (10) takes the form [6]

$$\psi(\mathbf{x}, t') = T \exp \left[-i \int_t^{t'} dt'' H(t'')/\hbar \right] \psi(\mathbf{x}, t) \quad (11)$$

where T is the time-ordering operator whose details are unimportant here (see Appendix A). What is important is the decomposition of \hbar ($= m_* c^2 t_*$) in the exponent of (11), leading

to

$$\int_t^{t'} \frac{dt'' H(t'')}{\hbar} = \int_t^{t'} \frac{dt'' H(t'')}{t_* m_* c^2}. \quad (12)$$

From the perspective of the PV theory, the normalization of dt'' by the Planck time t_* and H by the Planck-particle mass energy $m_* c^2$ strongly suggest that the scattering in the quantum-electrodynamic propagator theory is caused by the Planck-particle cores that pervade the vacuum state. This conclusion will be reinforced by the calculations to follow.

The normalized Hamiltonian operator H_0 can be expressed as

$$\begin{aligned} \frac{H_0}{m_* c^2} &= \frac{p^2/2m}{m_* c^2} = \frac{c\hat{\mathbf{p}} \cdot c\hat{\mathbf{p}}/2mc^2}{m_* c^2} \\ &= \frac{(-im_* c^2 r_* \nabla) \cdot (-im_* c^2 r_* \nabla)/2mc^2}{m_* c^2} = -\frac{r_* r_* \nabla^2}{2} \end{aligned} \quad (13)$$

where the equalities in (5) are used. Then the normalized Schrödinger equation becomes

$$ir_* \frac{\partial \phi}{c \partial t} - \frac{(-ir_* \nabla) \cdot (-ir_* \nabla)}{2} \phi = 0 \quad (14)$$

or

$$\left(it_* \frac{\partial}{\partial t} + \frac{r_* r_* \nabla^2}{2} \right) \phi = 0 \quad (15)$$

where t_* ($= r_*/c$) is the Planck time and the equations are dimensionless. The dimensionless aspect of the equations here and in what follows will help in recognizing the relationship between the Huygens principle and the propagator formalism.

The normalized inhomogeneous equation (9) becomes

$$\left(it_* \frac{\partial}{\partial t} + \frac{r_* r_* \nabla^2}{2} \right) \psi = \frac{V}{m_* c^2} \psi \quad (16)$$

where again the equation is dimensionless.

3 Electron-core propagator

Roughly speaking, the Huygens principle states that every point on a wavefront is itself the source of a spherical wavelet. In the present context, the Huygens principle takes the form [7, eqn. 6.29]

$$\phi(\mathbf{x}', t') = i \int d^3 x \frac{G_0(\mathbf{x}', t'; \mathbf{x}, t)}{\hbar} \phi(\mathbf{x}, t) \quad \text{for } t' > t$$

$$\phi(\mathbf{x}', t') = i \int d^3 x \frac{G_0(\mathbf{x}', t'; \mathbf{x}, t)}{(m_* c^2) t_*} \phi(\mathbf{x}, t) \quad (17)$$

and

$$\psi(\mathbf{x}', t') = i \int d^3 x \frac{G(\mathbf{x}', t'; \mathbf{x}, t)}{\hbar} \psi(\mathbf{x}, t) \quad \text{for } t' > t$$

$$\psi(\mathbf{x}', t') = i \int d^3 x \frac{G(\mathbf{x}', t'; \mathbf{x}, t)}{(m_* c^2) t_*} \psi(\mathbf{x}, t) \quad (18)$$

where the Green function propagators G_0 and G have the units “erg-sec per unit volume”. In the present paper, equations (17) and (18) are associated with what are defined as **internal-** and **external-**scattering processes respectively. The internal scattering refers to the free electron $\phi(\mathbf{x}, t)$ scattering off the pervaded PV space. The external scattering refers to the electron $\psi(\mathbf{x}, t)$ scattering off the pervaded PV space with an external potential $V(\mathbf{x}, t)$ perturbing that space. It will be seen in what follows that the units “erg-sec per unit volume” almost define the “pervaded vacuum space”.

Now begins the calculation of the wave function ψ resulting from the continuous interaction of the free-electron wave function ϕ with the perturbed vacuum state. The calculation will not be carried to completion, but only far enough (equation (25)) to suggest that the wave scattering takes place between ϕ and the pervaded vacuum space. Furthermore, many of the details in the following calculations based on reference [7] are unimportant to the present needs; so the calculations are heavily referenced in case the reader is interested in those details.

For $t = \Delta t_1$ [7, eqn. 6.30]

$$\left(it_* \frac{\partial}{\partial t_1} + \frac{r_* r_* \nabla^2}{2} \right) \psi(\mathbf{x}_1, t_1) = \frac{V(\mathbf{x}_1, t_1)}{m_* c^2} \psi(\mathbf{x}_1, t_1) \quad (19)$$

and

$$\left(it_* \frac{\partial}{\partial t_1} + \frac{r_* r_* \nabla^2}{2} \right) \psi(\mathbf{x}_1, t_1) = 0 \quad (20)$$

for $t \neq \Delta t_1$. Equation (19) refers to an external scattering as defined above.

The new wave function due to the external perturbation V in (19) can be expressed as [7, eqn. 6.31]

$$\psi(\mathbf{x}_1, t_1) = \phi(\mathbf{x}_1, t_1) + \Delta\psi(\mathbf{x}_1, t_1) \quad (21)$$

so the Schrödinger equation yields (using (15) for ϕ)

$$\begin{aligned} &\left(it_* \frac{\partial}{\partial t_1} + \frac{r_* r_* \nabla^2}{2} \right) \Delta\psi(\mathbf{x}_1, t_1) \\ &= \frac{V(\mathbf{x}_1, t_1)}{m_* c^2} [\phi(\mathbf{x}_1, t_1) + \Delta\psi(\mathbf{x}_1, t_1)]. \end{aligned} \quad (22)$$

It can be shown that the second terms on the left and right sides of (22) can be dropped [7, eqn.6.35], leading to

$$it_* \frac{\partial}{\partial t_1} \Delta\psi(\mathbf{x}_1, t_1) = \frac{V(\mathbf{x}_1, t_1)}{m_* c^2} \phi(\mathbf{x}_1, t_1) \quad (23)$$

which to first order in Δt_1 yields

$$\Delta\psi(\mathbf{x}_1, t_1 + \Delta t_1) = -i \frac{V(\mathbf{x}_1, t_1)}{m_* c^2} \phi(\mathbf{x}_1, t_1) \frac{\Delta t_1}{t_*} \quad (24)$$

where the differential $\Delta\psi(\mathbf{x}_1, t_1)$ coming from the approximation is ignored compared to the $\phi(\mathbf{x}_1, t_1)$ on the right side of (24).

For two consecutive time periods $\Delta t_1 \Delta t_2$, with an infinite past [where $\psi(x') \rightarrow \phi(x')$], it can be argued that [7, eqn. 6.43]

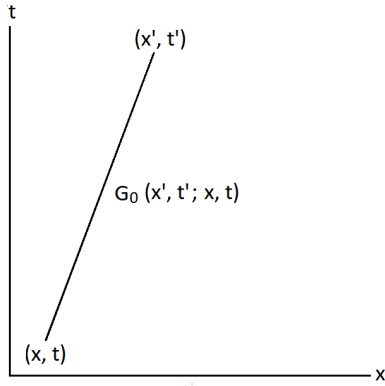


Fig. 1: The Feynman diagram for the propagation of the electron core $(-e_s, m)$ from (x, t) to (x', t') with no external scattering.

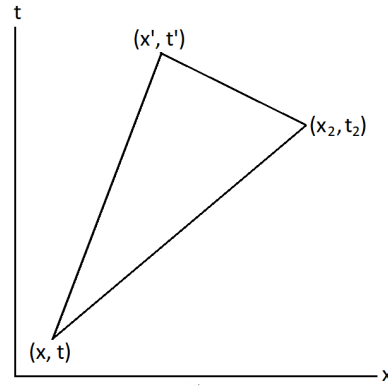


Fig. 3: The Feynman diagram for the propagation of the electron core $(-e_s, m)$ from (x, t) to (x', t') with one external scattering at (x_2, t_2) .

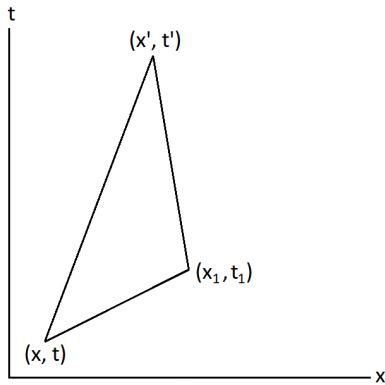


Fig. 2: The Feynman diagram for the propagation of the electron core $(-e_s, m)$ from (x, t) to (x', t') with one external scattering at (x_1, t_1) .

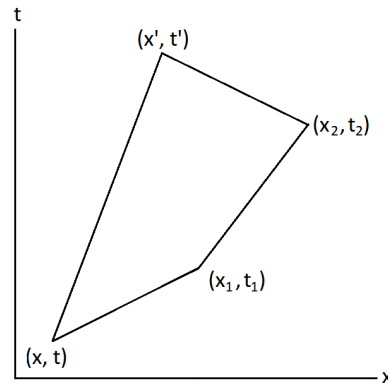


Fig. 4: The Feynman diagram for the propagation of the electron core $(-e_s, m)$ from (x, t) to (x', t') with a double external scattering at (x_1, t_1) and (x_2, t_2) .

$$\begin{aligned}
 \psi(x') = & \phi(x') + \int d^3x_1 \frac{\Delta t_1}{t_*} G_0(x'; 1) \frac{V(1)}{m_*c^2} \phi(1) \\
 & + \int d^3x_1 \frac{\Delta t_2}{t_*} G_0(x'; 2) \frac{V(2)}{m_*c^2} \phi(2) \\
 & + \int d^3x_1 \frac{\Delta t_1}{t_*} d^3x_2 \frac{\Delta t_2}{t_*} G_0(x'; 2) \\
 & \frac{V(2)}{m_*c^2} G_0(x'; 1) \frac{V(1)}{m_*c^2} \phi(1)
 \end{aligned} \tag{25}$$

where the obvious notations $(x) \equiv (\mathbf{x}, t)$ and $\phi(2) \equiv \phi(x_2)$ are used. The four terms in (25) represent respectively the propagation from (x, t) to (x', t') : a) as a free particle with no external scatterings; b) with one scattering at (x_1, t_1) ; c) with one scattering at (x_2, t_2) ; and d) with a double scattering at (x_1, t_1) and (x_2, t_2) in succession. The representations of these scatterings in Figures 1-4 are called Feynman diagrams [7, eqn. 6.43], where the horizontal axis represents space and the vertical axis represents time.

4 Conclusions and comments

A close examination of the previous calculations strongly suggests that the PV theory, which envisions a vacuum space pervaded by a degenerate collection of Planck-particle cores, provides a fundamental explanation for the Huygens principle and the scattering associated with the quantum-electrodynamic propagator formalism.

The retarded Green function G_0^+ associated with the Green function $G_0(\mathbf{x}', t'; \mathbf{x}, t)$ in equation (17) and in Figure 1 is given by the equations [7, eqn. 6.60]

$$\left(i\hbar \frac{\partial}{\partial t'} - H_0(x') \right) \frac{G_0^+(x'; x)}{\hbar} = \delta^3(\mathbf{x}' - \mathbf{x})\delta(t' - t) \tag{26}$$

for $t' > t$ and $G_0^+(x'; x) = 0$ for $t' < t$, where $x' = (\mathbf{x}', t')$ and $x = (\mathbf{x}, t)$; or

$$\left(it_* \frac{\partial}{\partial t'} + r_c r_* \nabla_x^2 \right) G_0^+(x'; x) = \delta^3(\mathbf{x}' - \mathbf{x})[t_*\delta(t' - t)] \tag{27}$$

where the parenthesis on the left and the bracket on the right of (27) are dimensionless.

Appendix A: Time-ordering operator T

The time-ordering operator [6] is defined by

$$T \exp \left[-i \int_t^{t'} dt'' H(t'')/\hbar \right] \equiv \quad (\text{A1})$$

$$\sum_{n=0}^{\infty} \frac{1}{n!} \left(\frac{-i}{\hbar} \right)^n \int_t^{t'} dt_1 \cdots \int_t^{t_{n-1}} dt_n H(t_1) \cdots H(t_n) \quad (\text{A2})$$

$$= \sum_{n=0}^{\infty} \frac{(-i)^n}{n!} \int_t^{t'} \frac{dt_1}{t_*} \cdots \int_t^{t_{n-1}} \frac{dt_n}{t_*} \frac{H(t_1)}{m_* c^2} \cdots \frac{H(t_n)}{m_* c^2} \quad (\text{A3})$$

where the final equality comes from the decomposition of the Planck constant, $\hbar = m_* c^2 t_*$, in (A2).

Submitted on April 14, 2018

References

1. Davies P. Superforce: the Search for a Grand Unified Theory of Nature. Simon and Schuster, Inc., New York, 1984.
2. Daywitt W.C. A Model for Davies' Universal Superforce. *Galilean Electrodynamics*, 2006, v. 5, 83.
3. Daywitt W.C. The Trouble with the Equations of Modern Fundamental Physics. *American Journal of Modern Physics. Special Issue: "Physics without Higgs and without Supersymmetry"*, 2016, v. 5(1-1), 22. See also www.planckvacuumDOTcom.
4. Carroll B.W., Ostlie A.D. An Introduction to Modern Astrophysics. Addison-Wesley, San Francisco, Boston, New York, Cape Town, Hong Kong, London, Madrid, Mexico City, Montreal, Munich, Paris, Singapore, Sydney, Tokyo, Toronto, 2007.
5. Daywitt W.C. The Planck Vacuum. *Progress in Physics*, 2009, v. 1, 20.
6. Fradkin E. Chapter 10: Observables and Propagators. Internet website: "Observables and Propagators, Fradkin".
7. Gingrich D.M. Practical Quantum Electrodynamics. CRC, The Taylor & Francis Group, Boca Raton, London, New York, 2006.

Predicting Total Angular Momentum in TRAPPIST-1 and Many Other Multi-Planetary Systems Using Quantum Celestial Mechanics

Franklin Potter

8642 Marvale Drive, Huntington Beach, CA 92646, USA

E-mail: frank11hb@yahoo.com

TRAPPIST-1 harbors at least 7 Earth-mass planets orbiting a 0.089 solar mass dwarf M-star. Numerous other multi-planetary systems have been detected and all obey a quantization of angular momentum per unit mass constraint predicted by quantum celestial mechanics (QCM) as derived from the general theory of relativity (GTR). The universality of this constraint dictates that the TRAPPIST-1 system should obey also. I analyze this recently discovered system with its many mean motion resonances (MMRs) to determine its compliance and make some comparisons to the Solar System and 11 other multi-planetary systems.

1 Introduction

In the past 25 years, more than 3500 exoplanets have been detected, many in multi-planetary systems with 4 or more planets [1]. Extreme examples include HD 10180 with 9 planets and TRAPPIST-1 with 7 planets. In each of the discovered systems the understanding of their formation and stability over tens of millions or even billions of years using Newtonian dynamics remains an interesting challenge.

A prediction of whether additional planets exist beyond those already detected is not an expected outcome of the dynamical studies. However, a different approach [2] called quantum celestial mechanics (QCM) offers the potential ability to predict the existence of additional angular momentum in the planetary system, which could indicate additional planets to be detected or additional mass in the form of rings or spherical shells of mass chunks orbiting the star, such as the Kuiper belt or the Oort Cloud in our Solar System.

The history of the formation of most of these planetary systems remains an active research area, ranging from *in situ* formation from a dust disk to pebble accretion followed by sequential inward migration toward the central star [3]. Their stability may depend upon numerous factors, and many research groups continue to investigate the long-term stability for millions of orbits over tens of millions of years, including in models for the history of our Solar System.

There is a recent paper [4] that considers the total angular momentum deficit (AMD) of multi-planetary systems with the proposal that the AMD is a way to classify their predicted stability. The AMD is defined by the total angular momentum difference

$$AMD = \sum_{k=1}^n \mu_k \sqrt{GM r_k} \left(1 - \sqrt{1 - \epsilon_k^2} \cos i_k \right) \quad (1)$$

between the maximum total orbital angular momentum when all the planets orbit in the same plane and the total angular momentum determined from the orbital data. The Solar System and HD 10180 are two examples discussed in which the outer system of planets is AMD-stable, the inner system

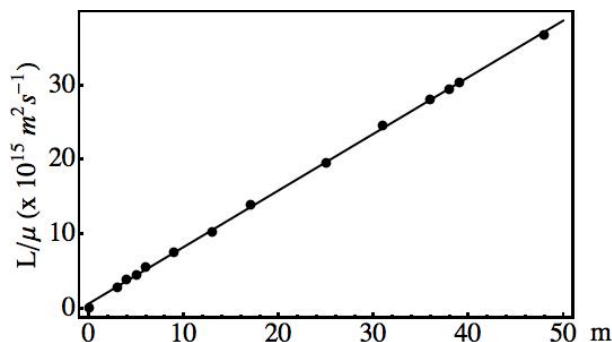


Fig. 1: Solar System fit to QCM total angular momentum constraint. The uncertainties are within the data circles.

of planets is AMD-unstable, and the whole system is AMD-unstable.

In fact, this AMD approach demonstrates that the AMD-unstable systems tend to have orbital period ratios concentrated around the lower integer mean motion resonance ratios such as 3:2 and 2:1, a result perhaps somewhat in conflict with expectations. This unexpected outcome is interesting because many planetary systems exhibit at least one mean motion resonance (MMR), which had been expected to contribute a stabilizing factor in parts of those systems. The AMD research therefore means that not all MMRs are beneficial toward stabilizing the planetary orbits.

The recently discovered TRAPPIST-1 system has 7 Earth-mass planets all within 0.1 au of its dwarf M-star of 0.089 solar masses [5]. Three of the planet pairs exhibit a 3:2 MMR and another pair exhibits the 4:3 MMR, yet studies indicate that this system has been in existence for at least 7 billion years. Perhaps an additional factor contributes to the stability of these multi-planetary systems.

We propose that the additional factor is the quantization of angular momentum per unit mass predicted by quantum celestial mechanics (QCM). The QCM theory [6] dictates that not all planetary orbits about the central star are available as equilibrium orbits but, instead, QCM determined equilib-

rium orbits exist only at specific radii. Bodies in orbits at all other radial distances will migrate towards these specific QCM equilibrium orbital radii.

In the following sections we review the QCM proposed angular momentum constraint that leads to a select set of orbital radii for all planetary systems and demonstrate its application to the Solar System, the 5 moons of Pluto, the 7 planets of TRAPPIST-1, and to numerous other exoplanetary systems, including HD 10180.

2 The QCM angular momentum constraint

The total angular momentum in a planetary system is an important physical parameter not often discussed. In 2003, H. G. Preston and F. Potter proposed [6] a new gravitational theory called Quantum Celestial Mechanics (QCM), which is derived from the general theory of relativity (GTR), that claims that all gravitationally bound systems in the Schwarzschild metric will exhibit the quantization of angular momentum per unit mass constraint

$$\frac{L}{\mu} = m \frac{L_T}{M_T} \quad (2)$$

with m being the orbit quantization integer, L the angular momentum of each orbiting body of mass μ , and L_T and M_T the total angular momentum and total mass of the planetary system.

In the simplest applications of QCM, one assumes that after tens of millions of years that the orbiting planet is at its equilibrium orbital radius r with a small eccentricity ϵ so that the Newtonian orbital angular momentum value $L = \mu \sqrt{GM r(1 - \epsilon^2)}$, with M being the star mass, can be used. For most multi-planetary systems, including the Solar System, TRAPPIST-1, and HD 10180, the values of ϵ are all less than 0.2 and will be ignored in the QCM analysis fit to the constraint.

Because the QCM quantization of angular momentum per unit mass constraint is derived from the general relativistic Hamilton-Jacobi equation via a simple transformation, one obtains a new gravitational wave equation [6]. In the familiar Schwarzschild metric this gravitational wave equation will apply to all gravitationally-bound systems with orbiting bodies. However, as in GTR, different metrics can be considered, including the static interior metric, for which the QCM analysis of the Universe [7] predicts a new interpretation of the cosmological redshift in agreement with the data, that all distant sources are in a more negative gravitational potential than all observers, i.e. the distant clocks tick slower.

3 Application of QCM to the Solar System

Our first application of QCM in the Schwarzschild metric was to our Solar System using the known masses and present spacings of its 8 planets. If only the orbital angular momentum of the 8 planets and the Sun are considered, so that L_T

$\approx 4 \times 10^{43} \text{ kg m}^2 \text{ s}^{-1}$, then this value of the total angular momentum meant that QCM predicted that all the planetary orbits should be within the radius of the Sun! Obviously, something was wrong.

At first, we suspected that our derivation of the constraint was incorrect. But a detailed check proved that our derivation had been done correctly, including the numerous approximations needed to obtain an equation with the most important factors. Therefore, in order to achieve the present day orbital spacings, we interpreted the QCM equations to be predicting much more angular momentum in the Solar System, about 50 times as much!

Indeed, we subsequently learned that the Solar System does have much more angular momentum in its system than the contributions from just the Sun and its planets. The Solar System has an enormous angular momentum contribution from the Oort Cloud with its approximately 100 Earth masses of ice chunks orbiting at about an average distance of 40,000 au, thereby dominating the total angular momentum of the Solar System by almost a factor of 50.

The new orbital fits of QCM using the constraint then agreed with the present orbital radii of the planets, and we predicted the total angular momentum in the Solar System to be the much higher value $L_T \approx 1.9 \times 10^{45} \text{ kg m}^2 \text{ s}^{-1}$. Fig. 1 shows our QCM fit to the 8 planets plus the 5 known dwarf planets, with m values 3, 4, 5, 6, 9, 13, 17, 25, 31, 36, 38, 39, 48.

So, for the first time, we were able to use the QCM angular momentum constraint to fit the equilibrium orbital radii of all the planets of the Solar System and to verify that the constraint could be an important factor in predicting additional angular momentum in a planetary system. One should note that the QCM fit does not require the division of the system into the inner planets and the outer planets, a prominent feature of other approaches, including AMD.

The successful application of the QCM angular momentum constraint to the Solar System encouraged us to try to find a definitive test. But the QCM constraint fit to the Solar System and to the orbiting satellites of the Jovian planets could not be considered definitive tests of QCM because their system total angular momentum values were not known to within 10%. So a decade long hunt began to find a multi-bodied system for which the physical parameters are known to be within a few percent.

4 Pluto system as a definitive test of QCM

Fortunately, in 2012, the dwarf planet Pluto was reported to have 5 moons. Their orbital stability was being studied in reference to the Pluto-Charon barycenter, and the moons are nearly in a 1:3:4:5:6 resonance condition!

An early QCM linear regression fit with $R^2 = 0.998$ to the angular momentum constraint for the Pluto system revealed more angular momentum could be present in this sys-

	m	r (au)	P (days)	P2/P1	$(n_2/n_1)^3$	L_{max} $10^{39} \text{ kg m}^2 \text{ s}^{-1}$	MMR(P)	MMR(n)
b	15	0.0115	1.51087	1.000	1.000	1.103		
c	18	0.0158	2.42182	1.603	1.675	1.802	1.603	1.675
d	21	0.0223	4.04961	2.680	2.600	0.540	1.672	1.552
e	24	0.0293	6.09961	4.037	3.815	1.828	1.506	1.467
f	28	0.0385	9.20669	6.094	5.954	1.651	1.509	1.560
g	31	0.0469	12.35294	8.176	8.000	2.066	1.342	1.344
h	36	0.0619	18.76700	12.421	12.366	0.826	1.519	1.546
						9.815		

Table 1: Fit of the 7 planets of TRAPIST-1 to the QCM angular momentum constraint.

tem, hinting that at least one more moon could exist. This fit used the smallest set of integers possible with m values 2, 6, 9, 10, 11, 12. A set with larger integers was also available beginning with $m = 4$ for a good fit but indicating a lower total angular momentum value for the system.

Then, in 2015, the New Horizons spacecraft sent back precise data about the Pluto system that established 5 tiny moons only. That limitation allowed us to have a definitive test [8] of QCM because the total angular momentum was then known to within 2.4%. With the m values 4, 10, 15, 16, 18, 19, the QCM angular momentum constraint applied to the Pluto system predicted $L_T = 6.28 \times 10^{30} \text{ kg m}^2 \text{ s}^{-1}$, a value commensurate with the value $L_T = 6.26 (\pm 0.14) \times 10^{30} \text{ kg m}^2 \text{ s}^{-1}$ calculated from the known physical parameters.

We therefore consider the Pluto system to be the definitive test of the QCM angular momentum constraint because we know the pertinent physical parameters to within 2.4%, and the predicted QCM total angular momentum determined from the slope of the QCM plot of L/μ vs m agrees with the total value determined in the standard way using Newtonian physics.

5 QCM constraint applied to TRAPPIST-1

There has been great interest in the TRAPPIST-1 system because at least 3 of the planets are in the so-called Habitable Zone where liquid water and perhaps some kind of life form could have evolved over its nearly 9 billion year history [10]. However, being so close-in to their M-star also means that these planets could be experiencing a severe UV radiation flux as well as particle winds emanating from the star. Studies of their atmospheric content are under way by researchers to determine whether water still exists or whether the UV radiation has dissociated any previously existing water vapor with the resulting particles having evaporated away to leave behind an arid surface environment [9, 11].

We know that the planetary system orbiting TRAPPIST-1 harbors at least 7 Earth-mass planets orbiting close-in to the dwarf M-star of $0.089 M_\odot$ [5]. More planets further out beyond 1 au could exist, a possibility that QCM may suggest by interpreting the constraint fit. The orbital period ratios

reveal that planet pairs d/e, e/f and g/h exhibit nearly a 3:2 mean motion resonance (MMR) and the pair f/g has a 4:3 MMR [9]. Planet pairs b/c and c/d do not have a first order MMR although their period ratios are near 5:3.

The formation of this system has been a challenge for modeling, and in a recent study [3] a pebble accretion and inward migration history have been proposed to accommodate its formation, including a process called resonance trapping as planets sequentially move inward and build.

The pertinent data for the 7 known planets and the predicted m values from the system's linear regression fit to the QCM angular momentum constraint are provided in Table 1. This set of m values is the lowest set of integers that achieved a linear regression least squares fit of $R^2 > 0.999$ for both plots: L/μ vs m and P_2/P_1 vs $(n_2/n_1)^3$, with $n = m+1$ for the assumed circular orbits. Of course, other integer sets with larger m values will also fit the constraint as well, but they will have a smaller slope and therefore a smaller system total angular momentum value calculated with (2).

In Fig. 2 is the plot of L/μ vs m with all uncertainties within the small circles around each data point. From the slope $8.77 \times 10^{12} \text{ m}^2 \text{ s}^{-1}$ of this QCM fit, one predicts a system total angular momentum of $1.56 \times 10^{42} \text{ kg m}^2 \text{ s}^{-1}$. The angular momentum from the star rotation plus the orbital motion of the 7 planets is much less, about $1.2 \times 10^{40} \text{ kg m}^2 \text{ s}^{-1}$, using the values given in Table 1 and a star rotation period of 3.295 days.

The angular momentum difference could be accommodated in several ways, including a larger integer for the first m value and larger integers overall, thereby reducing the QCM predicted total angular momentum. Or the difference could be due to the presence of at least one additional planet further out beyond a distance of about 1 au. For example, if the additional planet had the mass of Saturn, its orbit at about 3.8 au would be sufficient to account for the discrepancy between the total angular momentum values. And, of course, this system could have the equivalent of the Oort Cloud at a large distance from the star.

The period ratios provided in both columns 5 and 6 are referenced to planet b. For a circular orbit, $n = \ell+1$, and

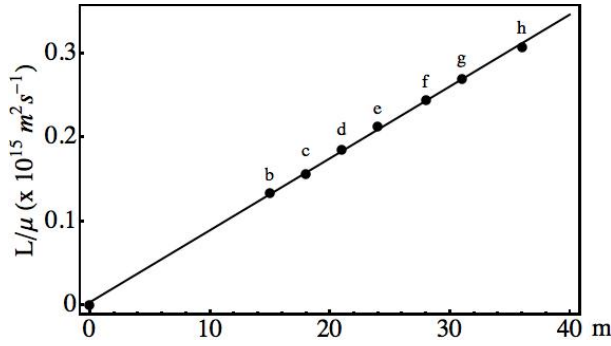


Fig. 2: QCM angular momentum constraint applied to the TRAPPIST-1 system of 7 planets close-in to the dwarf M-star. The uncertainties all lie within the data circles.

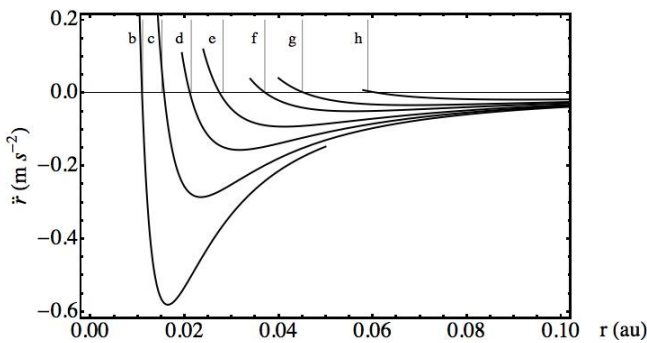


Fig. 3: The QCM predicted radial accelerations \ddot{r} for each of the 7 planets of TRAPPIST-1. Note that some planets should experience corrections to their radial positions over tens of millions of years.

we assume $\ell = m$, its maximum value. QCM predicts period ratios

$$\frac{P_2}{P_1} = \left[\frac{m_2 + 1}{m_1 + 1} \right]^3. \quad (3)$$

The largest discrepancy of the QCM predicted period ratios in column 6 from the actual values in column 5 is for planet e at 5.5%.

In the last two columns are the calculated MMRs for the adjacent planets when calculated from values in column 4, the MMR(P), and values calculated from column 6, for the MMR(n), revealing the amazing first order resonances d/e, e/f, g/h, and f/g, as well as the possible higher order resonances b/c and c/d. Planet c exhibits the biggest difference in QCM predicted values at about 7.2%.

Recall that QCM in the Schwarzschild metric predicts a specific but limited set of radii for circular equilibrium orbits that have both inward and outward forces acting, in direct contrast to Newtonian orbital dynamics which has an equilibrium orbit at all planetary orbital radii. For QCM the approximate expression for the effective gravitational potential is

$$V_{eff} = -\frac{GM}{r} + \frac{\ell(\ell + 1)L_T^2}{2r^2 M_T^2}, \quad (4)$$

where the angular momentum quantization integer ℓ originates in the θ -coordinate. We have taken $\ell = m$ for the expression. Whence, the expected value of the orbital radial acceleration near the equilibrium radius is defined by

$$\ddot{r}_{eq} = -\frac{GM}{r^2} + \frac{\ell(\ell + 1)L_T^2}{r^3 M_T^2}. \quad (5)$$

A computer simulation of the TRAPPIST-1 system could use this equation to study its long-term QCM dynamic stability contributions but must also include perturbations by the other planets. The net QCM accelerations are very small, varying from around a hundredth to a few tenths of a meter per second squared.

A plot of the QCM radial accelerations near the equilibrium radii for all 7 planets is shown in Fig. 3, where the vertical lines labelled b to h are the reported present radial orbital distances of the planets. As can be seen from the plot, a small radial movement inward for planet e is predicted to occur because its present radial acceleration is negative with respect to the QCM equilibrium orbital distance.

One would expect that the planets will oscillate about the QCM equilibrium orbital radii throughout their history, never settling at the exact radius at which no further radial acceleration would occur. Perturbations from the other nearby planets as they pass by will be larger than the QCM accelerations, but they last for short time intervals while the small QCM accelerations are acting constantly.

This TRAPPIST-1 system has existed for many billions of years, so some sort of stabilizing influence has been at play. We suspect that the QCM angular momentum constraint is the important additional factor, providing accelerations on both sides of the predicted QCM equilibrium orbital radius. A computer simulation will be needed to determine the outcomes over long time periods.

6 HD 10180 and other exosystems

The QCM quantization of angular momentum per unit mass constraint is expected to apply to all gravitationally bound systems described in the Schwarzschild metric.

In previous articles we analyzed multi-planetary systems with 4 or more planets and found that they all can fit the QCM angular momentum constraint. We list some of those systems for comparison in Table 2 in order of increasing star mass in column 2. Their m values and slope b are derived from the linear regression plots of L/μ versus m . The QCM value of L_T in column 6 is calculated from b and then compared to their known total angular momentum values (sum of columns 7 and 8).

Therefore, from the values in Table 2 we notice:

1. That our Solar System's b value is much larger than all the other multi-planetary system's b values. Why? Because the Solar System has the overwhelming angular momentum contribution from its Oort Cloud, a physi-

System	Star M_{\odot}	N	m values	b $10^{15} \text{ m}^2 \text{ s}^{-1}$	QCM L_T $10^{45} \text{ kg m}^2 \text{ s}^{-1}$	Star L_T $10^{42} \text{ kg m}^2 \text{ s}^{-1}$	Planets L_T $10^{42} \text{ kg m}^2 \text{ s}^{-1}$
TRAPPIST-1	0.089	7	15,18,21,24,28,31,36:	0.00877	0.00156	0.0113	0.012
GJ 667 C	0.31	7	16,21,26,29,34,39:55	0.0333	0.0206	0.00971	0.169
GJ 581	0.31	6	8,10,14,20,25:47	0.0456	0.0283	0.00454	0.229
HD 40307	0.75	6	9,12,16,19,22:35	0.0863	0.129	0.179	0.340
Tau Ceti	0.783	7	13,14,18,20:25,31,49	0.0923	0.145	0.0820	0.311
HR 8832	0.794	7	4,6,9,12:15,41,44	0.144	0.229	0.491	4.131
Kepler-20	0.912	6	8,10,12,15:18,24	0.105	0.191		0.846
Kepler-11	0.95	6	11,12,15,17,19:26	0.113	0.215		5.60
55 Cancri	0.95	5	3,8,12:23,62	0.160	0.304	0.118	78
Sun	1.0	8	:3,4,5,6,13,17,25,31	0.762	1.524	0.192	31
HD 10180	1.062	9	3,6,7,8,12,14:17,29,46	0.185	0.393	0.436	5.153
Kepler-90	1.20	8	14,15,17,28:33,36,43,50	0.0949	0.228	0.738	

Table 2: QCM angular momentum constraint applied to selected multi-planetary systems listed in order of star mass. N is the number of known planets which determine the m values for a linear regression fit $R^2 \geq 0.999$. The m values for planets with orbital radii less than Mercury’s are to the left of the colon. The predicted QCM L_T in column 6 is calculated using the QCM slope b times the star mass.

cal property that dictates QCM to predict the very large orbital spacings for its planets. We cannot say much more about the Solar System, i.e., predict whether more planets or dwarf planets exist, because the overwhelming but unknown total angular momentum contribution of the Oort Cloud precludes making such a prediction.

2. That for the TRAPPIST-1 system, with its incredibly small QCM b value, we expect another planet or more orbiting bodies because the QCM predicted total angular momentum value is much greater than the orbital contribution from its 7 known planets and the rotation of the central star. Perhaps the proposed pebble accretion and inward migration train is the explanation for its formation, but QCD would suggest otherwise, that the planets formed *in situ* by gathering the local dust accumulating at the QCM equilibrium radii, assuming that the total angular momentum in this system did not change significantly during their formation.
3. That even for the HD 10180 system fit, as shown in Fig. 4 with its 9 planets, the total angular momentum from its star rotation plus the known orbiting planets falls far short of the QCM predicted total angular momentum, so more orbiting mass is expected.
4. That all the systems in Table 2 are expected to have additional angular momentum based upon the predicted QCM value of L_T . If more planets in these systems are detected, they should have orbital radii corresponding to the listed QCM m values that dictate their allowed equilibrium orbital distances.

Perhaps another exosystem will be discovered in the near future that also has a large angular momentum contribution and very large QCM orbital spacings so that direct comparisons can be made to the Solar System in terms of the total angular momentum parameter.

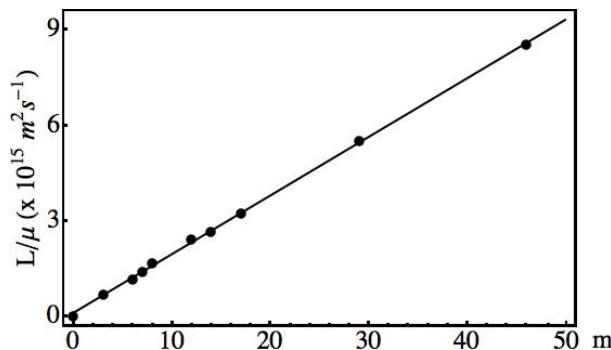


Fig. 4: QCM angular momentum constraint applied to HD 10180. Uncertainties lie within the data circles.

Note that both the 4 inner planets of the Solar System and the 7 planets of the TRAPPIST-1 system have been determined to be unstable by the AMD analysis [4]. Yet both systems have been in existence for more than 4 billion years, i.e., more than 4 billion Earth orbits. Perhaps the small QCM gravitational potential valleys around their QCM orbital equilibrium radii, such as those shown in Fig. 3, are contributing factors to their long-term stability. Or the existence of additional orbital mass further out contributes to their stability also. A computer simulation of these systems and the others that includes the QCM constraint could be done to determine whether this QCM effect is large enough to ensure their long-term stability.

7 Conclusions

Many multi-planetary systems have been discovered and they all had been determined previously to obey the QCM quantization of angular momentum per unit mass constraint. For most of those systems if not all of them, additional angular momentum is predicted by QCM, angular momentum which

could be contributed by additional planets or spherical shells of ice.

Now the interesting TRAPPIST-1 system of 7 Earth-like planets has been shown to obey the angular momentum constraint for each known planet in the system. The QCM predicted total angular momentum of its planetary system is $1.56 \times 10^{42} \text{ kg m}^2 \text{ s}^{-1}$ versus the estimated value of $1.2 \times 10^{40} \text{ kg m}^2 \text{ s}^{-1}$ for the 7 planets plus the star rotation contribution. This large total angular momentum discrepancy could indicate that either at least one more planet could exist beyond several 1 au or that a set of m values with larger integers would be a better fit to decrease the predicted total angular momentum.

Also, for the TRAPPIST-1 system, from the determined radial acceleration values near to the QCM predicted orbital equilibrium radii, several planets could migrate slightly. For example, planet e has a present radial distance that should decrease slightly over several thousand years in order to reach its nearby predicted QCM orbital equilibrium radius. Perturbations from the other planets will be important to consider in a computer simulation of its behavior as the planet migrates to its true QCM equilibrium orbital radius.

We also provide a list of 12 multi-planetary systems so that a direct comparison of our Solar System QCM parameters can be made to other systems. The major difference is that our Solar System contains significantly more angular momentum than any other known planetary system discovered. Our QCM theory uses this information to predict the allowed equilibrium orbital distances, an approach that explains why almost all other multi-planetary systems with smaller total angular momentum values can have so many planets within the orbital radius of Mercury. Dynamically, a larger repulsive orbital angular momentum term in the QCM radial acceleration equation will result in the planets forming at larger orbital equilibrium radii.

Finally, the long-term stability of these multi-planetary systems remains a challenge for the traditional modeling using Newtonian universal gravitation without additional constraints. The consideration of the total angular momentum deficit (AMD) has introduced a method to classify their stability but is incomplete. Perhaps the QCM quantization of angular momentum per unit mass approach will be the additional constraint needed in order to better understand the formation and stability of multi-planetary systems.

Acknowledgements

We thank Sciencegems.com for continued support. Also, this research has made use of the Exoplanet Orbit Database and the Exoplanet Data Explorer at exoplanets.org.

Received on April 20, 2018

References

1. Han E., et al. Exoplanet Orbit Database. II. Updates to Exoplanets.org. *PASP*, 2014, v. 126 (943), 827.
2. Potter F. Multi-planet Exosystems All Obey Orbital Angular Momentum Quantization per Unit Mass predicted by Quantum Celestial Mechanics (QCM). *Progress in Physics*, 2013, v. 9 (3), 60–61.
3. Ormel C., Liu B., Schoonenberg D. Formation of TRAPPIST-1 and other compact systems. arXiv: astro-ph/1703.06924.
4. Laskar J., Petit A. AMD-stability and the classification of planetary systems. arXiv: astro-ph/1703.07125.
5. Gillon M., Triaud A. H. M. J., Demoy B.-O., et al. Seven temperate terrestrial planets around a nearby ultracool dwarf star TRAPPIST-1. *Nature*, 2017, v. 542, 456–460.
6. Preston H. G., Potter F. Exploring large-scale gravitational quantization without \hbar in planetary systems, galaxies, and the Universe. arXiv: gr-qc/0303112.
7. Potter F., Preston H. G. Cosmological Redshift Interpreted as Gravitational Redshift. *Progress in Physics*, 2007, v. 3 (2), 31–33.
8. Potter F. Update on Pluto and its 5 Moons Obeying the Quantization of Angular momentum per Unit Mass Constraint of Quantum Celestial Mechanics. *Progress in Physics*, 2016, v. 12 (1), 56–58.
9. Luger R., Sestovic M., et al. A seven-planet resonant chain in TRAPPIST-1. *Nature Astronomy*, 2017, v. 1, (Article 0129).
10. Burgasser A. J., Mamejek E. E. On the Age of the TRAPPIST-1 System. arXiv: astro-ph/1706.02018.
11. Borrier V., De Wit J., Bolmont E., et al. Temporal Evolution of the High-energy Irradiation and the Water Content of TRAPPIST-1 Exoplanets. arXiv: astro-ph/1708.09484v1.

On the Classical Scaling of Quantum Entanglement

Pierre A. Millette

E-mail: PierreAMillette@alumni.uottawa.ca, Ottawa, Canada

In this paper, we consider the implications of the classical scaling of quantum entanglement observed experimentally. The probability of preserving entanglements over classical scales and preventing the entanglement from collapsing due to physical interactions is exceedingly small, indicating a fragile entanglement process. We propose a physically robust entanglement process that persists to classical scales as observed. We use a formulation of quantum mechanics that gives precedence to the physical rather than the mathematical aspects of the theory and its transition to the classical domain, using a physical interpretation instead of the literal interpretation of the Hilbert space of the standard formalism. We clarify the difference between separable (product) and non-separable (entangled) states, and the local realism nature of the product states which obey Bell's inequality compared to the non-local nature of the entangled states which violate Bell's inequality. We note that the truly quantum mechanical processes such as the double-slit interference pattern, potential barrier tunneling, and in particular the entanglement process as we show in this paper, depend on the quantum mechanical phenomenon of wave-particle duality. In entanglement experiments, the quantum mechanical results obtained are from the *wave* aspect of the wave-particle quantum object (q-object), just like the interference pattern in double-slit experiments, not the particle aspect of the q-object which is currently unknowingly assumed. The wave aspect of the q-object gives rise to the non-local behaviour as would be expected from the quantum mechanical calculations, while the particle aspect exhibits local causal behaviour. This explains why the entanglement process is robust: the wave-particle q-objects of entangled states have definite physical characteristics at emission time and are free of fragile evanescent properties. In addition, we conclude that "spooky action at a distance" (SAAD) is not required.

1 Introduction

Quantum entanglement is a quantum mechanical property of a composite quantum system consisting of two or more subsystems (such as particles), describing a situation where a quantum subsystem is linked to another via a specific process leading to correlations between observable physical properties of the subsystems. The two-particle *spin-singlet* state

$$|\psi^-\rangle = \frac{1}{\sqrt{2}} \left(|\uparrow_1 \downarrow_2\rangle - |\downarrow_1 \uparrow_2\rangle \right) \quad (1)$$

is an example of state entanglement in bipartite systems [1, p. 19].

Schrödinger first introduced the term *entangled state* to describe the non-separable pure states of quantum systems [2], [1, p. 17]. Consider for example the emission of two photons of opposite polarization from a given process, such as the stimulated emission of polarization-entangled photons (see for example [3, 4]). The emitted photons are then conceived of as "entangled" pure states. The system is described by the wavefunction [4]

$$|\psi\rangle = \frac{1}{\sqrt{2}} \left(|\cup_1\rangle |\cup_2\rangle + |\cup_1\rangle |\cup_2\rangle \right) \quad (2)$$

where \cup_i and \cup_i represent the right-hand and left-hand circularly polarized photons for $i = 1$ or 2 . This wavefunction

represents what we know of the entangled system, or alternatively represents our lack of knowledge of the specific properties of each photon that is emitted. All we know is that if one emitted photon is right-hand circularly polarized, then the other will be left-hand circularly polarized, and vice versa. Eq. (2) is a statement of this situation.

The predominant interpretation (the orthodox viewpoint [5]) is that the wavefunction (2) represents a physical description of the emitted photons in an unresolved evanescent state, and that once a measurement is performed on one of them, the wavefunction collapses, the measured photon's actual properties are then known and an instantaneous propagation of that information is perceived by the other photon so that it can assume the complementary properties required by the process – "spooky action at a distance" (SAAD) as Einstein called it, a process that some physicists like to think of as quantum magic, an approach that speaks more of metaphysics than physics. The reasons for the acceptance of this description will be considered in greater detail in Section 5.

Over the past decades, experiments have been devised to extend the range of quantum entanglements, to the point where classical scales have been achieved. This includes both the size of entangled objects (*e.g.* [6–10]) and the distances over which entanglement has been maintained (*e.g.* [11, 12]).

These are particularly stunning results as any interaction

of one of the entangled components with its environment will collapse the entanglement. The probability of preventing such interactions and preserving entanglements over classical sizes and distances is exceedingly small. As noted by Jaeger [1, p. 20] “Indeed, *pure* such states of two-particle systems are exceptional rather than typical in the world; typically, a system very soon interacts with a number of other systems, so that, even if it were prepared in a pure state, it is typically described by a mixed state”.

The probability that a photon can travel a distance x without interaction is given by [13] [14, Section 3.3.1] [15, p 304]

$$P_{no-int}(x) = \exp(-n_p \sigma x) \quad (3)$$

where n_p is the particle number density and σ is the total photon interaction cross-section including absorption and scattering. For propagation of photons in the atmosphere, $n_p \sim 2.5 \times 10^{25} \text{ m}^{-3}$ [16] and $\sigma \sim 180 \text{ barn/molecule} \equiv 1.8 \times 10^{-26} \text{ m}^2/\text{molecule}$ [17]. Using these values in (3), the no-interaction probability becomes

$$P_{no-int}(x) = e^{-0.45 x} \quad (4)$$

where x is in meters. We see that for classical distances x , the probability $P_{no-int}(x)$ increasingly becomes very small. For example, $P_{no-int}(1 \text{ m}) = 0.64$, $P_{no-int}(10 \text{ m}) = 0.011$, $P_{no-int}(100 \text{ m}) = 2.9 \times 10^{-20}$, $P_{no-int}(1 \text{ km}) = 3.6 \times 10^{-196}$. For the value of 143 km of [11, 12] the probability that a photon can travel such a distance without interaction is astronomically small.

Hence the probability of preserving entanglements over classical sizes and distances and preventing the entanglement from collapsing due to physical interactions is exceedingly small. The question has to be raised: in light of these successful classical-scale experiments, are we currently misunderstanding the quantum entanglement process such that instead of a fragile entanglement situation as the above considerations indicate, we can derive a quantum entanglement process that leads to a physically robust entanglement situation that persists to classical scales as observed?

2 Quantum entanglement questions

Questions have been raised concerning entanglement and its extension to the classical (or macro) domain [18]. There is no doubt that some processes generate particle or photon pairs that have a definite relationship (correlation) between them (which are referred to as being entangled) and these relationships are confirmed experimentally. At stake here is the interpretation of the quantum entanglement process, and the impact of the understanding of this process on the development and technological applications of this quantum mechanical process – a misinterpretation can lead to considerations that are not physically realistic.

Questions have also been raised on the limited applicability of Bell’s inequality [19–21], based on the assumptions

used in its derivation. Bell [22] uses a single continuous parameter λ described by a probability distribution $\rho(\lambda)$: the basic limitation of this approach is that it imposes a quantum mechanical calculation approach on the analysis. Bell’s derivation is only applicable to a specific class of hidden variable theories that can be represented by his starting equation and assumptions, which Jaynes [20] refers to as Bell theories. Some hidden variable theories don’t need to satisfy Bell’s starting equation to reproduce quantum mechanical results, as evidenced by Bohmian mechanics [23]. Bell’s inequality is thus found to apply to a limited set of circumstances and situations, not to every quantum system. Selleri [24] provides a comprehensive review of the proofs of Bell’s inequality.

Actual experimental demonstration of entanglement is a challenge. Entanglement experiments detect both entangled components within the same time window (see Subsection 5.3), so there is no way to confirm the presence or absence of SAAD – it is assumed to be present purely based on the predominant interpretation discussed in Section 1. Zhao [19] has proposed various experiments to clarify the physical properties of entanglement, including one to determine if the collapse of the entangled wavefunction due to the measurement of one component causes the transformation of the other component due to SAAD as is supposed in the orthodox interpretation. No reports of these experiments having been performed have surfaced – their execution should be given a high priority to help us better understand the phenomenon of entanglement.

3 Literal or physical interpretation?

To be able to answer the question posed at the end of Section 1 on a physically robust entanglement process, we need to have a better understanding of the physical description of quantum mechanics and of its transition to the classical domain. The orthodox view in the standard formalism of quantum mechanics is done via entanglement, wavefunction collapse and decoherence [25]. This is a literal interpretation of the Hilbert space mathematical theory of quantum mechanics developed by von Neumann and Dirac [26, 27]. However, as noted by Home and Whitaker [15, see p. 309], “[t]o conclude, there are aspects of classical reality pertaining to the macro-physical world that cannot be made consistent with quantum theory in any limit, at least using the standard formalism and decoherence models.”

This thus leads us to consider other approaches to understand this problem. There are other interpretations of quantum mechanics which satisfy its principles – the book by Home [14] provides an excellent exposition of the conceptual foundations of quantum physics. As is well-known [28], the various formulations of quantum mechanics provide the same results (Schrödinger wave equation, Heisenberg matrix formulation, Dirac standard formalism, Feynman path integral, Bohm quantum potential among others) – the differences be-

tween them lie in the insights that these different formulations can provide. To understand the process under discussion, what is required is a physical interpretation based on a formulation of quantum mechanics that gives precedence to the physical rather than the mathematical aspects of the theory, and of its transition to the classical domain.

A physical theory of quantum mechanics which offers a logical transition into classical physics was first developed before it was displaced by the preferred standard formalism. This initial theory was instrumental in the development of quantum mechanics. Here we briefly recap this approach.

In classical mechanics [29], the phase space description of a system is given in terms of generalized coordinates $q = \{q_i; i = 1, 2, \dots, N\}$ and canonical momenta $p = \{p_i; i = 1, 2, \dots, N\}$ and its time evolution is described in terms of its Hamiltonian $H(q, p)$ using Hamilton's equations

$$\dot{q}_i = \frac{\partial H}{\partial p_i}, \quad \dot{p}_i = -\frac{\partial H}{\partial q_i}. \tag{5}$$

The Lagrangian of the system determines its dynamics in configuration space in terms of the coordinates $\{q_i\}$ through the Euler-Lagrange equations

$$\frac{\partial L}{\partial q_i} - \frac{d}{dt} \left(\frac{\partial L}{\partial \dot{q}_i} \right) = 0, \quad i = 1, 2, \dots, N. \tag{6}$$

If a statistical description of the system is desired, the state of the system is described in terms of a probability function $P(q, p)$ defined on the phase space, and its time evolution is given by

$$\frac{dP}{dt} = \{P, H\} + \frac{\partial P}{\partial t}, \tag{7}$$

where the Poisson bracket $\{P, H\}$ is given by

$$\{P, H\} = \sum_i \left(\frac{\partial P}{\partial q_i} \frac{\partial H}{\partial p_i} - \frac{\partial H}{\partial q_i} \frac{\partial P}{\partial p_i} \right). \tag{8}$$

The quantum mechanical description of the system derived from the foregoing considerations sees the dynamical variables (q, p) now interpreted as operators (\hat{q}, \hat{p}) acting on complex wavefunctions $\psi(q)$ generating observables and satisfying the commutation relation

$$[\hat{q}_i, \hat{p}_j] = i\hbar \delta_{ij}, \tag{9}$$

where \hbar is Planck's reduced constant. This transition from a classical to a quantum mechanical description, known as *canonical quantization*, is effected (done) by the replacement of classical variables by quantum operators according to

$$q_i \rightarrow \hat{q}_i, \quad p_i \rightarrow \hat{p}_i \tag{10}$$

and (classical) Poisson brackets by (quantum) commutators according to

$$\{A, B\} \rightarrow \frac{1}{i\hbar} [\hat{A}, \hat{B}]. \tag{11}$$

The close relation between the classical and quantum dynamical equations is evident in the similarity between the classical equation of motion (7) and the quantum equation of motion as derived by Heisenberg,

$$\frac{d}{dt} \langle A \rangle = \frac{1}{i\hbar} \langle [\hat{A}, \hat{H}] \rangle + \left\langle \frac{\partial A}{\partial t} \right\rangle. \tag{12}$$

This result is a manifestation of Ehrenfest's theorem [30, see pp. 389–394] which holds that quantum mechanical expectation values $\langle A \rangle$ obey the classical equations of motion. This similarity points to the relation between the classical probability functions defined on the (q, p) phase space and the quantum mechanical expectation values obtained from the (\hat{q}, \hat{p}) operators acting on the complex wavefunctions $\psi(q)$ representing our knowledge of the system, which in the end obey the classical equations of motion.

This approach provides a physical interpretation that can be used to better understand the classical scaling of quantum entanglement. One of the characteristics of the above considerations is the physical reality of the underlying quantum mechanical system as it evolves into a classical system. In the following section, we consider the nature of quantum states as this has an impact on the robustness of entangled states.

4 The nature of quantum states

Jaeger [1, pp. 19–22] clearly communicates the importance of understanding the difference between separable (product) and non-separable (entangled) states. Over the past quarter century, the definition of entanglement has been extended, from information theory, to include mixed states that are separable when given as combination of products of subsystem states. Separable subsystem states are entirely uncorrelated (not entangled), while the entangled mixed states are the inseparable states – however, “[t]he problem of determining whether or not a given state of a composite system is entangled is known as the *separability problem*.” [1, p. 21]. These entangled mixed states tend to somewhat muddle the entanglement water.

When considering separable (product) states, as noted by Jaeger [1, p. 21], “...the outcomes of local measurements on any separable state can be simulated by a local hidden-variables theory, that is, the behavior of systems described by such states can be accounted for using common-cause explanations”. In other words, *separable* states can have definite physical properties when they are prepared.

It is important to note that Bell's inequality is violated only by entangled (non-separable) states. As noted by Jaeger [1, p. 22], “[t]he quantum states in which correlations between [components] A and B can violate a Bell-type inequality are called *Bell correlated*, or *EPR correlated*. If a bipartite *pure* state is entangled, then it is Bell correlated with certainty, as was first pointed out by Sandu Popescu and Daniel Rohrlich [31] and by Nicolas Gisin in the early 1990s [32].

However, no simple logical relation between entanglement and Bell correlation holds for the mixed entangled states”.

Home [14, pp.203–209] also makes the point. He concludes “an arbitrary mixture of factorable or product state vectors always satisfies Bell’s inequality” as first shown by [33,34], while “[f]or any given nonfactorable state vector of correlated quantum systems it is always possible to choose observables so that Bell’s inequality is violated by quantum mechanical predictions.” [14, pp.205, 208] which was first demonstrated by [32] as seen previously.

Hence we have two different types of quantum states depending on whether they are product (separable) or entangled (non-separable) states. Separable states are consistent with local realism – they can be physical and local, while entangled states are not consistent with local realism, based on Bell’s inequality. The normal reaction would be that there should be one consistent behaviour across all states, that the entangled states’ behaviour trumps the separable states’ behaviour, and hence quantum states are not consistent with local realism.

However, as seen in Section 2, questions have been raised about Bell’s inequality, and this difference in behaviour between separable and entangled states may indicate that there is a problem with our understanding of Bell’s inequality and of entanglement in general. We explore this question in greater details in the next section, and in doing so, show that we can in fact derive a robust entanglement process as observed in the classical scaling of quantum entanglement.

5 A robust entanglement process

The considerations of Section 3 reinforce the underlying physical building blocks of quantum mechanics: the superposition principle, Heisenberg’s uncertainty principle and wave-particle duality. These are crucial to physically understand the entanglement process and demonstrate why it is a robust process. While the superposition property results from the linear wave equations used in the theory and Heisenberg’s uncertainty principle results from the fact that quantum mechanical canonically conjugate dynamical variables are Fourier transform pairs of variables [35], wave-particle duality is a purely quantum mechanical property and is undoubtedly the most important of these. The truly quantum mechanical processes such as the double-slit interference pattern, potential barrier tunneling, and in particular the entanglement process as we will see in this section, depend on the quantum mechanical phenomenon of wave-particle duality. It is critical to analyze quantum phenomena in terms of wave-particle duality to fully understand them.

5.1 Non-existence of hidden-variables?

Home [14] does an extensive review of all proofs of the non-existence of hidden-variable theories in quantum mechanics and concludes “[h]aving established that contrary to folklore,

no a priori compelling argument excludes the possibility of contextual hidden variable theories, the entire enterprise of developing a more complete description of quantum phenomena beyond the ambit of the standard interpretation becomes logically legitimate”, and provides a reference to an example: “A pedagogically instructive model example of how a contextual hidden variable model can reproduce the standard quantum mechanical results is discussed by [36], who show in detail how such a model can provide an objectively real treatment of decaying, oscillating, and regenerating kaons” [14, pp.195–196]. A contextual hidden variable model is one “in which the value obtained by a measurement is a function of the premeasurement value as well as the measurement context.” [14, p.37].

In addition, the basic deficiency of hidden-variable non-existence proofs is that they are derived within the context of quantum mechanics. By its very nature, quantum mechanics is a probabilistic theory – so it is not surprising that such “proofs” find that deterministic results cannot be derived from quantum mechanics. The reader is referred to [21] for an example of this approach in the assumptions used by Bell in the derivation of his inequality, which leads to the conclusion that “it is not surprising that Bell’s inequality is not satisfied in systems that obey quantum mechanics”.

It is important to note that the label “hidden-variable theories” is attached indiscriminately to more complete theories of quantum mechanics. However, as in the case of Bohmian mechanics, a deterministic quantum physics theory does not need to include hidden variables. The proper path to such a theory is to start outside of quantum mechanics, derive a deterministic microscopic theory, and show that quantum mechanics can be derived from it – see [44] for an example of this approach.

Home [14] continues “[t]here are strong physical grounds for suspecting that the standard framework (formalism and interpretation) of quantum mechanics is fundamentally inadequate, though its empirical success to date is unquestionably impressive” [14, p.37]. Home identifies the following aspects of quantum mechanics that are not well understood in the standard framework: the quantum measurement paradox, the classic limit of quantum mechanics, nonlocality of quantum mechanics arising from entanglement, and wave-particle duality [14, pp.37-38]. These are the very factors at play in the robustness of the entanglement process as discussed in this paper.

5.2 Wave-particle q-objects

Entanglement experiments compare the behaviour of classical particles with quantum mechanical results that are unknowingly assumed to represent the particle aspect of the wave-particle quantum object (which for brevity we refer to as a “q-object”). It is important to realize that a q-object does not behave as a classical object due to its explicit wave-particle

nature. For the wave aspect of a macroscopic object, its de Broglie wavelength is extremely small and its effect is negligible – however, in the quantum mechanical domain the impact of the wave-particle nature of the q-object becomes significant as observed in quantum physics. It is interesting to note that the impact of wave-particle duality has been observed at mesoscopic scales as reported in [6]. Thus a q-object is an object where the effect of wave-particle duality cannot be neglected.

In entanglement experiments, the quantum mechanical results obtained are from the *wave* aspect of the wave-particle q-object, just like the interference pattern in double-slit experiments. Hence, the results obtained in Bell experiments [38] and other entanglement experiments devised since then are the quantum mechanical results of the wave aspect of the wave-particle q-objects which are different from the particle results, again as seen in double-slit experiments (classical double-particle pattern versus quantum mechanical wave interference pattern). Similarly in Hardy experiments [39], the non-zero probability $P(A_1, B_1)$ [40] obtained in contradistinction to the local realist probability of zero is due to the *wave* aspect of the wave-particle q-object.

Wave-particle duality is still somewhat of a mystery in quantum mechanics. It is still understood mostly in terms of Bohr's principle of wave-particle complementarity which holds that the wave aspect and the particle aspect of an object are complementary aspects of a quantum object [14, see Chapter 5]. However, wave-particle duality arises naturally in the theory of Spacetime Continuum Elastodynamics (*STCED*) [57, 58] which is briefly covered in the Appendix and is considered in greater detail in [44]. This model provides a natural explanation for wave-particle duality, where an object, represented as a spacetime deformation, is composed of transverse and longitudinal modes, with the transverse mode corresponding to the wave aspects of the deformation and the longitudinal mode corresponding to the particle aspects of the deformation.

A wave-particle q-object is thus a hybrid object consisting of both wave and particle aspects which manifest themselves differently in experiments, depending on the type of measurement. We examine the experiments of Aspect *et al.* [41–43] using single-photon states covered in Home [14, Section 5.4] to demonstrate how they can be fully understood in terms of *STCED* wave-particle duality.

In the “light pulses on a beam splitter” experiment (Home's Fig. 5.2), for a pulsed photodiode light pulse, the wave aspect is expected to apply from the *STCED* wave-particle model – indeed, as Home comments “[t]he striking feature is that even under this apparently quantum condition, light pulses arriving at the beam splitter continued to behave as classical waves, and the inequality $[P_C \geq P_T P_R]$ was never observed to be violated” [14, p. 288], where P_T is the probability that a single count is transmitted, P_R is the probability that a single count is reflected, and P_C is the probability of a

coincidence for that single count.

For a source of single photon pulses from an excited atom transition, using the same experimental setup, the particle aspect is expected to apply from the *STCED* wave-particle model – indeed, “a clear-cut violation of the inequality $[P_C \geq P_T P_R]$ ” was observed. “This confirmed single particle behavior of the single-photon states.” [14, p. 288].

The experiment was then modified as per Home's Fig. 5.3 by removing the detectors on either side of the beam splitter and recombining the two beams using mirrors and a second beam splitter. Using the source of single photon pulses from an excited atom transition as previously, this time the wave aspect is expected to apply from the *STCED* wave-particle model as it is being treated as a wave (recombining the two beams) – indeed, the experiment “showed interference effects dependent on the difference in path lengths along two possible routes of single-photon pulses.” [14, p. 288].

This provides experimental confirmation of the *STCED* wave-particle model where the wave-particle q-object consists of both wave and particle aspects which manifest themselves differently depending on the type of measurement. The behaviour is physical and logical. In addition, nothing precludes the wave-particle q-object from having the full physical properties encoded in the q-object. The results obtained in the case of non-rotated detectors are in agreement with local results that would be obtained classically, because there are no specific quantum effects coming out of the quantum mechanical calculations in this case.

This indicates that the entangled q-objects are emitted with deterministic physical properties. The wave aspect gives rise to the non-local behaviour (within causality requirements due to the particle aspect of the q-object) as would be expected from the quantum mechanical calculations, while the particle aspect exhibits local causal behaviour [44]. This explains why the entanglement process is robust: the wave-particle q-objects of entangled states have definite physical, not evanescent, characteristics at emission time.

5.3 Physical approach

This leads us to consider a physical approach which posits that the photons (for example), as wave-particle q-objects, are emitted with specific properties, but that due to our lack of knowledge of their detailed characteristics, can only be probabilistically characterized with the wavefunction ψ as a combination of the possible states and their probabilities (the realistic viewpoint [5]). Once a measurement is performed on one of the photons, its properties are resolved, thereby increasing our knowledge of the system, and allowing us to specify the properties of the other photon – a simple physical understanding of the process [21]. Such a process can easily scale to classical objects and distances, and is undeniably very robust as the q-objects' properties are determined at emission time, not evanescent depending either on an experimenter's whim

or thought process, or on not having an interaction that would destroy the entanglement on its way to measurement resolution. The classical-scale experiments considered previously are then seen to be a confirmation of this approach.

The wavefunction is thus seen to be a probabilistic description of our (limited) *knowledge* of a quantum mechanical system, not a complete physical description of the system, with this probability being proportional to the *intensity* of the wavefunction as seen in [44]. This explains the laws of quantum probability [45,46]. We note the same behaviour for electromagnetic radiation, where the intensity is proportional to the energy density of the field, which can be converted to a probability by normalization, as seen in [44].

As a result of the measurement process, the original wavefunction description is superceded (the so-called collapse of the wavefunction) and is replaced by a more accurate wavefunction description of the quantum mechanical system that takes into account the results of the measurement process. As [37] puts it, “When a detector clicks the wavefunction does not ‘collapse’ from all over space to a point, it is simply that only part of it is now relevant.” It is important to note that this measurement process is effected (done) by the interaction of the quantum mechanical system with an outside agency, whether it is a measurement apparatus or an interaction with another quantum mechanical system.

This is a simple logical description of the physical process that does not require metaphysical “spooky action at a distance” explanations and, by the principle of Occam’s razor, is a superior explanation of the entanglement process. It should be noted that the imaginary actors “Bob” and “Alice” which are used in the explanation of entanglement and SAAD, even though the explanation is presented as a sequential series of events, are both aware of the same experimental information within the same time window, as mentioned in Section 2, and hence fully satisfy Jaynes’ analysis of entanglement experiments as discussed in [20,21].

As Home points out, “[c]ontrary to a widely held misconception, we stress that no experiment probing quantum locality has yet tested quantum correlations measured across spacelike separation unambiguously.” [14, p. 233]. In photon polarization correlation experiments [38], “[t]he claim of spacelike separation is usually based on ensuring that a photon on one side reaching a photomultiplier detector is space-like separated from its partner passing the polarization analyzer on the other side.” However, a typical photomultiplier detector requires about 30 ns for a current pulse to be generated following the arrival of a photon, which provides a different spacelike separation than that obtained from the resolution time of a photomultiplier which is usually of order 1 ns [14, p. 233].

It should be noted that the model proposed in this paper is independent of these so-called “loopholes”. They are mentioned to indicate the difficulty of performing such experiments which raises cautionary notes on the concomitant

dangers of wishful thinking and unrecognized assumptions, limitations and interpretation of the results.

5.4 Evidence for SAAD?

So why introduce a mysterious agent, “spooky action at a distance”, when none is required? As we asked in Section 1, what prompts the acceptance of this description as part of the orthodox interpretation? The reason is that SADD is believed to be supported by the experimental evidence. However, the aforementioned considerations and the analysis of Jaynes [20,21,47] show that the experimental evidence can be explained without resorting to metaphysics, that the problem results from the assumption that a conditional probability represents a physical influence instead of the physically-correct logical inference that it is.

As Home and Whitaker write [15, p. 238],

In one out of four cases, Alice is lucky with her measurement, and Bob’s particle immediately becomes an identical replica of Alice’s original. Then it might seem as if information has traveled instantly from Alice to Bob. Yet this strange feature cannot be used to send *usable information instantaneously*, because Bob has *no* way of knowing that his particle is already an identical replica. Only when he *learns* the result of Alice’s Bell-state measurement, which is transmitted to him via classical means, can he exploit the information in the teleported quantum state.

where the emphasis is in the original text and we have in addition highlighted the word “learns”.

In other words, what is believed to be “spooky action at a distance” is actually the experimenters’ knowledge of the system suddenly increasing as a result of the measurement process, and the experimenters being in a position to logically infer the properties of the distant component, which is confirmed in the measurement performed on the distant component. In actual practice, in entanglement experiments, both measurements are done in the same time window (see Sections 2 and 5.3).

There is also a certain intellectual inertia at play. As Bell [48] commented, “Why is the pilot wave picture [Bohm’s] ignored in text books? Should it not be taught, not as the only way, but as an antidote to the prevailing complacency? To show that vagueness, subjectivity, and indeterminism, are not forced on us by experimental facts, but by deliberate theoretical choice?” All very good questions.

6 Quantum information causality

The emerging concept of *information causality* [49–51] is an attempt to preserve causality based on the underlying premise that it is information that is the core element in the analysis of the entanglement process. The approach followed is to impose this concept as a principle of nature to avoid the special relativistic causality problems raised by SAAD. This concept

unwittingly reflects Jaynes' analysis of entanglement experiments in that it focuses on information – however, Jaynes' analysis [20, 47] already accomplishes this without having to introduce an additional constraint in the guise of a new causality principle, and in so doing, also eliminates the need for SAAD.

7 Weak quantum measurements

Weak quantum measurements [52–56] is another emerging concept in quantum mechanics that has an impact on the understanding of the entanglement process. What is interesting with this approach is that it is possible to make minimal-interacting measurements, which leaves the collapse of the wavefunction in the literal interpretation of the mathematical standard formalism of quantum mechanics in a quandary: how can any measurement be done without collapsing the wavefunction?

The accepted explanation [54] is that the quantum state is not collapsed into eigenvectors, but instead, by a weak coupling of the measurement device and the system, is biased by a small angle such that the measurement device shows a superposition of several eigenvalues. The current status is summarized as follows: “weak measurement theory presents a plethora of strange quantum phenomena, not yet completely understood.” [54]. There is no doubt that even a weak interaction measurement will have an impact on the system, and this approach, certainly experimentally valid, puts the wavefunction collapse of the literal interpretation of quantum mechanics into question.

The proposal of weakly interacting measurements was also introduced in [35] in the context of the application of the Nyquist-Shannon Sampling Theorem to quantum measurements. The author showed that Brillouin zones in Solid State Physics are a manifestation of the Nyquist-Shannon Sampling Theorem at the quantum level, where the translational symmetry of atoms in a solid resulting from the regular lattice spacing, is equivalent to an effective sampling of the atoms of the solid giving rise to the Brillouin zones. This raised the possibility of investigating new experimental conditions leading to new measurements previously considered unreachable, a possibility that is also considered possible in the literature on weak quantum measurements.

8 Discussion and conclusion

In this paper, we have considered the classical scaling of quantum entanglement. This implies a physically robust entanglement process, contrary to the fragile entanglement process that the standard formalism interpretation implies given that the probability of preserving entanglements over classical sizes and distances and preventing the entanglement from collapsing due to physical interactions is exceedingly small.

Actual experimental demonstration of entanglement, other than testing the Bell inequality, is a challenge. Entangle-

ment experiments detect both entangled components within the same time window, so there is no way to confirm the presence or absence of “spooky action at a distance” (SAAD) which is assumed to be present based on the standard formalism interpretation.

To better understand the entanglement process and determine a robust entanglement process, we have considered a physical interpretation based on a formulation of quantum mechanics that gives precedence to the physical rather than the mathematical aspects of the theory used in the literal interpretation of the Hilbert space formulation.

We have considered the transition from a classical to a quantum mechanical description, known as *canonical quantization*, which is effected (done) by the replacement of classical variables by quantum operators, and have noted that one obtains closely related classical and quantum (Heisenberg) equations of motion. This result is a manifestation of Ehrenfest's theorem which holds that quantum mechanical expectation values obey the classical equations of motion.

We have considered the difference between separable (product) and non-separable (entangled) states. Mixtures of product (separable) states always satisfy Bell's inequality *i.e.* separable states can have definite physical properties when they are prepared. Bell's inequality fails only for entangled (non-separable) states. Hence separable states are consistent with local realism – they can be physical and local, while entangled states are not consistent with local realism, based on their violation of Bell's inequality.

We have seen that these considerations reinforce the underlying physical building blocks of quantum mechanics: the superposition principle, Heisenberg's uncertainty principle and wave-particle duality which is the most important of these. The truly quantum mechanical processes such as the double-slit interference pattern, potential barrier tunneling, and in particular the entanglement process as we have seen in this paper, depend on the quantum mechanical phenomenon of wave-particle duality. It is thus critical to analyze quantum phenomena in terms of wave-particle duality to fully understand them.

We have noted Home's [14] conclusion reached after an extensive review of all proofs of the non-existence of hidden-variable theories, that “no a priori compelling argument excludes the possibility of contextual hidden variable theories”, giving legitimacy to the development of a more complete description of quantum phenomena beyond the standard interpretation. He further identifies the aspects of quantum mechanics that are not well understood in the standard framework: the quantum measurement paradox, the classic limit of quantum mechanics, nonlocality of quantum mechanics arising from entanglement, and wave-particle duality, which are the very factors at play in the robustness of the entanglement process as discussed in this paper.

We have noted that in entanglement experiments, the quantum mechanical results obtained are from the *wave* aspect of

the wave-particle quantum object (which for brevity we refer to as a “q-object”), just like the interference pattern in double-slit experiments. A q-object is an object where the effect of wave-particle duality cannot be neglected.

Hence, Bell’s inequality is violated in the quantum mechanical problem, that is the wave aspect of the wave-particle q-object, which is different from the particle results, as seen in double-slit experiments (particle versus wave patterns). However, nothing precludes the wave-particle q-object from having the full physical properties encoded in the q-object when the entangled q-objects are emitted. The wave aspect then gives rise to the non-local behaviour (within causality requirements due to the particle aspect of the q-object) as would be expected from the quantum mechanical calculations, while the particle aspect exhibits local causal behaviour. This explains why the entanglement process is robust: the wave-particle q-objects of entangled states have definite physical characteristics at emission time.

This has lead us to consider a physical approach which posits that the photons (for example), as wave-particle q-objects, are emitted with specific properties, but that due to our lack of knowledge of their detailed characteristics, can only be probabilistically characterized with the wavefunction ψ as a combination of the possible states and their probabilities (the realistic viewpoint). Performing a measurement on one of the photons resolves its properties which allows us to specify the properties of the other photon – a simple physical understanding of the entanglement process. Such a process can easily scale to classical objects and distances, and is undeniably very robust as the q-objects’ properties are determined at emission time, not evanescent as in the standard formalism. The classical-scale experiments considered previously are then seen to be a confirmation of this approach.

We have also considered the emerging concept of *information causality* which is an attempt to preserve causality based on the underlying premise that it is information that is the core element in the analysis of the entanglement process, which is correct. However, Jaynes’ analysis [20, 47] already accomplishes this without having to introduce an additional constraint in the guise of a new causality principle, and in so doing, also eliminates the need for SAAD.

We have also considered weak quantum measurements which is another emerging concept in quantum mechanics. There is no doubt that even a weak quantum measurement will have an impact on the system, and this approach, certainly experimentally valid, puts the wavefunction collapse of the literal interpretation of quantum mechanics into question.

It should be noted that quantum cryptography and quantum computing are then seen to depend on the *wave* aspect of the wave-particle q-object. This fundamental understanding should help accelerate the progress of these new development programs.

The resolution of the robustness of the entanglement process in classical scale quantum entanglement experiments is

thus achieved within the wave-particle q-object explanation of the process in which entangled state q-objects have definite physical characteristics at emission time. Strong evidence has been provided to support this proposal.

The design of experiments to provide experimental evidence requires that experimentalists shift the paradigm used to test quantum theories. Currently experiments are designed to try to prove the applicability of quantum mechanics to entangled states by verifying various inequalities such as Bell’s. The experiments suggested by Zhao [19] try to clarify the physical properties of quantum entanglement and includes experimental tests of the locality of the measurements of Bell states, experimental tests of the constituents of Bell states, and experimental tests of determinism in quantum measurements. In addition, even though the entanglement experiments currently performed agree with the model proposed in this paper, specific experiments need to be performed to test the model under conditions that emphasize that quantum entanglement behaviour results from the *wave* aspect of the wave-particle q-objects.

Appendix: wave-particle duality in *STCED*

It should be noted that wave-particle duality is considered in greater detail in [44] within the theory of the Elastodynamics of the Spacetime Continuum (*STCED*) [57, 58]. As shown in *STCED*, energy propagates in the spacetime continuum as wave-like deformations which can be decomposed into *dilatations* and *distortions*. *Dilatations* involve an invariant change in volume of the spacetime continuum which is the source of the associated rest-mass energy density of the deformation. On the other hand, *distortions* correspond to a change of shape of the spacetime continuum without a change in volume and are thus massless. Thus the deformations propagate in the continuum by longitudinal (*dilatation*) and transverse (*distortion*) wave displacements. This provides a natural explanation for wave-particle duality, with the transverse mode corresponding to the wave aspects of the deformation and the longitudinal mode corresponding to the particle aspects of the deformation.

Received on April 26, 2018

References

1. Jaeger G. Entanglement, Information, and the Interpretation of Quantum Mechanics. Springer-Verlag, Berlin, 2009.
2. Schrödinger E. Die gegenwaertige Situation in der Quantenmechanik. *Die Naturwissenschaften*, 1935, v. 23, 807; Discussion of probability relations between separated systems. *Proc. Cambridge Philos. Soc.*, 1935, v. 32, 446.
3. Lamas-Linares A., Howell J. C. and Boowmeester, D. Stimulated emission of polarization-entangled photons. *Nature*, 2001, v. 412, 887–890.
4. Hayat A., Ginzburg P. and Orenstein, M. High-rate entanglement source via two-photon emission from semiconductor quantum wells. *Physical Review B*, 2001, v. 76, 035339.

5. La Rosa A. Introduction to Quantum Mechanics. Portland State University Lecture Notes, Portland, 2017, Chapter 12, Quantum Entanglement.
6. Arndt M., Nairz O., Vos-Andreae J., Keller C., van der Zouw G., Zeilinger A. Wave-particle duality of C_{60} molecules. *Nature*, 1999, v. 401, 680–682.
7. Nairz O., Arndt M., and Zeilinger A. Quantum interference experiments with large molecules. *American Journal of Physics*, 2003, v. 71, 319–325.
8. Lee K. C., Sprague M. R., Sussman B. J., Nunn J., Langford N. K., Jin X. M., Champion T., Michelberger P., Reim K. F., England D., Jaksch D., Walmsley I. A. Entangling macroscopic diamonds at room temperature. *Science*, 2011, v. 334 (6060), 1253–1256.
9. Dolde F., Jakobi I., Naydenov B., Zhao N., Pezzagna N., Trautmann C., Meijer J., Neumann P., Jelezko F., and Wrachtrup J. Room-temperature entanglement between single defect spins in diamond. *Nature Physics Letters*, 2013, DOI: 10.1038/NPHYS2545, 139–143.
10. Belli S., Bonsignori R., D’Auria G., Fant L., Martini M. and Peirone S. Entangling macroscopic diamonds at room temperature: Bounds on the continuous-spontaneous-localization parameters. arXiv: quant-ph/1601.07927v3.
11. Xiao S. M., Herbst T., Scheldt T., Wang D., Kropatschek S., Naylor W., Wittmann B., Mech A., Kofler J., Anisimova E., Makarov V., Jennewein Y., Ursin R and Zeilinger A. Quantum teleportation over 143 kilometres using active feed-forward. *Nature Letters*, 2012, v. 489, 269–73.
12. Herbst T., Scheidl T., Fink M., Handsteiner J., Wittmann B., Ursin R. and Zeilinger A. Teleportation of Entanglement over 143 km. arXiv: quant-ph/1403.0009v3.
13. Townsend R. H. D. Stellar Astrophysics. University of Wisconsin-Madison Lecture Notes, Madison, 2008, Section 10, Radiation & Matter.
14. Home D. Conceptual Foundations of Quantum Physics, An Overview from Modern Perspectives. Plenum Press, New York, 1997.
15. Home D., Whitaker A. Einstein’s Struggles with Quantum Theory, A Reappraisal. Springer, New York, 2007.
16. Value for “dry air” from “Molecular number density” table in Wikipedia under entry “Number density”, accessed 10 March 2018.
17. Hubbell J. H. Photon Cross-Sections, Attenuation Coefficients, and Energy Absorption Coefficients from 10 keV to 100 GeV. Nat. Bur. Stand. (US) Report NSRDS-NBS-29, Washington DC, 1969, pp. 45–46.
18. Bruno N., Martin A., Sekatski P., Sangouard N., Thew R. T. and Gisin N. Displacement of entanglement back and forth between the micro and macro domains. *Nature Physics Letters*, 2013, DOI: 10.1038/NPHYS2681, 1–4.
19. Zhao H. L. On Bell’s Joint Probability Distribution Assumption and Proposed Experiments of Quantum Measurement. arXiv: physics.gen-ph/0906.0279v4.
20. Jaynes E. T. Clearing Up Mysteries – The Original Goal. In Skilling J., ed. Proceedings Volume, Maximum Entropy and Bayesian Methods. Kluwer Academic Publishers, Dordrecht, 1989, pp. 1–27.
21. Millette P. A. On the Applicability of Bell’s Inequality. *Progress in Physics*, 2016, vol. 12 (3), 211–215.
22. Bell J. S. On the Einstein–Podolsky–Rosen Paradox. *Physics*, 1964, v. 1, 195–200. Reprinted in Bell J. S. Speakable and Unspeakeable in Quantum Mechanics. Cambridge University Press, Cambridge, 1987, pp. 14–21.
23. Dürr D., Teufel S. Bohmian Mechanics: The Physics and Mathematics of Quantum Theory. Springer-Verlag, Berlin, 2009.
24. Selleri F., ed. Quantum Mechanics Versus Local Realism: The Einstein–Podolsky–Rosen Paradox. Plenum, New York, 1988.
25. Joos E., Zeh H. D., Kiefer C., Giulini D., Kupsch J., Stamatescu I.-O. Decoherence and the Appearance of a Classical World in Quantum Theory, Second Edition. Springer-Verlag, Berlin, 2003.
26. von Neumann J. Mathematical Foundations of Quantum Mechanics. Princeton University Press, Princeton, (1932) 1996.
27. Dirac P. A. Lectures on Quantum Mechanics. Dover Publications, New York, (1964) 2001.
28. Styer D. F., Balkin M. S., Becker K. M., Burns M. R., Dudley C. E., Forth S. T., Gaumer J. S., Kramer M. A., Oertel D. C., Park L. H., Rinkoski M. T., Smith C. T. and Wotherspoon T. D. Nine formulations of quantum mechanics. *Am. J. Phys.*, 2002, v. 70 (3), 288–297.
29. Leinaas J. M. Non-Relativistic Quantum Mechanics. University of Oslo Lecture Notes, Oslo, 2003.
30. Ballentine L. E. Quantum Mechanics, A Modern Development. World Scientific Publishing, Singapore, 1998.
31. Popescu S. and Rohrlich D. Generic quantum nonlocality. *Phys. Lett. A*, 1992, v. 166, 293.
32. Gisin N. Bell’s inequality holds for all non-product states. *Phys. Lett. A*, 1991, v. 154, 201.
33. Capusso V., Fortunato D. and Selleri F. Generic quantum nonlocality. *Int. J. Theor. Phys.*, 1973, v. 7, 319.
34. Home D. and Selleri F. *Riv. Nuov. Cim.*, 1991, v. 14 (9), 1.
35. Millette P. A. The Heisenberg Uncertainty Principle and the Nyquist-Shannon Sampling Theorem. *Progress in Physics*, 2013, v. 9 (3), 9–14. arXiv: quant-ph/1108.3135.
36. Home D. and Selleri F. *J. Phys. A*, 1991, v. 24, L1073.
37. Holland P. R. The Quantum Theory of Motion. Cambridge University Press, Cambridge, 1993.
38. Aspect A., Dalibard J. and Roger G. Experimental test of Bell’s inequalities using time-varying analyzers. *Phys. Rev. Lett.*, 1982, v. 49, 1804–1807.
39. Hardy L. Nonlocality for Two Particles without Inequalities for Almost All Entangled States. *Phys. Rev. Lett.*, 1993, v. 71, 1665–1668.
40. Guo W. J., Fan D. H. & Wei L. F. Experimentally testing Bell’s theorem based on Hardy’s nonlocal ladder proofs. *Sci China-Phys Mech Astron*, 2015, v. 58, 024201-1–5.
41. Grangier P., Roger G. and Aspect A. *Europhys. Lett.*, 1986, v. 1, 173.
42. Aspect A. and Grangier P. *Hyp. Int.*, 1987, v. 37, 3.
43. Aspect A. In Miller A. I., ed. Sixty-Two Years of Uncertainty. Plenum, New York, 1990, pp. 45–59.
44. Millette P. A. Wave-Particle Duality in the Elastodynamics of the Spacetime Continuum (STCED). *Progress in Physics*, 2014, vol. 10 (4), 255–258.
45. Feynman R. P. The Concept of Probability in Quantum Mechanics. Lecture, 1951.
46. Feynman R. P., Leighton R. B., Sands M. Lectures on Physics, Volume III: Quantum Mechanics. Addison-Wesley Publishing Company, Reading, Massachusetts, 1965, Chapter 3, Probability Amplitudes.
47. Jaynes E. T. Probability in Quantum Theory. In Zurek W. H., ed. Complexity, Entropy and the Physics of Information. Addison Wesley Publishing, Reading, MA, 1990.
48. Bell J. S. On the Impossible Pilot Wave. *Foundations of Physics*, 1982, v. 12, 989–999. Reprinted in Bell J. S. Speakable and Unspeakeable in Quantum Mechanics. Cambridge University Press, Cambridge, 1987, pp. 159–168.
49. Pawłowski M., Paterek T., Kaszlikowski D., Scarani V., Winter A. and Zukowski M. Information causality as a physical principle. *Nature Letters*, 2009, vol. 461, doi:10.1038/nature08400, T101–104.
50. Pitalúa-García D. Quantum information causality. arXiv: quant-ph/1210.1943v3.

51. Ringbauer M., Fedrizzi A., Berry D. W. and White A. G. Information Causality in the Quantum and Post-Quantum Regime. arXiv: quant-ph/1406.5034v2.
 52. Fuchs C. A. Information Gain vs. State Disturbance in Quantum Theory. arXiv: quant-ph/9605014.
 53. Vaidman L. Weak Value and Weak Measurements. arXiv: quant-ph/0706.1348.
 54. Tamir B. and Cohen E. Introduction to Weak Measurements and Weak Values. *Quqnta*, 2013, vol. 2 (1), 7–17.
 55. Svensson B. E. Y. Pedagogical Review of Quantum Measurement Theory with an Emphasis on Weak Measurements. *Quqnta*, 2013, vol. 2 (1), 18–49.
 56. Vaidman L. Weak Value Controversy. arXiv: quant-ph/1703.08870.
 57. Millette P. A. Elastodynamics of the Spacetime Continuum. *The Abraham Zelmanov Journal*, 2012, vol. 5, 221–277.
 58. Millette P. A. Elastodynamics of the Spacetime Continuum: A Spacetime Physics Theory of Gravitation, Electromagnetism and Quantum Physics. American Research Press, Rehoboth, NM, 2017.
-

Matter in a Space of a Fractional Dimension. A Cosmological System of Spaces and Evolution of the Universe

Mikhail N. Mashkin

E-mail: mnmashkin@yandex.ru

In this article, we propose a model of evolution of the Universe from topological spaces as a sequence generating one space from another. While the Universe is modelled in the form of a fraction-dimensional space, where time is the manifestation of the fractional dimension of the space.

Introduction

The origin of the Universe is a key topic in modern physics. Expansion of the Universe still demands an explanation.

Forty years ago, the physicist A. D. Sakharov has introduced a hypothesis: objects of the three-dimensional space are compositions of objects of a two-dimensional space and a one-dimensional space.

Based on this hypothesis, we propose a new cosmological model. In the framework of this cosmological model, the three-dimensional space is generated by its sub-spaces of lower dimensions. So forth this cosmological model and the process generating the spaces are described in detail.

The cosmological model of the Universe

The topological approaches described in Alexandrov's *Combinatorial Topology* [1] are used here to introduce the new cosmological model of the Universe. So we have:

R^{-1} — a space, which dimension is -1 that means a lack of space;

R^0 — a space of zero dimension means a space of energy, which is similar to energy of a quark;

R^1 — a space, which dimension is 1, means a space of electric energy;

R^2 — a space, which dimension is 2, means a space of magnetic energy;

R^3 — a space, which dimension is 3, means a space of gravitational energy (the "weight space");

R^1 , R^2 and R^3 — Euclidean spaces. Dimension of such a space is the number of freedom degrees of a material point located therein.

The process generating the aforementioned topological spaces is as follows.

The space R^0 . As a result of inflation [2] as symmetrization, an R^{-1} space generates an R^0 space. The space R^0 is not Euclidean. Each object located in a space contains a part of the total energy of the space. As such one, the space R^0 contains two groups of symmetric objects. The additive energy of objects located in the space is zero. Interaction between objects of one group is proportional to their distance from each other. Objects of the space R^0 uniquely define this space itself. Hence, the space R^0 is a space of quark-like energy.

Distances between the objects is determined by the difference in energies of these objects. Time is a factor of evolution of the space. This evolution factor (time) is manifested in the redistribution of energy between the objects, and in the change in the objects' number in this space (i.e. transition from one state of the space into another state of the space). When interaction between the objects of the space reached symmetry, time disappears. In this case, the space R^0 arrives at a singular state. As is known, a space is identical to a specific type of energy. Quark-like energy is identical to the space R^0 . So, quark-like energy and generates the space R^0 .

The space R^1 . Due to symmetrization of the singularity of the space R^0 , synthesis of two objects which are attributed to two different groups of the space R^0 generates an object of a higher-dimensional space R^1 . This is a space of electric energy (see above). Thus the space of electric energy is generated. Objects of the space R^1 are charges. The numerical value of such a charge is equal to the modulus of the energy difference of two objects attributed to the space R^0 . Interaction between two charges is proportional to the multiplying result of their numerical values. Time in the space R^1 is determined by transformation of energy of the space R^0 into electric energy. The space R^1 evolves from the space R^0 to the singularity state. Singularity of a space is another space in which time is absent. So, after the entire energy of the space R^0 is transformed into electric energy, time disappears. Energy of each single charge is unlimitedly and continuously distributed along the space R^1 according to the interaction.

The space R^2 . Due to symmetrization of the singularity state of the space R^1 , charges in the space are separated from each other by the sign of difference of the objects attributed to the groups of the space R^0 . The groups of charges differ by their signs. Synthesis of two charges bearing different signs generates an object of a higher-dimensional space R^2 (a space of magnetic energy, see above). Thus the space of magnetic energy is generated.

Consider the generation process by the example of a single photon. The photon is a result of synthesis of two charges bearing different signs (the space R^1), which are equal in their absolute values. The photon energy is continuously and unlimitedly distributed along the space R^2 . Interaction between two photons is inversely proportional to the distance between

them, and is proportional to the product of their energies. A single photon is an object of the magnetic energy space R^2 . Objects in the space R^2 have the rotational degree of freedom (the spin).

The space R^2 evolves from the singularity state of the space R^1 to its own state of singularity. After converting electrical energy into magnetic energy, the space R^2 arrives at its own singularity state: time disappears in the space.

The space R^3 . As a result of symmetrization of the singularity state of R^2 , objects of the space are separated by the rotational degree of freedom (the spin). Synthesis of two objects, which are located in the space R^2 and bear oppositely directed spins, generates an object of a higher-dimensional space R^3 (a space of gravitational energy, see above). Thus the space of gravitational energy, R^3 , is generated. Objects of the space R^3 are composed of objects of the spaces which dimensions are 1 and 2. The mass of objects of R^3 is continuously and unlimitedly distributed along the space.

Evolution of the space R^3

At present, the process converting magnetic energy of the space R^2 into gravitational energy of the space R^3 is in progress. We suggest to refer magnetic energy of the space R^2 as dark energy (the vacuum-like substance according to Gliner [3,4]). In these terms, mass (gravitational energy) is represented by matter and dark matter. Dark matter is a result of conversion of the magnetic energy into the gravitational energy. In the process of evolution of the space R^3 , the shared part of the gravitational energy increases. This leads to slowing the clock down in this space. The process of passage of light in a space is analogous to the process of registration of time by a clock. The speed of light in this case is the conversion factor of the length in a duration of time. This coefficient is a constant of the space R^3 . The process of passage of light in the space R^3 is the process of motion of a photon in the space R^2 . In the space R^3 , there are regions of absorption and emission of the photon. The photon's trajectory in the space R^2 is mapped into the region of its registration in the space R^3 in the relation "one-to-many". Thus the photon is tunneling in the space R^3 . With the increase in the mass fraction in space, the redshift effect arises: a clock slow down with the process of passage of light. Density of the gravitational energy of the space R^3 depends on the speed of light. The energy density of a space, reduced to time duration, is a constant value [5]: $d_t c_t^{r-1} = const$, where d_t is the density of matter at a given point of the space; c_t is the speed of light (the speed of time) at the given point of the space; r is the dimension of the space at the given point.

Matter in a space of a fractional dimension

Consider how we percept the space of our world. At present, the space is three-dimensional: three spatial coordinates with triangulation of three dimensions are required. The fourth

coordinate is time. In this case, the qualitative difference between the coordinate of time and the coordinates of space is emphasized. It is suggested that there exists an infinite set of three-dimensional spaces. However, under certain conditions (such as that the light speed in vacuum is constant), the time coordinate can be expressed in terms of linear length and vice versa. This allows us to assume that the time coordinate and the space coordinates have the same nature. In this case, the question about the infinite set of three-dimensional spaces does not vanish. On the basis of the above, we consider the problem of generation of spaces in the framework of the theory of topology sets.

Consider metric spaces R^n . In accordance with [1], an empty set has a dimension of $n = -1$. A set R^0 containing only one point X_i has a dimension of $n = 0$. To go to a higher dimensional space, it is necessary to perform a continuous mapping of one point $X_i \in R^0$ into a continuous set of points $X \subseteq R^1$. Here are two ways to display the sequence: 1) in the form of the ε -displacement (see §1.1 of Chapter 6 in [1]), where the continuity sequence of the subsequent point from the previous one is observed; and 2) the transfer method, where this condition is not satisfied. Introducing the notion of a sequence maps, we thereby define the time factor. Here the time factor determines the process generating a space with a higher dimension from a space of a lower dimension. Using only the shift method to generate a space gives a set that has a beginning, i.e. the starting point of reference. To exclude the starting point of reference, it is necessary to use, at least once, the transfer method. To generate all points of the set R^1 , an infinite set of steps (an infinite amount of time) is required.

Time is a quantitative characteristic of the displayed space. Introducing the time factor is equivalent to introducing a characteristic of the density of the mapping flow — the speed of time. By the speed of time, we understand the ratio of the number of displayed points of a higher dimension space to the number of points of a space of a smaller (than that generated these points) dimension. This determines the multiplicity: how many points of the higher dimension space is displayed by one point of the lower dimension space. The instant fulfillment of the mapping (the multiplicity is infinite) is identical to the infinite speed of time, which in all cases is dimensionless. Hence, the complete numerical axis (line) in the set attributed to the metric space R^1 can be obtained by instant mapping one point $X_i \in R^0$ into a continuous set of points $X \subseteq R^1$ using two methods: the shift and carry methods.

In this case, metric spaces with an integer dimension can be represented as spaces with the zero time speed (that means that time is absent — there is no generation process, the number of displayed points is zero). The Hilbert space can be decomposed into an infinite number of metric spaces of a finite dimension (see §2.4 of Chapter 1 in [1]), and the following relation is fulfilled: $R^{n-1} \subseteq R^n$. And the cardinality of the set $\{R^{n-1}\}$ is equal to infinity: $|\{R^{n-1}\}| = \infty$. This assumes that the speed of time is infinite when creating a space,

in which n is an integer, from a space of a lower dimension. Under the condition that the complete covering of R^n is not fulfilled (the speed of time is finite), the covered subset of R^n can be represented by a space R^d having a dimension d , where $(n - 1) \leq rd \leq n$, i.e. a space with a fractional dimension. It is proposed to define spaces, in which the speed of time is finite and differs from zero, as fraction-dimensional spaces. The time speed function depends on the numerical value of the space dimension, which is a real number. It monotonically decreases within the interval of dimensions $(n - 1) < d < n$, see Fig. 1 below.

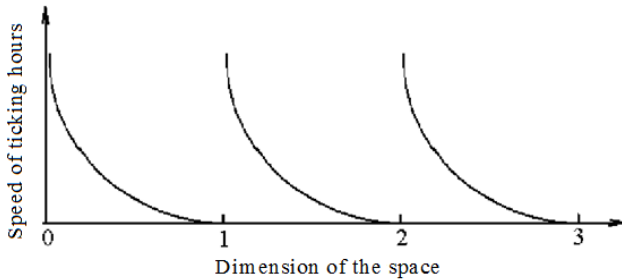


Fig. 1: The time speed of fraction-dimensional spaces.

The characteristic of the speed of time in the regions of our space is the speed of light. In this case, the distance from the point of radiation to the absorption point of a photon matches with the respective time duration registered by a remote clock. For example, the speed of light registered by our clock in this way on the boundary of the Universe exceeds the speed of light registered in our region of the space. When the numerical value of the time coordinate is reduced (with the respective numerical values the spatial coordinates) to the same measurement units, the magnitude of the speed of light is also dimensionless. Analysis of the speed of light in vacuum and material media shows that with the increasing density of matter the speed of light decreases. Reduction of the speed of light is accompanied by an increase in the dimension of space, see Fig. 1. This allows us to use the numerical value of the space dimension as the energy characteristic of the space. The density of matter has an inverse relation to the speed of time within an integer interval of the space dimension, see Fig. 2 below.

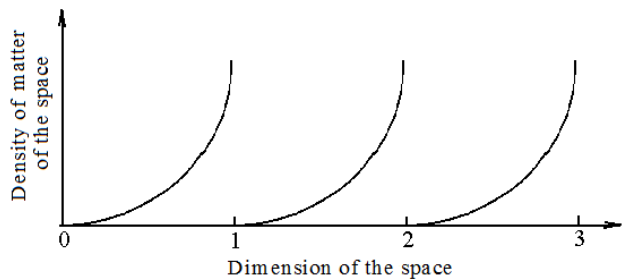


Fig. 2: The energy density of a fraction-dimensional space.

The boundary on the left of the fractional dimension (to an integer value of the space dimension) gives an infinite set of $(n - 1)$ -dimensional spaces having zero energy density. The boundary on the right is an n -dimensional space with an infinite density of matter, see Fig. 2. In this case, two versions representing a fraction-dimensional space are possible:

1. The space of an integer dimension R^{n-1} with the inclusions (domains or points and their neighborhoods, the set K) wherein the space is fraction-dimensional;
2. The space R_t^{n-1} containing the set S of points, each of which is a space of an integer dimension, and where covering Π by the set S of the space R_t^{n-1} is incomplete.

The first assumes that there exists a single integer-dimensional space containing a set of inclusions. The second — a set of integer-dimensional spaces. The latter is impossible under the previously stated assumption that an integer space contains infinite dense matter or is a continuum of integer spaces of lower dimensions. It is more preferable to assume that at all points of S we have the same space, but for each matter density d (time speed) the respective subset of points of this space is R_d^{n-1} . These subsets do not intersect with each other:

$$\bigcup R_{di}^{n-1} \cap R_{dj}^{n-1} = \emptyset, \quad \forall i \neq j; i, j = 1, 2, \dots \infty.$$

All this is equivalent to the fact that each point of the space has one numerical value of the matter density parameter, i.e.

$$R^{n-1} \cap \bigcup R_{di}^{n-1} = R^{n-1}, \quad i = 1, 2, \dots \infty.$$

In the case, where is a chain of the sets of points with zero numerical value of the matter density, interaction between the points at the ends of this chain occurs without time i.e. instantly (the speed of time is infinite there). However, the density of matter at each point of this chain is zero in this case as well as the space dimension of this set R^n . This is limiting and unreachable by definition. Moreover, the set R_d^{n-1} is uniquely mapped into one point of the space R_t^{n-1} . This implies the continuity of the mapping of R^{n-1} into R_t^{n-1} . The region of the set R_t^{n-1} , for given numerical values of d , belongs to the set of positive values of the numerical axis. Boundary of this region is the set of points in which the matter density of the space (i.e. the speed of time) is not defined. This corresponds to whole-dimensional spaces in which the time factor is absent. Suppose that the covering of Π remains unchanged. Corresponding to this covering, the average fractional dimension is $m_d = M[d] = const$. The numerical characteristic of the coating, in turn, is proportional to m_d . If density of the coating is $d_{\Pi} = f(\Pi)$, then $m_d = d_{\Pi}$. From here, in a fraction-dimensional space, two time processes are possible:

1. The process of convergence of points of the set $S \subset R_t^{n-1}$ with each other upto coincidence (absorption), which makes possible to equalize the matter density throughout the entire space R^{n-1} ;

2. The process inverse to the convergence of points. Separation of one point into at least two points.

These two processes compete and provide a mapping of K into S , previously considered in two ways: the shift and carry methods. Due to the shift and transfer of points of the set R_t^{n-1} , mutual absorption of the points is possible. This should be accompanied with the reverse: the generation of points. This condition ensures that the covering of the same set R_t^{n-1} — the conservation law of the dimension (covering) of the space — remains constant. On the other hand, the covering Π is incomplete, but ensures the mapping S into the range of possible numerical values of the set R_t^{n-1} , — the positive numerical axis. This mapping is also determined by the fractional dimension through the time flow, and determines dynamics of the interaction processes of points of the set $K = \{R_d^{n-1}\}$ with each other. Therefore, **the space of a fractional dimension is dynamic**. The point of the set R_t^{n-1} corresponds to R_d^{n-1} — the set of points with the same density of matter of the space R^{n-1} . That is, in the absence of interaction with the remaining points, its position is determined only upto the set R_d^{n-1} . In this case, the point of the latter can be defined (perhaps) simultaneously at all points of R_d^{n-1} . That is, each such point has no distinctive features over the others. In the case of absorption (synthesis), it is possible and necessary to generate (divide) points of the spaces R_t^{n-1} and K . This is a necessary condition for generating a space (i.e. transfer). On the other hand, at a sufficiently high density of matter in the localization region of the point, the time speed is sufficiently small: displacement or transfer in this case almost does not require time. This also gives rise to the effect of supposedly simultaneous finding of one point in all places (points) of the localization region.

Results

Spaces of fractional dimensions contain local inhomogeneities in which the fractional dimension of the space differs from the fractional dimension of the vacuum region (which is the neighborhood of the inhomogeneity, the localization space). These are material objects. A local inhomogeneity is manifested in the numerical values of the parameters of the fields of a material object. The numerical values of the field parameters show the energy distribution of the space in the object's localization region. Combinations of the fields as the distribution characteristics of energies of the space give a description to the whole variety of the material objects. Degeneration of a fraction-dimensional space in the part of material objects leads to the appearance of zero-dimensional parameters that is quantum numbers. This quantum mechanism determines the discreteness of the set of phenomena there. A space with a unit inhomogeneity is an integer (for example, the three-dimensional space) everywhere, except for the heterogeneity itself. For an observer, it turns into a point because transition from one point to another does not require

time. The very region of heterogeneity is a point at which the density of matter is infinite high. Passage through this point requires an infinite amount of time. Such a point is limiting, boundary, open, that is unreachable. Another boundary, with a uniform density of matter throughout the space, is also unreachable. Hence, we have an open interval for describing the entire set of material objects in a fraction-dimensional space.

Conclusion

So, a model of the cosmological system of spaces is proposed here. When considering this model, evolution of the Universe is discussed as well as the problem of description of fraction-dimensional spaces. Such spaces are defined as a results of energy conversion from the moment of inflation to R^3 . The concept of singularity as a space in which time is absent is proposed. A “fractional space” is defined as a space in which the process of energy conversion from one type to another takes place. In this case, time is a factor of the process of energy conversion. Dynamics of fraction-dimensional spaces is predicted. These research results are a basis to calculate numerical values of the characteristics of such spaces.

Acknowledgements

I am thankful to Svyatoslav Petrovich Gabuda (April 23, 1936 — April 7, 2015), a Soviet/Russian physicist, Professor and Doctor of Physical and Mathematical Sciences, for valuable discussions.

Submitted on April 17, 2018

References

1. Alexandrov P.S. Combinatorial Topology. Volumes 1, 2, and 3 bound as one. Mineola (NY), Dover Publications, 1998 (reprinted from the 1957, 1959, and 1960 editions).
2. Linde A. Particle Physics and Inflationary Cosmology. Chur (Switzerland), Harwood Academic Publishers, 1990; arXiv: hep-th/0503203, p. 1–6.
3. Gliner E.B. The vacuum-like state of a medium and Friedman cosmology. *Soviet Physics Doklady*, 1970, v. 15, no. 6, 559–561.
4. Gliner E.B. Algebraic properties of the energy-momentum tensor and vacuum-like states of matter. *Soviet Physics JETP*, 1966, v. 22, no. 2, 378–382.
5. Mashkin M.N. Matter in a space of a fractional dimension (*in Russian*) <http://www.sciteclibrary.ru/rus/catalog/pages/6525.html>

Calculation of the Density of Vacuum Matter, the Speed of Time and the Space Dimension

Mikhail N. Mashkin

E-mail: mnmashkin@yandex.ru

An example of calculating the density of vacuum matter is presented based on the hypothesis of fractional dimension of our space. The speed of time and the dimension of our space are calculated.

Introduction

In the previous paper [1], we showed the hypothesis that the reduced density of space energy is constant:

$$d_t c_t^{r-1} = const, \tag{1}$$

where d_t is the density of matter (substance) at a given point in the space; c_t is the speed of light (proportional to the speed of time) at the given point in the space; r is the dimension of the space at the given point.

The previous analysis of this hypothesis showed that this formula exactly coincides with the topological thickness of the space with a non-integer dimension value, i.e.,

$$M = X Y Z^{r-2}, \tag{2}$$

where X, Y, Z are equivalent sets. Their permutations do not change the result of their Cartesian product.

Calculation of the numerical value of r can be performed based on the definition of fractional dimension, as a property of self-similar objects (fractional dimension is a dimension in the form of a fraction, for example, 23900/10000).

In our case, self-similar objects are convex bodies in n -dimensional spaces, for example, in the three-dimensional Euclidean space.

We will use a volume relative increase as an increment that provides fractional dimension (non-integer dimension). This is due to the alleged expansion of space, which is determined by the Hubble constant*.

When moving at a measured distance in seconds, assuming that the speed of light in vacuum is constant, we obtain the value of the Hubble constant in units of acceleration:

$$\begin{aligned} H_a = H c_v &= \frac{(55 \div 75) \times 10^3 \times 3 \times 10^8}{3.086 \times 10^{22}} = \\ &= (5.35 \div 7.29) \times 10^{-10} \text{ m/s}^2, \end{aligned} \tag{3}$$

where c_v is the speed of light in vacuum.

Let us take a ball with a single radius equal to 1 second, i.e. 3×10^8 m as a basis for calculating the initial volume of a convex body. Further we will call the radius as a unit length.

*The Hubble constant is defined currently within $H = 55 \div 75$ km/(s Megaparsec).

As a time interval for comparison, we will select the time of transmission of a signal at a distance of the unit length, i.e. the time of 1 s.

As an increment, we will determine the increment of the initial volume v_1 during the passage of the signal at a distance of the unit length, see Fig. 1.

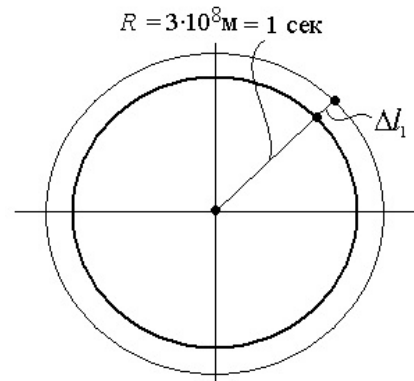


Fig. 1: A ball with a radius of a unit length.

In this case, the increment of the unit length is equal to:

$$\begin{aligned} \Delta l_1 &= \frac{\int_1^2 H_a t dt}{c_v} = \frac{1.5 H_a}{c_v} = \frac{1.5 \times (5.35 \div 7.29) \times 10^{-10}}{3 \times 10^8} = \\ &= (2.68 \div 3.65) \times 10^{-18} \text{ s}. \end{aligned} \tag{4}$$

The relative increment is the ratio of the increment to the finite length:

$$\Delta r_1 = \frac{\Delta l_1}{1 + \Delta l_1} \approx (2.68 \div 3.65) \times 10^{-18}. \tag{5}$$

The relative increment of the initial volume v_1 is equal to:

$$\Delta v_1 \approx 3 \Delta r_1 = (8.04 \div 10.95) \times 10^{-18} \approx 10^{-17}. \tag{6}$$

When the numerical value of r equals 3, the dimension of the constant in formula (1) is equal to

$$\frac{[\text{kg}][\text{m}]^2}{[\text{m}]^3[\text{s}]^2} = \frac{[\text{kg}]}{[\text{m}][\text{s}]^2}$$

or $L^{-1} M T^{-2}$, i.e. Pascal.

Hence, this can be interpreted as the modulus of the volume compression/expansion of the three-dimensional space.

In case when $3 > r > 2$, we will refer to the reviewed constant to as the module of the extension of a non-integer dimension space.

Then the formula (1) can be represented in the form of:

$$d_t c_t^{r-1} = M_r, \tag{7}$$

where M_r is the module of the expansion of the space of non-integer dimension, taken in Pascals.

Calculation of the density of vacuum matter

Using the ratio (7), we can calculate the density of vacuum matter. With this, it is possible to accept in first approximation the vacuum density inside material bodies as that equal to the density of their substance.

Let us take the following approximations: the space dimension is constant, i.e. $r = const$, and is $r \approx 3$; the effects of light dispersion are not taken into account.

Formula (1) contains three interrelated parameters: density, the speed of light and the space dimension. Consider the relationship between the speed of light and the matter density in detail. The table data of the refractive index (optical density) and the density of precious stones are shown in Fig. 2.

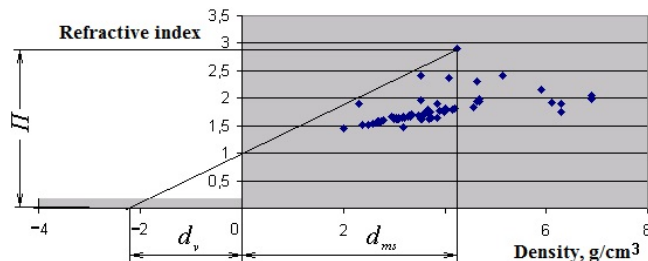


Fig. 2: The precious stones density.

Analysis of Fig. 2 allows us to suggest that the refractive index is linearly dependent on the matter density. Hence, we obtain the formula of the vacuum matter density outside material bodies:

$$d_v = \frac{d_{ms}}{\Pi - 1}, \tag{8}$$

where d_{ms} is the density of substance, $\Pi = c_v/c_{ms}$ is the refractive index, c_{ms} is the speed of light in the substance.

Here are the tabular data of the stones, used in jewelry industry. The data give the minimum of the calculated density of vacuum for diamonds and synthetic rutile (see Table for detail).

In the above calculations, we used the average density of substance. However, under real conditions inside real substances there are nodes of the crystal lattice in the form of ions or atoms which have a finite volume and their own density. For example, for a diamond we have the radius of the

The group of stones	Stone	Density, g/cm ³	Refract. index	Calc. vacuum density, g/cm ³
Colorless stones	Diamond	3.52	2.42	2.48
	Synthetic rutile	4.25	2.9	2.24

carbon atom $r_a = 0.077$, and the distance between the reflection planes (interatomic) $d = 0.356$ nm. Hence, the density of the carbon atom itself is $6,274$ g/cm³. Let us calculate the maximum reduced density between two carbon atoms located from each other at a distance d using the following formula:

$$d_{red.} = \frac{m_c}{V_{c_1}} + \frac{m_c}{V_{c_2}}, \tag{9}$$

where $V_{c_1} = \frac{4\pi}{3} r_1^3$ is the volume of a sphere with the first carbon atom in the center, $r_1 = 0.0385 \div 0.3165$ nm, $V_{c_2} = \frac{4\pi}{3} (0.356 - r_1)^3$ is the volume of a sphere with the second carbon atom in the center, m_c is the mass of the carbon atom.

Calculation by formula (9) shows that approximately 50% of the space between carbon atoms has a density of about 1 g/cm³. Hence, the estimated density of vacuum substance obtained by formula (8) is less than 0.7 g/cm³. The actual numerical value, obviously, is much lower, since the reduced density assumes uniform distribution of the substance of the carbon atom within the sphere.

Calculation of the space dimension and the speed of time

On the other hand, it follows from the definition of fractional dimension of space, that any volume of a space generates a volume in a certain multiplicity, which is equal to the speed of time [1]. For vacuum it is:

$$dt \approx \Delta t = \Delta v_1 = 10^{-17}, \tag{10}$$

i.e. any volume of a space, when a signal passes through it, generates a relative, additional volume equal to the speed of time.

The generation of the volume corresponds to a certain amount of gravitational energy. This amount can be compared to a quantum of energy which, taking into account formula (10), gives the ratio:

$$M_r V_1 dt = h, \tag{11}$$

where V_1 is the generated unit volume, 1 m^3 , h is the Planck constant (6.626×10^{-34} J s).

Our three-dimensional space is flat. The critical Friedman density of our space is about $d_f = 1 \times 10^{-28}$ kg/m³. From here, we calculate the dimension of our space:

$$r = \frac{\log h - \log V_1 - \log d_f - \log dt}{\log c_v} + 1 = \frac{\log 6.626 - 34 - 0 + 28 + 17}{8 + \log 3} + 1 = 2.395; \tag{12}$$

where $c_t \simeq c_v = 3 \cdot 10^8$ m/s; $d_f = d_t = 10^{-28}$ kg/m³; $V_1 = 1$ m³; $dt = 10^{-17}$.

If the space has a Friedman energy density, the photon speed in the region of the carbon atom is (on the average):

$$c_c = \sqrt{\frac{d_f}{d_c}} c_v = \sqrt{\frac{1 \times 10^{-28}}{6274}} c_v = 1.26 \times 10^{-16} \times 3 \times 10^8 = 37.9 \text{ nm/s}, \quad (13)$$

where d_c is the average density of matter inside the sphere of a carbon atom.

At the obtained speed of light inside the sphere of the carbon atom, the wavelength of visible radiation is:

$$\lambda_c = 1.26 \times 10^{16} \lambda_{mv} = 1.26 \times 10^{-16} \times 600 \times 10^{-9} = 7.56 \times 10^{-23} \text{ m}, \quad (14)$$

where λ_{mv} is the wavelength of visible radiation. This is about 10^{13} times less than the diameter of a carbon atom. This gives a possibility of interaction between the waves of visible radiation and a carbon atom which is represented as a drain funnel (the source — reverse funnel — tornado). That is the **photon**, as an object of magnetic energy, behaves as a **time magnetic monopole**: it can be absorbed and emitted.

Results

Substantiation and calculation of the density of space matter have been done. The concept of the time speed has been specified. The time speed of our space has been calculated. A formula for calculating the fractional dimension of our space has been obtained. The calculation of the fractional dimension of our space has been performed.

So, on the basis of representation of the fractional dimension of a space as a space with the presence of time, the following calculations were done: the density of vacuum matter, the speed of time and the dimension of our space.

Further calculation of the numerical values of the following properties — the substance density of material objects, the vacuum and space density as a whole — can be continued dealing with (see [1] for detail): conversion of magnetic energy into dark matter; dark matter interaction with matter; synthesis of objects of our space; a three-dimensional model of distribution of density of the outer space mass.

Submitted on April 17, 2018

References

1. Mashkin M.N. Matter in a space of a fractional dimension. A cosmological system of spaces and evolution of the Universe. *Progress in Physics*, 2018, v.14, issue 3, 131–134.

Fully Classical Quantum Gravity

Thomas C. Andersen

NSCIR, 8 Bruce St. B 841, Thornbury, Ontario, N0H 2P0, Canada
E-mail: tandersen@nscir.ca

It's an experimental fact that quantum objects in the ground state do not radiate electromagnetic energy, but what are the limits on our knowledge of the gravitational equivalent of this? In semiclassical gravity it is the expectation values of quantum particle positions that form the source for the Einstein equations, thus a particle or atom in a ground state emits no gravitational radiation. Here we instead assume a fully classical quantum gravity — the internal components of objects in a pure quantum state are assumed to classically radiate gravitational waves. The effects of this theory of microscopic gravity on the measured properties of the hydrogen atom, along with possibilities to experimentally measure the effects of atomic or nuclear scale gravitational radiation are explored.

1 Introduction

The quantum gravity problem remains unsolved in physics today. There are many possible solutions proposed, but almost all of them suppose the existence of the graviton. The graviton should have the same energy relation as the photon:

$$E_{\text{graviton}} = \hbar\nu. \quad (1)$$

There not only exists no experimental confirmation of this relationship for gravity, it is also widely known that an experiment to detect a single graviton is well beyond the capabilities of any present or future realizable experiment. Gravity may simply be a non quantum effect. Rosenfeld in 1963 is still very much relevant [1].

There is no denying that, considering the universality of the quantum of action, it is very tempting to regard any classical theory as a limiting case to some quantal theory. In the absence of empirical evidence, however, this temptation should be resisted. The case for quantizing gravitation, in particular, far from being straightforward, appears very dubious on closer examination.

2 Other classical gravity theories

Semiclassical gravity can be summarized as a classical gravitational field coupled to quantum matter fields. While semiclassical gravity is widely thought of as a workable limiting approximation until a quantum theory of gravity is discovered, there are researchers who treat semiclassical gravity as a real possibility and hence in need of experimental tests [2]. The semiclassical equations for quantum gravity are as from Møller [3] and Rosenfeld [1]:

$$R_{\mu\nu} - \frac{1}{2}g_{\mu\nu}R = \frac{8\pi G}{c^4}\langle\Psi|T_{\mu\nu}|\Psi\rangle. \quad (2)$$

While seemingly straightforward, semiclassical gravity has subtleties, especially in determining the quantum expectation value (see Appendix A of Bahrami [4]).

Another classical treatment of quantum gravity comes from Roger Penrose with the *Gravitization of Quantum Mechanics* [5] where he posits that gravity connects not to the expectation value, but rather directly to each superposed quantum state. Gravitation causes collapse as the gravitational field of multiple superposed states becomes too energetic.

3 Fully classical quantum gravity

Fully classical quantum gravity (FCQG) uses Einstein's equations as given,

$$R_{\mu\nu} - \frac{1}{2}g_{\mu\nu}R = \frac{8\pi G}{c^4}T_{\mu\nu} \quad (3)$$

with the coupling to microscopic matter being on some assumed sub-quantum level, where particle positions always have a definite value, as in for instance de Broglie-Bohm mechanics [6]. Of course if one uses Bohmian mechanics in its entirety, then gravitation is also quantized, and particles will not radiate from their ground states. We thus assume here that quantization does not apply to gravity at all, that particle trajectories are real and that they interact directly and classically using the laws of Einstein's general relativity. In many ways it is similar to the program of stochastic electrodynamics (SED) [7], in that classical fields couple directly to sub-quantum particle motions. Indeed if one is to assume a SED like explanation of quantum behaviour, then gravity should also be treated classically.

4 Gravitational radiation from atoms and nucleons

Ashtekar [8] for example elucidates the need for a quantum theory of gravity by citing Einstein in 1916:

...Nevertheless, due to the inner-atomic movement of electrons, atoms would have to ra-

diate not only electro-magnetic but also gravitational energy, if only in tiny amounts. As this is hardly true in Nature, it appears that quantum theory would have to modify not only Maxwellian electrodynamics, but also the new theory of gravitation.

Using instead Rosenfeld's position that we must rely on experiment to show the need for quantum gravity, consider the energy loss rate of a circa 1916 style Bohr planetary hydrogen atom in the ground state, using Eddington's [9] formula for the gravitational energy radiated by a two body system (in the approximation that one mass is much heavier):

$$\frac{dE}{dt}(\text{atom}) = -\frac{32Gm_e^2r_h^4\omega^6}{5c^5} = -10^{-43}\text{eV/s.} \quad (4)$$

Which even over the age of the universe amounts to an energy loss due to gravitational waves for a hydrogen atom in the ground state of only 10^{-25} eV. Why was Einstein worried about such a small rate of gravitational energy loss for a hydrogen atom? In contrast the electromagnetic lifetime of the classical hydrogen atom is about 10^{-11} s which of course helped lead to the discovery of quantum mechanics.

As a comparison to the above estimate, a quantum mechanical prediction of the lifetime of the $3_p - 1_s$ state for emitting a graviton is about 1.9×10^{39} s [10, 11], which is within a few orders of magnitude of the fully classical estimate above.

This energy loss is of no experimental significance. So we can conclude that the stability of atomic orbitals is not an experimental indication of a need for quantum gravity. In other words we cannot experimentally determine if atoms radiate gravitational waves continuously or not.

4.1 Gravitational radiation from within nuclei

The Sivram-Arun paper *Thermal Gravitational Waves* [12] is an expansion of Weinberg's results in his 1972 book [10]. Both calculate the gravitational wave (GW) emission from nuclei passing each other thermally in an astrophysical hot plasma (stars). In fully classical quantum gravity we make the additional assumption that gravitational waves are also produced by nucleon motion inside each individual nucleus, even in the ground state, greatly increasing GW emission and making it happen at any temperature, since it arises from internal nucleon movements within each nucleus. Calculating an estimate for the GW emission would depend on the model one uses for the nucleus. The Fermi gas model of the nucleus assumes that the nucleons are free to move inside the potential well of the nucleus. Since we are assuming that gravity is fully classical, we can use the same calculations as that of Weinberg and Sivram to arrive at an estimate of gravitational wave emission from nucleons inside nuclei.

4.2 A GW nuclear emission/absorption model

Taking the calculation of Weinberg to nuclear material, Sivaram finds a rate of 10^{-16} eV/s per neutron [12] (using their neutron star calculation). Fully classical quantum gravity would then suggest that the Sun emits about 10^{22} watts of 10^{22} Hz gravitational wave energy, as opposed to the 10^9 watts at a lower atomic frequency that Weinberg calculates from plasma conditions only.

Another way to arrive an estimate for GW emission in nuclei is to treat a nucleus as having several nucleons moving in it at some typical internal velocity. The speed of nucleons is given by their kinetic energy in the Fermi gas model with a peak momentum of about 250 MeV/c. Using only one pair of these peak energy nucleons and setting $r = 1$ fm, Eddington's formula for a bar of mass 2 nucleons, spinning at a nuclear 10^{23} Hz, predicts an emission rate of about 10^{-9} eV/s.

While these two approaches to calculate the GW emission of a nucleus in the fully classical model differ by several orders of magnitude, GW emission rates near these levels hint that such effects (or perhaps more likely a lack of effect) might be measurable in the lab.

Experiments might need to use differential absorption effects to arrive at results. Absorption models are harder to quantify, as the cross section estimate is quite uncertain due to unknown detailed information on particle substructure.

Within this fully classical quantum model each nucleon will have its own characteristic spectrum of nucleon-frequency gravitational waves, depending on the structure and size of the atomic nucleus. Experiments similar to those done to look for "big G" could use dissimilar materials for the masses whose force of attraction is to be measured. It's notable that experiments to determine Newton's constant G have had great difficulty obtaining consistent results. Most measurements of G do not agree with each other to within the errors carefully determined by the experimenters [13].

Another experimental avenue would be to search for GW interaction effects between the bulk of the earth and masses in a lab of dissimilar materials.

5 Emission/absorption parameter space

Fig. 1 is a sketch of allowed emission and absorption parameters. Some — but not all — combinations of emission and absorption parameters are ruled out by experiment. Towards the upper left of the image limited absorption combined with higher emission would mean that the stochastic background of gravitational waves would be too energetic, having for example energy greater than the baryonic mass in the universe. The phrase "stability of nuclei" refers to the experimental fact that nuclei live for billions of years. On the right a ruled out region exists where absorption cross sections are not physically likely. The top line shows a calculation for the gravitational wave emission rate of a proton due to parton (quark) motion. "Nuclear emission (high)" refers to the Eddington

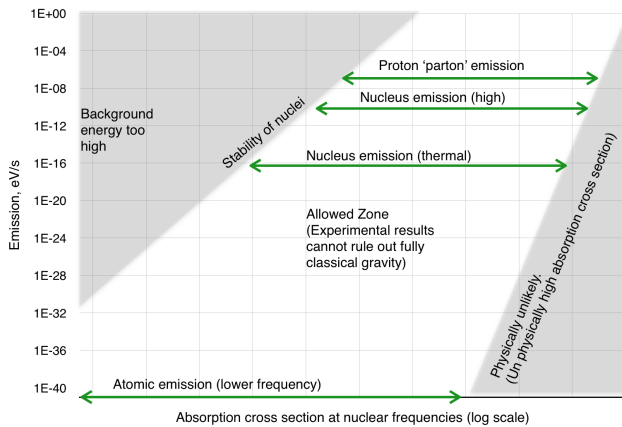


Fig. 1: Nuclear frequency gravitational wave emission and absorption. The elusive nature of gravitational wave detection means that even fully classical quantum gravity cannot be experimentally ruled out. The frequency of the gravitational waves is that of nucleons ($\omega \approx 10^{22}$ Hz).

emission rate for a heavy nucleus, while the lower nucleus emission rate is calculated assuming thermal Coulomb GW emission inside each nucleus.

6 Discussion

Due to the weak nature of gravitational effects on subatomic particles, even fully classical gravity cannot be experimentally ruled out at this time. Quantum gravity experiments that are possible with today's technology are very rare, this proposal represents an opportunity to test one of the tenants of quantum gravity.

Null results from experiments as described here will be able to constrain the allowed parameter space of a fully classical theory of microscopic gravity, thus suggesting that gravity needs to be quantized.

These tests are also a test of the ubiquity of quantum mechanics. With a non null result the conceptual foundations of quantum mechanics would be in question, as gravity might then be determined to be outside of the realm of quantum mechanics.

Submitted on April 1, 2018

References

1. Rosenfeld L. On Quantization of fields. *Nuclear Physics*, 1963, v. 40, 353–356.
2. Großardt A. Newtonian self-gravity in trapped quantum systems and experimental tests. arXiv:1702.04309 [quant-ph].
3. Møller C. Les theories relativistes de la gravitation. Colloques Internationaux CNRS, Paris, p. 91, 1962.
4. Bahrami M., Großardt A., Donadi S., and Bassi A. The Schrödinger Newton equation and its foundations. arXiv:1407.4370 [quant-ph], 2014.
5. Penrose R. On the Gravitization of Quantum Mechanics 1: Quantum State Reduction. *Found. Phys.*, 2014, v. 44, 557–575.
6. Bohm D. A suggested interpretation of the quantum theory in terms of "hidden" variables. I. *Physical Review*, 1952, v. 85(2), 166–179.
7. De la Peña L., Cetto A.M., and Hernández A.V. The Emerging Quantum, 2015.
8. Ashtekar A., Reuter M., and Rovelli C. From General Relativity to Quantum Gravity. arXiv:1408.4336 [gr-qc], 2014.
9. Eddington A.S. The Propagation of Gravitational Waves. *Proceedings of the Royal Society of London A: Mathematical, Physical and Engineering Sciences*, 1922, v. 102(716), 268–282.
10. Weinberg S. *Gravitation and cosmology : principles and applications of the general theory of relativity*. Wiley, 1972.
11. Boughn S. and Rothman T. Aspects of graviton detection: graviton emission and absorption by atomic hydrogen. *Classical and Quantum Gravity*, 2006, v. 23(20), 5839–5852.
12. Sivaram C. Thermal Gravitational Waves. arXiv:0708.3343, 2007.
13. Rosi G., Sorrentino F., Cacciapuoti L., Prevedelli M., and Tino G.M. Precision measurement of the Newtonian gravitational constant using cold atoms. *Nature*, 2014, v. 510(7506), 518–21.

Kirchhoff's Law of Thermal Emission: Blackbody and Cavity Radiation Reconsidered

Pierre-Marie Robitaille

Department of Radiology and Chemical Physics Program, The Ohio State University, Columbus, Ohio 43210, USA.
E-mail: robitaille.1@osu.edu

Kirchhoff's law of thermal emission asserts that, given sufficient dimensions to neglect diffraction, the radiation contained within arbitrary cavities must always be black, or normal, dependent only upon the frequency of observation and the temperature, while independent of the nature of the walls. In this regard, it is readily apparent that all cavities appear black at room temperature within the laboratory. However, two different causes are responsible: 1) cavities made from nearly ideal emitters self-generate the appropriate radiation, while 2) cavities made from nearly ideal reflectors are filled with radiation contained in their surroundings, completely independent of their own temperature. Unlike Kirchhoff's claims, it can be demonstrated that the radiation contained within a cavity is absolutely dependent on the nature of its walls. Real blackbodies can do work, converting any incoming radiation or heat to an emission profile corresponding to the Planckian spectrum associated with the temperature of their walls. Conversely, rigid cavities made from perfect reflectors cannot do work. The radiation they contain will not be black but, rather, will reflect any radiation which was previously incident from the surroundings in a manner independent of the temperature of their walls.

1 Introduction

Kirchhoff's law of thermal emission was formulated in 1859 [1, 2]. It is often presented as stating that, at thermal equilibrium, the emissivity of an object, ϵ_v , is equal its absorptivity, α_v . However, this should properly be considered as 'the law of equivalence', first proposed by Balfour Stewart [3] in 1858.

Kirchhoff's law extended much beyond Stewart's [3] and stated that, given thermal equilibrium, the radiation contained within an arbitrary cavity was depended only on the temperature of the enclosure and on the frequency of observation [1, 2]. Such radiation was completely independent of the nature of the walls [1, 2]. It was because of Kirchhoff's law that blackbody, or normal, radiation has always been viewed as independent of the lattice and unlinked to a physical cause [4]. Clearly, if Kirchhoff was correct and blackbody radiation was independent of the nature the walls, then such radiation could not be ascribed causality in the emitting structure.

Yet, it has been known for over 200 years that the radiation emitted from objects was highly variable [5]. In 1804, Leslie reported that the emission of surfaces depended on their nature and established the primacy of lampblack as a blackbody surface [6]. As a result, lampblack or soot, along with graphite, soon gained a dominant role in the construction of laboratory blackbodies (see [7] and references contained therein). The nature of the surface producing a thermal spectrum clearly did matter, in stark contrast to Kirchhoff's claims relative to cavity radiation [1, 2].

In the early 19th century, blackbodies were simply objects made from graphite or coated with materials such as soot and lampblack. Carbon black was also employed, a pigment used

in paints since pre-historic times [8]. Eventually, blackbodies became increasingly sophisticated devices, typically cavities. Other good absorbers of radiation slowly moved onto the scene relative to the construction of laboratory blackbodies [9–11], but graphite, soot, and carbon black retained their pre-eminent role [12]. Max Planck soon benefited from the construction of advanced cavities [9–11], when he formulated the blackbody solution [13, 14]. Contrary to Kirchhoff law [1, 2] the nature of the walls was thereby proven to be important on a practical level. It governed the quality of a blackbody. The quest for ever blacker surfaces [15–22] has now turned to novel structural absorbance approaches guided by samples as diverse as butterflies [23, 24] and birds [25]. Yet still today, many blackbodies in national laboratories are based upon the use of graphite (e.g. [26, 27]).

It remains true that blackbodies are specialized cavities which depend entirely on the nature of their walls [7, 9–12, 26, 27]. Laboratory blackbodies are made from materials that have an elevated emissivity over the range of interest, as is widely known throughout metrology. This fact alone is sufficient to illustrate that Kirchhoff's law cannot be valid.

As such, it is surprising that many still believe that any arbitrary cavity can produce a blackbody spectrum. In the laboratory, this was never the case. Planck himself [13] was dependent on the work of leading scientists in order to obtain a spectrum with the blackbody frequency distribution [9–11]. If Kirchhoff law had been correct [1, 2], this should not have been necessary.

The author has previously stated that Kirchhoff's law was not valid (see [4, 7, 12] and references therein), as it has no proper theoretical [28] or experimental proof. Planck's equa-

tion [13, 14] remained unlinked to a physical mechanism [4] because of Kirchhoff's law [1, 2]. As a result, physics was prevented from accounting for the production of a thermal photon from a simple cavity made from a block of graphite. Blackbody radiation remained, according to Kirchhoff, independent of the nature of the walls [1, 2]. In this respect, Planck's equation [13] was unique in spectroscopy. This has enabled scientists, in disciplines other than condensed matter physics, to infer that thermal photons could be produced without having recourse to a physical lattice, as was clearly required when emitted from graphite [4]. This has also enabled Max Planck to claim that his equation had universal significance [14, §164]. But in reality, Planck's solution was strictly limited to actual blackbodies (e.g. [7, 9–11, 26, 27]) and not to all cavities.

Thus, cavity radiation is reconsidered herein as to refute Kirchhoff's law [1, 2] and place a proper perspective on cavity radiation. In order to do so, cavities were constructed from materials which acted as nearly perfect absorbers or reflectors of radiation in the infrared. The results are discussed in terms of the work required to convert incident energy into normal radiation within the blackbody cavity. Conversely, the existence of nearly perfectly reflecting cavities is discussed in the context of resonant cavities used in magnetic resonance imaging [29], microwave cavities [30, 31], and lasers [32]. The findings demonstrate that cavity radiation is absolutely dependent on the nature of the walls. Consequently, Kirchhoff's law was never valid [4, 7, 12] and Planck's equation is not universal, as confirmed by a wide array of experimental results [29–32].

For the sake of brevity, the challenge to Kirchhoff's law presented herein can be limited to the study of a single approach without any loss in content. In 1954, de Vos published his *Evaluation of the Quality of a Blackbody* in the journal *Physica* [33]. This article has become a classic in blackbody radiation. de Vos [33] examined the quality of cavities constructed from materials with varying emissivity by noting the change upon incident radiation. This radiation was allowed to enter a cavity, exit, and be monitored with a detector placed at various angles. For cylindrical cavities, de Vos was concerned with the ratio of the length of the cavity to its diameter. He demonstrated that the radiation within cavities appeared to become increasingly isotropic as this ratio was increased [33]. However, de Vos had not demonstrated that all cavities will be black, independent of incident radiation. In fact, de Vos was concerned with the degree to which the surface of the cavity was either specular or white [33]. He did not evaluate whether a cavity could actually emit photons at the correct temperature. Thus, his work provided only limited insight into blackbody radiation [33]. He did analyze to what extent the surface property of a cavity affected the change of incoming light into fully diffuse reflection [33]. However, if a cavity was not constructed of a near ideal absorber, it was not necessarily black unless it was able to receive the proper

incident radiation from its surroundings.

At the same time, if a cylindrical hole of sufficient depth was placed in a material with an elevated emissivity, the findings from de Vos suggest that the resulting cavity should indeed be black [33]. This approach was therefore implemented in this work in order to construct a simple blackbody cavity from small blocks of graphite. In parallel fashion, nearly perfectly reflecting cavities were constructed from blocks of brass, copper, and aluminum.

2 Materials and methods

Infrared images were obtained using a CompactPro thermal imaging camera (Seek Thermal, Inc., Santa Barbara, CA 93117; Thermal.com) interfaced with an Android (version 4.4.2) cell phone, as shown in Fig. 1A.

The camera had a focusable lens and a 32° field of view. It was equipped with a 320×240 thermal sensor, had a temperature range of -40 to 330°C , and was capable of obtaining ei-

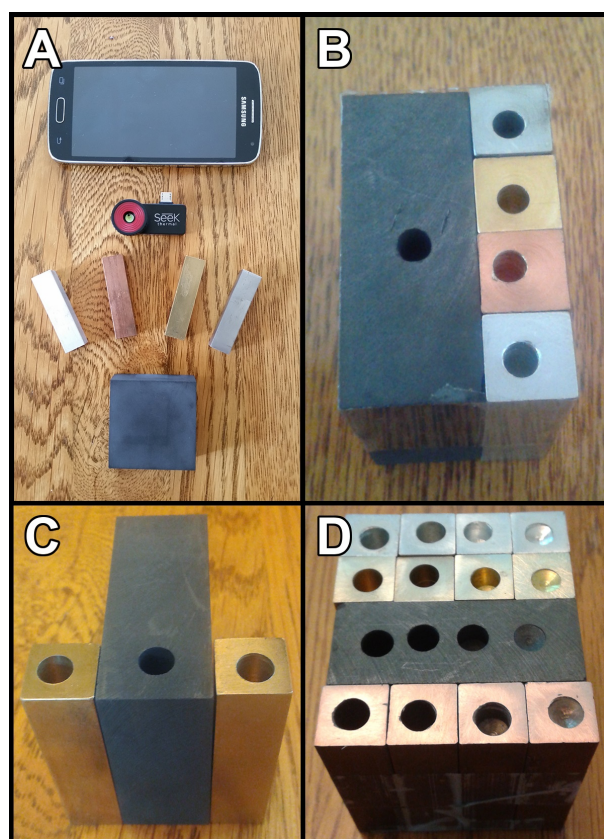


Fig. 1: A) Photograph of the Android phone, Seek Thermal camera, and aluminum, copper, brass, steel, and graphite blocks; B) Block assembly I (graphite on the left, then on the right from top to bottom: steel, brass, copper, aluminum). Note that two small scratches are visible near the graphite cavity. C) Block assembly II (brass, graphite, brass). D) Block assembly III (horizontal rows from top to bottom: aluminum, brass, graphite, copper).

ther still images or video. All images were obtained with the camera operating in white mode, except for Fig. 2A, where black mode was utilized.

Cylindrical cavities were constructed by drilling a small hole into $12.5 \times 12.5 \times 50$ mm blocks of copper, aluminum, brass, and steel (Specific Gravity Metal Blocks, EISCO, Haryana 133001, India). The expected emissivity of the copper, brass, and steel holes should be on the order of 0.03-0.1 [34]. The type of steel was unknown. A $20 \times 50 \times 50$ mm 99.9% Purity Graphite Ingot Block EDM Graphite Plate Milling Surface (Otoolworld, China) was used to build the reference blackbody using the same approach.

Cavities were produced with a drill press using either standard $\frac{3}{16}$ " or $\frac{1}{4}$ " diameter drill bits or a DeWalt Pilot Point $\frac{1}{4}$ " diameter drill bit to the depth described in the figure legends. Cavities were examined at room temperature or after having reached steady state while being heated on a hotplate (Cuisinart, East Windsor, NJ) to a temperature of approximately $\sim 304^\circ\text{C}$. Small graphite particles were made from 2 mm mechanical pencil refills (Menards, Eau Claire, WI) cut to a length of 0.5 cm and inserted into the cavities of interest.

Experiments were initiated at room temperature, by placing the camera at a distance of ~ 20 cm above the table surface and therefore ~ 15 cm above the surface of the block assembly. The eye of the camera was positioned directly over the center of this assembly. In order to document the effect of ambient radiation on the cavities, a galvanized steel rod was placed in an oven, heated to $\sim 232^\circ\text{C}$, and then brought near the cavities, as described in the figures.

3 Results

Thermal images are presented in Fig. 2 with the corresponding schematic representations outlining the position of the rod in Fig. 3. In Fig. 2A, a thermal image is presented in black mode, revealing that all the cavities appeared nearly the same at room temperature. In this image, there was also reflection of thermal radiation from the body of the observer onto the block assembly. Thus, on cursory examination, Kirchhoff's law appeared valid as all cavities essentially contained the same radiation. Still, the block was positioned within a room filled with radiation at the same temperature. Therefore, it was important to determine whether the cavities were generating radiation on their own or simply manifesting the radiation in their surroundings.

For other studies, the camera was switched to white mode and the cavities all appeared black, as seen in Fig. 2B. Next, in Fig. 2C-F (see schematics in Fig. 3C-F), a heated galvanized steel rod was placed above their surface. The rod had been heated to $\sim 232^\circ\text{C}$. In Fig. 2C, the rod was positioned to the right of the steel cavity (see schematic Fig. 3C). With the heated rod in this position, the graphite and steel cavities could not be filled with its radiation. These two remain pretty much as they were with just a tiny spec of reflection at

the graphite cavity. Thus, radiation from the rod was reaching this cavity as well, as expected. At the same time, the aluminum, copper, and brass cavities were immediately filled with radiation from the rod.

The rod was then moved to the left in Fig. 2D, as shown in Fig. 3D. Notice, once again, that there was no effect on the graphite cavity and that only a slight reflection was observed at the top of the steel cavity. However, all the others were filled with radiation from the rod. In particular, note the pattern in the brass cavity revealing that it was still not able to fully convert incoming radiation into isotropic ejected radiation. This indicated this cavity should be deeper to render the radiation fully isotropic, as suggested in de Vos' classic work [33].

In Fig. 2E, the rod was placed near the center of the block as represented in Fig. 3E. The three cavities from aluminum, copper and brass were again filled with rod radiation, but the graphite cavity remained unaffected and the steel cavity almost unaffected. However, reflection of rod radiation could be observed in the scratches on each side of the graphite cavity. As such, radiation from the rod was clearly reaching this cavity. Finally, in Fig. 2F, the rod was positioned just to the right of the steel cavity as shown in Fig. 3F. In this position, the steel cavity was no longer black. Now, it could be observed that rod radiation was able to partially fill the steel cavity. Nonetheless, the bottom of this cavity was darker, thereby indicating that steel had a much higher emissivity than the aluminum, copper, or brass cavities, but was not on par with graphite. The aluminum, copper, and brass cavities all appeared filled with radiation from the rod.

Next, the effect of inserting a small piece of graphite into the cavities was examined as shown in Fig. 4. In Fig. 4A (see schematic 4D), the graphite cavity was indistinguishable from the surface of the block at thermal equilibrium. Both cavities within the brass blocks were clearly visible.

When the heated steel rod was brought in close proximity to the cavities, its radiation was reflected off the surfaces and the signal to noise of the resulting image increased, as shown in Fig. 4B (schematic 4E). However, the central graphite cavity appeared black and both of the brass cavities became filled with rod radiation. This revealed that real blackbodies do work and convert any incident radiation to that corresponding to the temperature of their walls. Conversely, the two brass cavities on each side became filled with radiation originating from the steel rod. Again, the reflecting cavities were not black, as they manifested the radiation present in their surroundings in a manner independent of the temperature of their own walls. When the graphite particle was introduced into each of the cavities, it was unable to make the brass cavities fully black, as clear signs of radiation from the heated rod remained, as shown in Fig. 4C (schematic 4F).

Next, consider the findings from block assembly III, as displayed in Fig. 5. Initially, this assembly was monitored at room temperature, in equilibrium with its surroundings, as

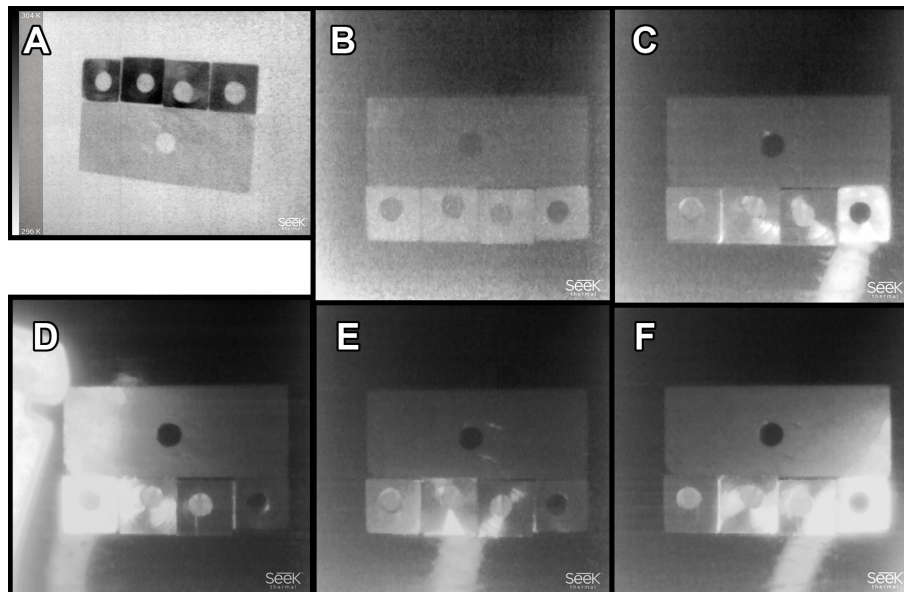


Fig. 2: A) Infrared image obtained from the Block Assembly I (see Fig. 1B) with the camera operating in black mode. For this image the camera was hand held. All the cavities were made using a standard $\frac{3}{16}$ " drill bit to a depth of 1" and appeared to contain the same radiation; B-F) Infrared images obtained from the block assembly with the camera in white mode. The lens of the camera was exactly 15 cm directly above the top of the block assembly or 20 cm above the top of the table. In these images, photons emitted from the heated rod and reflected prior to detection are observed as a white streaks on the images. B) The galvanized steel rod was not near the block assembly. Thermal radiation from the observer was likely to account for the good signal to noise on this image; C) The heated galvanized steel rod was placed on the right near the steel cavity; D) The heated galvanized steel rod was placed on the left side near the aluminum cavity. In this case, both the rod and its reflection are clearly visible; E) The heated galvanized steel rod was placed at the center of the block assembly. The two small scratches near the graphite cavity reflected radiation, demonstrating that radiation from the rod was reaching this cavity as well; F) The heated galvanized steel rod was placed just to the right of the steel cavity.

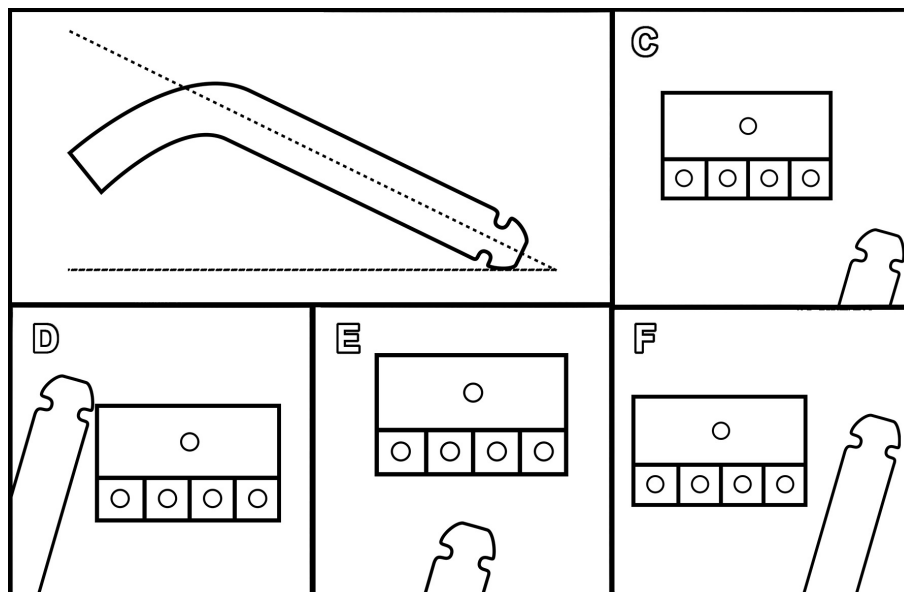


Fig. 3: Schematic representation illustrating the position of the heated rod relative to the block assembly. In the upper left, a vertical cross section is presented. For Fig. 2C-F, the rod was held using locking pliers at an angle of $\sim 25-30^\circ$ relative to the table. C-F) top view illustrating the rod position in Figs. 2C-F, respectively.

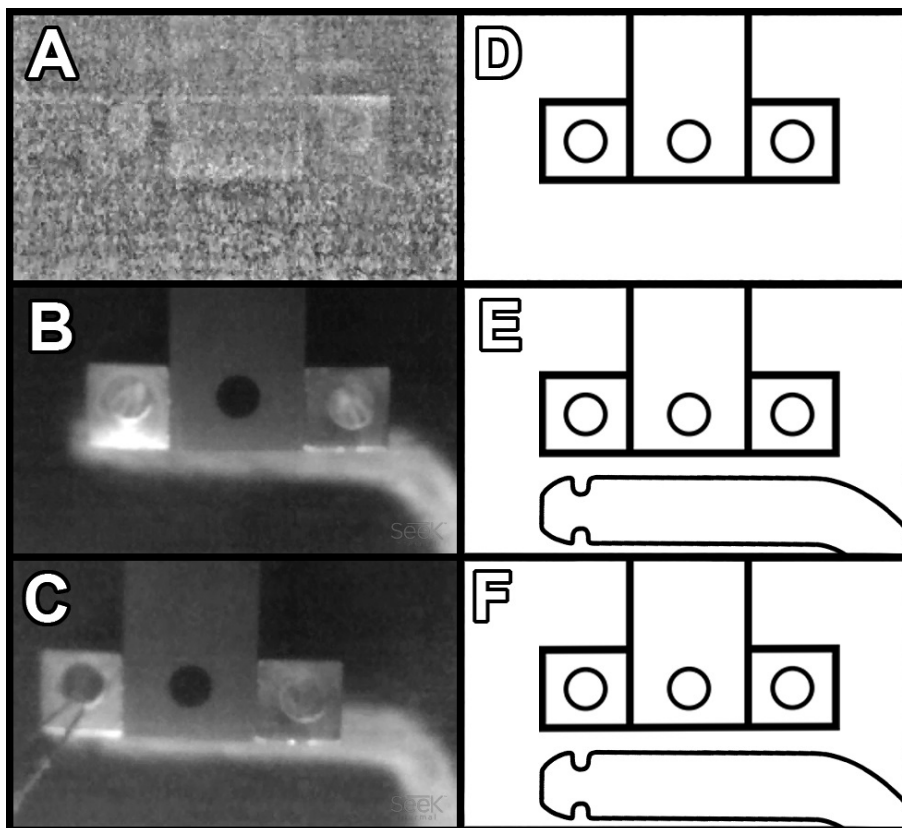


Fig. 4: Infrared images (A-C) and their schematic representations (D-F). The cavities were drilled with a DeWalt Pilot Point $\frac{1}{4}$ " diameter drill bit to the depth $1\frac{1}{4}$ ". A) Infrared image obtained from the Block Assembly II (see Fig. 1C) at room temperature without any heated rod present (schematic in D). B) Image obtained while placing a heated steel rod in close proximity to the cavities (schematic in E). C) Repeat of B, but this time, a graphite particle was suspended from two strings into the left brass cavity such that the center of the particle was exactly 1 cm from the top of the block (schematic in F). Graphite particles were also inserted at the bottom of the other two cavities. In B and C, the stem of the rod was parallel to and about 7 cm above, the top of the table (or a height of about 2 cm above the top of the block). In schematics E and F, the rod was illustrated such that its position from left to right could be accurately represented relative to the block. However, in the plane of the image, the rod was actually positioned just below the field of view considered by the schematic, or about one rod width from the block.

shown in Fig. 5A (corresponding schematic, 5C).

Once again the infrared camera was positioned a distance of ~ 15 cm from the top of the block. The cavities within the graphite portion of the block under those conditions were indistinguishable from the graphite surface. The image was noisy, as expected, since the observer was well removed from the block during data acquisition. At the same time, the cavities made within the aluminum, brass, and copper blocks were clearly visible and distinct from one another, demonstrating that they did not contain identical radiation. Since these cavities were made from highly reflective materials, this implied that the space surroundings of the block contained some anisotropic radiation.

In Fig. 5B, the same block was examined (schematic 5D). This time, the hands of the investigator were positioned on each side of the block, such that thermal equilibrium was not maintained and the associated radiation could be observed

filling the aluminum, brass, and copper cavities. Clearly, these nearly perfectly reflecting cavities were not black, but contained radiation emitted by their surroundings. Conversely, under these conditions, the three deepest graphite cavities, located on the left of the third row, remained essentially unaffected. At the same time, the shallowest cavity, made from the tip of the drill bit and located on the right of the third row, was sensitive to this challenge (Fig. 5B, D). There were reflections of thermal photons off the surfaces of each block which altered the appearance of the images as well. This study served to exemplify, once again, that real blackbodies could do work converting radiation incident upon their walls to black radiation manifesting their temperature. Conversely, rigid perfectly reflecting cavities could not do work. They contained the radiation present in their surroundings in a manner independent of their own temperature and such radiation was clearly observed in the aluminum, brass, and copper

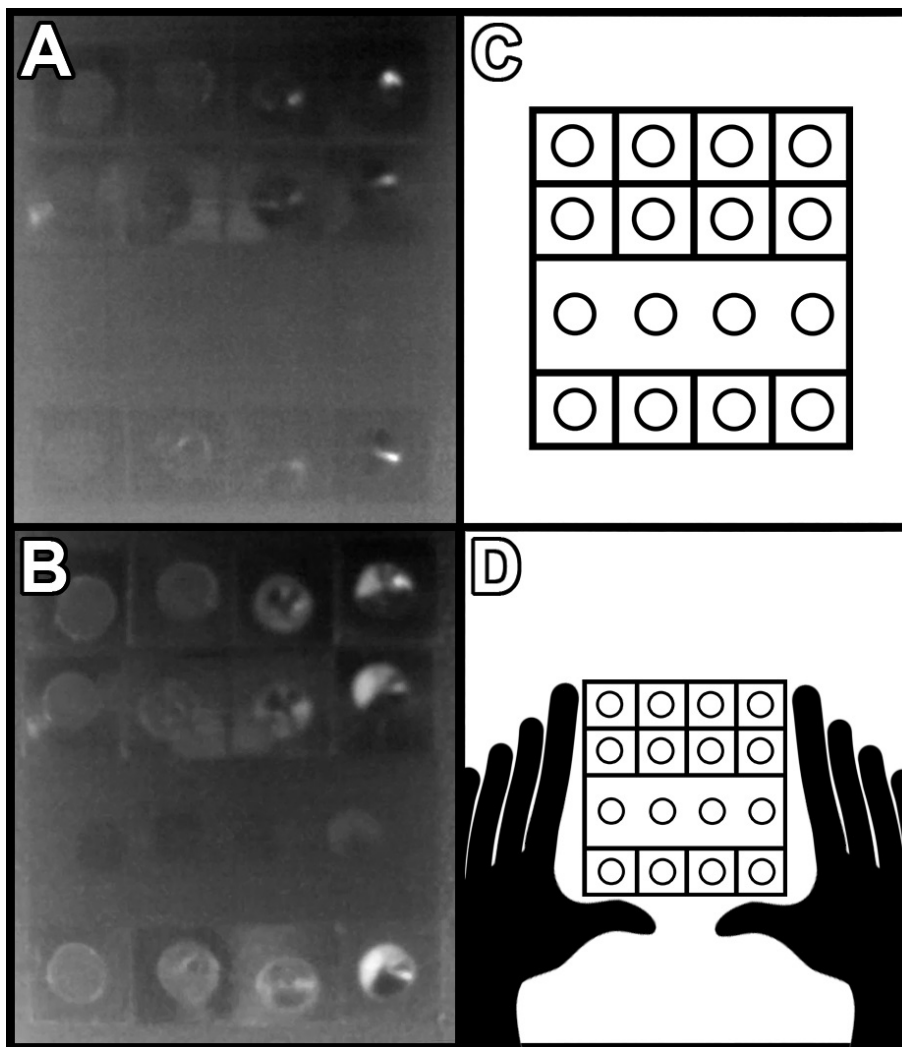


Fig. 5: A) Infrared image obtained from the Block Assembly III (see Fig. 1D) at room temperature. The corresponding schematic is displayed in C (reduced by 25%). B) Same as in A, but this time the hands of the investigator were placed near the sides of the block such that thermal photons from the first two fingers of each hand could challenge the cavities, as seen in the schematic representation D (reduced by ~50%). The horizontal rows from top to bottom correspond to aluminum, brass, graphite, copper. These cylindrical cavities were made using a standard $\frac{1}{4}$ " drill bit to different depths (from right to left: 1) depth corresponding to just the cone of the drill bit, 2) depth to $\frac{1}{4}$ ", 3) $\frac{3}{4}$ " and 4) $1\frac{1}{4}$ ".

cavities.

At this point Block Assembly III was placed onto the surface of a hotplate brought to a temperature of $\sim 304^\circ\text{C}$, as shown in Fig. 6.

Under these conditions, the graphite cavities located on the third row all appeared to contain isotropic radiation closely manifesting their equilibrium temperature. This indicated that these cavities were able to convert heat energy located in their walls to blackbody radiation. Even the cavity produced with only the tip of the drill bit, on the right, contains isotropic radiation. Conversely, the cavities constructed from aluminum, brass, and copper did not all contain such

radiation. Rather, they showed clear signs that their radiation originated from the hotplate and was a property of the surroundings, not the cavity itself.

While the $1\frac{1}{4}$ " aluminum (top row, left most) and copper (bottom row, left most) cavities appeared to contain isotropic radiation, the brass cavity of the same depth (second row, left most) clearly did not. In addition, careful examination revealed that crescents were visible in the aluminum, brass, and copper $\frac{3}{4}$ " cavities (second column) as well. With the exception of graphite, the $\frac{1}{4}$ " cavities (third column) did not contain isotropic radiation at the appropriate temperature and neither did the corresponding conical cavities made from just the tip

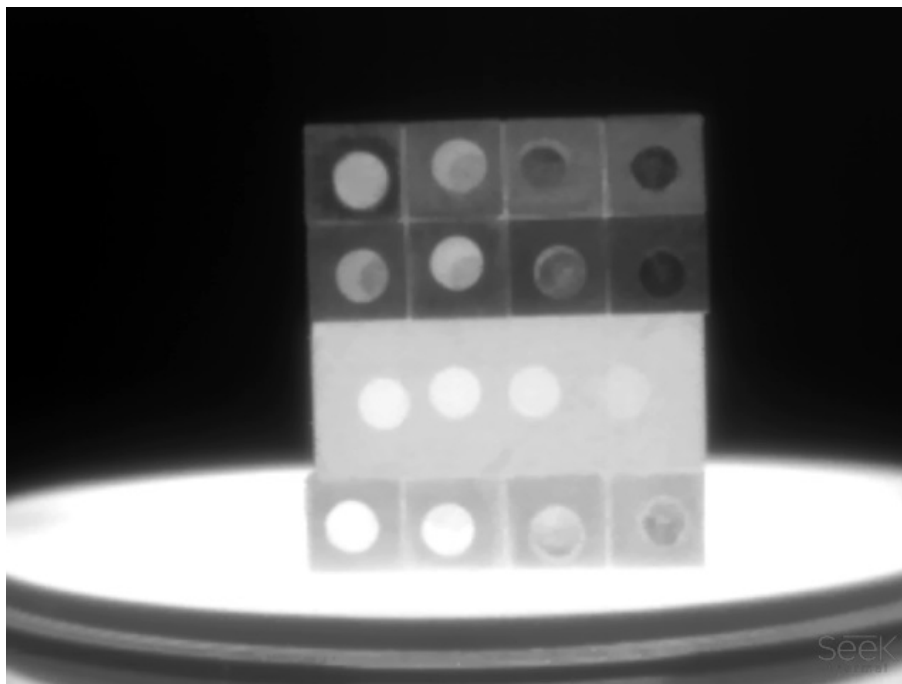


Fig. 6: Infrared image obtained from the Block Assembly III (see Fig. 1D) positioned on a hotplate surface at a temperature estimated at $\sim 304^{\circ}\text{C}$ using the thermal camera. In order to acquire this image, the camera was mounted on a tripod such that its lens was ~ 20 cm from the face of the block.

of the drill bit (fourth column). For instance, note the inability of any of the smallest cavities, made from these materials, to sustain radiation at the proper temperature. Crescent patterns also appeared in cavities constructed from aluminum, brass, and copper, even at a depth of $\frac{3}{4}$ " (second column), despite the fact that the radiation in the graphite cavity at the same depth was clearly isotropic. At a depth of $1\frac{1}{4}$ ", the brass cavity (second row, first column) still displayed such patterns.

When the block assembly was cooled, it was apparent that the copper blocks had become highly oxidized and this, in addition to their proximity to the hotplate, might help explain their superior performance when compared to aluminum and brass.

Still, these results revealed that real blackbodies, represented herein by the graphite cavities, could do work and manifested the radiation appropriate to the temperature of their own walls. Conversely, the aluminum, brass, and copper cavities illustrate that nearly ideal reflectors could not do work, but contained the radiation present in their surroundings which was independent of the nature of their walls.

4 Discussion

The approach to, and departure from, thermal equilibrium has been the subject of countless studies by Fourier [35], Dulong [36], Petit [36], de la Provostaye [37], and Desains [37] (see [38] for a full review). In similar fashion, through the stud-

ies presented herein, a greater understanding has been sought about the nature of the radiation within cavities. This was accomplished both under conditions of thermal equilibrium and also by considering challenges which represent small departures from equilibrium. However, these challenges were important because they served to highlight the nature of the radiation which filled a cavity and thereby help to establish the identity of those objects which properly constituted blackbodies.

4.1 Blackbodies defined

Prior to formulating his law, Kirchhoff first defined a blackbody by stating that *"This investigation will be much simplified if we imagine the enclosure to be composed, wholly or in great part, of bodies which, for infinitely small thickness, completely absorb all rays which fall upon them"* [2, §7]. Kirchhoff therefore recognized the importance of surface absorptivity in the blackbody problem.

Surprisingly however, when Max Planck would later define the blackbody in his classic text [14], he completely rejected Kirchhoff's approach writing: *"In defining a blackbody Kirchhoff also assumes that the absorption of incident rays takes place in a layer 'infinitely thin'. We do not include this in our definition"* [14, §10]. Planck then changed the characteristics of a blackbody surface: *"A rough surface having the property of completely transmitting the incident radiation is described as 'black'"* [14, §10]. With this defini-

tion, Planck removed absorbance of the surface itself from the requirements for creating a blackbody and inappropriately placed the focus on transmittance. Planck adopted this new definition because he was preparing to advance a proof of Kirchhoff's law which ignored absorbance at the boundary of two materials [14, §35-37]. But in doing so, Planck moved away from physical reality. His approach proved invalid [39]. Nearly ideal absorbance for thin surfaces remains the hallmark of all materials used to construct quality blackbodies [7, 9–11, 25, 27].

4.2 The mathematical form of Kirchhoff's Law

In advancing his law [2], Kirchhoff did not have recourse to experimental verification. He first stated that the emissive power of an object, E , divided by its absorptive power, A , was equal to a universal function which depended only upon temperature, T , and frequency, ν ($E/A = e$ where $e = f\{T, \nu\}$). He then immediately replaced absorptive power, A , with absorptivity, α_ν , such that $E/\alpha_\nu = f\{T, \nu\}$. For actual blackbodies, it is clear that α_ν can be set to 1 and $E = f\{T, \nu\}$. However, Kirchhoff's expression becomes undefined when α_ν is set to zero, as would occur if the cavity was constructed from a perfect reflector. Planck himself recognized the undefined nature of Kirchhoff's law under those conditions (see §48, §51, §52 in [14]).

Thus, relative to Kirchhoff's relationship, two limits are involved. The first, addresses cavities constructed from perfect absorbers, such that α_ν can be set to 1. The second, involves cavities constructed from perfect reflectors, such that α_ν can be set to zero and the law becomes undefined. Perfectly reflecting cavities never followed Kirchhoff's law. They are important however as they form the basis for many resonant devices [29–32]. In any event, Kirchhoff had no mathematical basis for arguing that all cavities must contain black radiation which is dependent only upon temperature and frequency.

4.3 Laboratory blackbodies

Clearly, laboratory blackbodies [4, 7, 12, 26, 27], including those utilized to provide Planck with data [9–11], were specialized cavities constructed from highly absorbing materials. This observation alone was sufficient to conclude that Kirchhoff's law was invalid.

In the infrared, it was evident that the graphite cavities used in this study were able to maintain their internal radiation in a manner which was essentially independent of any radiative challenge. They acted as real blackbodies and could do work. They could ensure that the radiation they contained was governed by the nature and the temperature of their own walls. They converted incoming energy, whether in the form of incident radiation or heat, into normal radiation with the correct frequency distribution.

Conversely, cavities constructed from aluminum, brass,

and copper acted as nearly ideal reflectors. They contained the radiation which was incident from their surroundings and showed no ability to convert this radiation to black radiation corresponding to the temperature of their own walls. In this regard, it was evident that perfect reflectors could not do work. They were unable to effect any change upon incident radiation other than that which would occur given specular or diffuse reflection.

de Vos noted the extent to which cavities could make radiation isotropic as a function of the ratio of their diameter and depth [33]. However, perfectly reflecting cavities, by definition, could not emit radiation. As such, the radiation which they contained must remain completely independent of the temperature of their walls and dependent solely on the radiation contained in their surroundings. de Vos's analysis of the quality of a cavity in terms of its ability to convert incoming radiation into ejected isotropic radiation, while of interest, actually had little bearing on the behavior of real blackbodies. This was because real blackbodies depended on the nature of their surfaces, not on the dimension of a cavity, in order to ensure that the emitted radiation would be both isotropic and black. A cavity in fact, should not be required, provided that the surface material was black and that no external radiation was able to contaminate this emission. This explained in part the interest in materials with elevated emissivity values [9–11, 26, 27] and highly absorbing surfaces [15–22]. Cavities did enable blackbody radiation to be contained, but they were not necessary for its production.

4.4 Cavities and work

Perhaps the central feature of all actual blackbodies was that they must have the ability to do work and convert any incident energy into the frequency distribution corresponding to the temperature of their own walls. In this sense, the work performed by a blackbody conformed to the standard definition whereby energy was converted from one form to another. Blackbodies accomplished this task in two ways. First, they were able to alter the frequency of incoming radiation and re-emit it with the blackbody frequency distribution corresponding to the temperature of their walls. Secondly, they could convert heat energy located in their own walls into thermal radiation associated with this temperature. In either case, only absorbers of radiation could act as blackbodies, as only they could serve as emitters. Radiation was absorbed by the walls and re-emitted in a manner which depended on the density of states and thereby upon temperature.

Conversely, rigid perfect reflectors could only redirect incoming radiation in a specular or diffuse manner. A change in phase occurred without any change in frequency. Therefore, no work was done, as a change in the energy distribution of the incoming radiation did not occur. Furthermore, perfect reflectors could not harness the energy contained in their walls and thereby emit radiation. Unable to absorb, they could not

emit.

The reality that rigid perfectly reflecting cavities cannot do work is the basis for resonant cavities in ultra high field magnetic resonance imaging (UHFMRI) [29], electron paramagnetic resonance (EPR) [30], microwave communications [31] and the resonant cavities used for building coherent radiation following stimulated emission in lasers [32]. All of these disciplines strive to build highly reflective resonant cavities with optimal quality factors, $Q = f/\delta f$, where f is the frequency of interest and δf full width at half maximum of the resonance. Q-factors are inversely proportional to surface resistance echoing Planck's desire for infinitely large conductivity.

In clinical MRI, dielectric losses in the human body will dominate Q-factors for any resonator [26]. As a result, little can be gained in this discipline from building resonators from materials more sophisticated than copper or silver.

However, lasers do not experience these limitations. As a result, resonant cavities in lasers can benefit from the construction of highly reflective Bragg super-mirrors, which can have reflectance values of 99.9999% [40–42]. Ion-beam interference coating mirrors [43] are associated with LIGO [44]. Specialized mirrors are also used in high precision atomic clocks to generate optical cavities with low thermal noise in that setting [45]. Laser cavities can thus achieve Q-factors of 10^{10} , or more [46].

The use of resonant cavities in UHFMRI [29], EPR [30], microwave technology [31], and lasers [32] proves that Kirchhoff's law is not valid. These cavities critically depend on their nearly perfectly reflecting nature which allows them to serve as resonant devices, unable to alter incoming radiation by making it black. It is evident that the radiation in these cavities is absolutely dependent upon the radiation which was incident upon them and completely independent of the temperature of their walls. Absorption of incident photons, transformation into thermal vibrations, and re-emission into thermal photons does not occur in perfectly reflecting cavities. Kirchhoff and Planck cannot claim otherwise, when they assert that all cavities contain black radiation [1, 2, 14].

4.5 Max Planck and Kirchhoff's law

Max Planck attempted to prove the validity of Kirchhoff's law in the opening sections of *The Theory of Heat Radiation* [14, §1-52]. Upon close examination, the derivation was discovered to be unsound [39]. In order to construct his proof, Planck actually redefined the very nature of a blackbody and no longer required, as did Kirchhoff, the ability to absorb radiation over an *infinitely small thickness* [2, §1]. In contrast to Kirchhoff, Planck permitted radiation to enter a medium without absorption/emission at its surface [14, §36-37]. When considering a medium with a vanishingly small absorptivity, he allowed for their use as blackbodies by invoking infinite thickness [14, §10]. Thus, Planck's proof of Kirchhoff's law

used transmission and, at times, improperly ignored absorption. Additionally, his proof relied on the use of polarized light [14, §35-37] and the use of Brewster's angle, when heat radiation is never polarized [47].

In this regard, it is noteworthy that in order to address the blackbody problem Max Planck actually focused his attention on the perfectly reflecting, rather than the perfectly absorbing, wall [14]. Planck had defined the reflector as: "*the surface of an absolute conductor (metal) of infinitely large conductivity*" [14, §55]. Planck's focused on perfectly reflecting cavities despite the fact that such cavities cannot function as proper blackbodies.

Indeed, Planck understood that "*In a vacuum bounded by perfectly reflecting walls, any state of radiation may persist*" [14, §51]. However, he advanced that such radiation could be converted to blackbody radiation at the correct temperature with the simple addition of a small particle of carbon [14, §51]. He believed that this particle acted as a catalyst and provided no heat energy of its own [14, §51]. However, Fig. 3 demonstrated that the addition of a carbon particle alone was not sufficient to produce the desired radiation. In fact, it was doubtful that Planck or his contemporaries ever tested the concept, as a small particle of graphite could never do enough work to fully convert the radiation, incident upon a cavity, into fully black radiation. The second law has always restricted what the carbon particle could achieve. In addition, Planck's use of the carbon particle [14, §51] could easily lead to a violation of the 1st law.

Using a thought experiment, it could be demonstrated that the catalyst argument violated the 1st and 2nd laws of thermodynamics [48]. Planck himself recognized that the radiation contained in a perfectly reflecting cavity was undefined [14, §48, §51, §52]. As such, the energy contained in these radiation fields could not be transformed to the proper frequency distribution, unless it exactly matched the energy required at the temperature of interest. Since the radiation was undefined, any attempt to transform radiation of arbitrary energy content to that with the proper frequency distribution for a given temperature risked violating the 1st law of thermodynamics. Planck could not be assured that the energy density within the cavity enabled the carbon particle to make the radiation black at the correct temperature. Only when the correct energy density was initially present in the cavity, could Planck avoid violating the 1st law. Furthermore, the carbon particle must do work to transform heat energy into radiation and fill the cavity. It could never act as a catalyst. Planck's attempt to address the undefined nature of the radiation in a perfectly reflecting cavity, by the insertion of a carbon particle, stood in opposition to the laws of thermodynamics [48].

Throughout his text on *The Theory of Heat Radiation* [14], Max Planck attributed all of the energy to the radiation field and included none in the walls of the cavity. Obviously, if this was done, the solution could not depend on the nature of the walls. However, the approach was not justified. Real

cavities have energy in their walls. The most important example is the perfectly reflecting cavity, wherein thermal equilibrium is governed by the conduction of energy in the walls, not within a radiation field. By definition, such walls have no means of interacting with radiation and, therefore, a radiation field cannot be used to set equilibrium in a perfectly reflecting cavity. Perfectly reflecting cavities are responsive to the radiation incident upon their openings only through reflection. The reflection can be either specular, white, or a mixture. However, any effect on the incoming light in a perfectly reflecting cavity will occur in a manner completely devoid of any relationship to the temperature of its walls. The radiation within perfectly reflecting cavities is determined by history and environment, not temperature.

5 Conclusions

For more than 150 years [12], Kirchhoff's law of thermal emission [1, 2] has governed much of scientific thought in physics and astronomy, despite the fact that it lacked proper theoretical [28] and experimental proof [4, 7, 12, 28, 38, 39, 48]. Now it is clear that cavities do not all contain the same radiation, independent of the nature of their walls. Perfect reflectors are unable to convert incoming radiation into the Planckian distribution corresponding to their wall temperature. In the absence of wall motion, they are unable to do any work and merely sustain the radiation in their surroundings. If this incident radiation is phase coherent, then perfect reflectors can even sustain standing waves, as required in UHFMRI [29], EPR [30], microwave telecommunication [31] and lasers [32]. Had Kirchhoff's law been valid, then none of these modalities would exist, as no cavity would become resonant and all incident radiation would become destined to adopt the blackbody profile.

Kirchhoff's law is demonstrably false. Real blackbodies can do work on any incoming radiation and, as shown herein, they appear to do so instantly. They exclusively contain radiation which reflects the temperature of their walls, not the presence of the radiation in their surroundings. It is this ability to do work in the ideal blackbody, and the inability to do work in the perfect reflector, which determines the real behavior of cavities. That is also why laboratory blackbodies are always constructed from materials which possess relatively elevated emissivity values over the frequencies of interest [4, 7, 9–12, 26, 27]. The production of a blackbody spectrum absolutely requires the presence of a vibrating lattice and is intrinsically tied to the nature of the walls [4], contrary to Kirchhoff's claim [1, 2].

As a result, Max Planck's long advocated universality [14, §164] as to time, length, mass, and temperature was never valid. The concept was entirely dependent on the notion that Kirchhoff's law was correct, but this was never the case. As a consequence, the units of measure remain a product of humanity's definitions and science constrained by this fact.

Though Planck's equation remains correct for actual blackbodies, it is no longer reasonable to proclaim that black radiation can be produced simply through arbitrary cavities in thermal equilibrium. Such assertions are incorrect as evidenced by the preeminent role of graphite and soot in the construction of actual blackbodies [4] and as modern technology readily demonstrates [29–32].

Acknowledgement

The author would like to thank Joseph Luc Robitaille for assistance in conducting these experiments and relative to the preparation of the figures. An earlier partial version of this work was archived on viXra.org as follows: Robitaille P.-M. and Robitaille J.L. Kirchhoff's Law of Thermal Emission: What Happens When a Law of Physics Fails an Experimental Test? viXra:1708.0053 submitted on 2017-08-06.

Dedication

This work is dedicated to Joseph Benoît Martin Robitaille.

Received on May 8, 2018

References

1. Kirchhoff G. Über den Zusammenhang zwischen Emission und Absorption von Licht und Wärme. *Monatsberichte der Akademie der Wissenschaften zu Berlin*, 1860 (sessions of Dec. 1859), 783–787.
2. Kirchhoff G. Über das Verhältnis zwischen dem Emissionsvermögen und dem Absorptionsvermögen. der Körper für Wärme und Licht. *Poggendorfs Annalen der Physik und Chemie*, 1860, v. 109, 275–301. (English translation by Guthrie F.: Kirchhoff G. On the relation between the radiating and the absorbing powers of different bodies for light and heat. *Phil. Mag.*, 1860, v. 20, 1–21).
3. Stewart B. An account of some experiments on radiant heat, involving an extension of Prévost's theory of exchanges. *Trans. Royal Soc. Edinburgh*, 1858, v. 22 (1), 1–20 (also found in Harper's Scientific Memoirs, Ames, J. S., ed. The Laws of Radiation and Absorption: Memoirs of Prévost, Stewart, Kirchhoff, and Kirchhoff and Bunsen, translated and edited by Brace D. B., American Book Company, New York, 1901, pp. 21–50).
4. Robitaille P.-M. On the validity of Kirchhoff's law of thermal emission. *IEEE Trans. Plasma Science*, 2003, v. 31 (6), 1263–1267.
5. Wedgwood T. Experiments and observations on the production of light from different bodies, by heat and by attrition. *Phil. Trans. Roy. Soc. Lond.*, 1792, v. 82, 28–47; Wedgwood T. Continuation of a paper on the production of light and heat from different bodies. *Phil. Trans. Roy. Soc. Lond.*, 1792, v. 82, 270–282.
6. Leslie J. An Experimental Inquiry into the Nature and Propagation of Heat. T. Gillet, Salisbury Square, 1804.
7. Robitaille P.-M. Blackbody radiation and the carbon particle. *Progr. Phys.*, 2008, v. 3, 36–55.
8. Winter J., FitzHugh E. W. Pigments based on Carbon. In: Berrie B.H., ed. Artists' Pigments: A Handbook of Their History and Characteristics, 1986, v. 4, 1–37.
9. Hoffmann D. On the experimental context of Planck's foundation of quantum theory. In: Revisiting the Quantum Discontinuity, Max Planck Institute for the History of Science, Preprint 150, 2000, 47–68.
10. Lummer O., Pringsheim E. Kritisches zur schwarzen Strahlung. *Annalen der Physik*, 1901, v. 6, 192–210.

11. Rubens H. and Kurlbaum F. Anwendung der Methode der Reststrahlen-zur Prüfung der Strahlungsgesetzes. *Annalen der Physik* v. 2, 649–666; Rubens H., Kurlbaum F. On the heat radiation of longwave-length emitted by black bodies at different temperatures. *Astrophys. J.*, 1901, v. 74, 335–348.
12. Robitaille P.-M. Kirchhoff's Law of Thermal Emission: 150 Years. *Progr. Phys.*, 2009, v. 4, 3–13.
13. Planck M. Über das Gesetz der Energieverteilung im Normalspektrum. *Annalen der Physik*, 1901, v. 4, 553–563.
14. Planck M. The Theory of Heat Radiation. P. Blakiston's Son & Co., Philadelphia, PA, 1914.
15. Brown R. J. C., Brewer P. J., Milton M. J. T. The physical and chemical properties of electroless nickel–phosphorus alloys and low reflectance nickel–phosphorus black surfaces. *J. Mater. Chem.*, 2002, v. 12, 2749–2754.
16. Yang Z. P., Ci L., Bur J., Lin S. Y., Ajayan P. M. Experimental observation of an extremely dark material made by a low-density nanotube array. *Nano Lett.*, 2008, v. 8 (20), 446–451.
17. Kravets V. G., Schedin F., Grigorenko A. N. Plasmonic blackbody: Almost complete absorption of light in nanostructured metallic coatings. *Phys. Rev. B*, 2008, v. 78, 205405.
18. Vorobyev A. Y., Topkov A. N., Gurin O. V., Svich V. A., Guo C. Enhanced absorption of metals over ultrabroad electromagnetic spectrum. *Appl. Phys. Lett.*, 2009, v. 95, 121106.
19. Liu X., Coxon P. R., Peters M., Hoex B., Cole J. M., Fray D. J. Black silicon: fabrication methods, properties and solar energy applications. *Energy Environ. Sci.*, 2014, v. 7, 3223–3263.
20. Guo J., Guo X., Xu W., Zhang Z., Dong J., Peng L. A Zn-Ni coating with both high electrical conductivity and infrared emissivity prepared by hydrogen evolution method. *Applied Surface Science*, 2017, v. 402, 92–98.
21. Sun W., Du A., Feng Y., Shen J., Huang S., Tang J., Zhou B. Super Black Material from Low-Density Carbon Aerogels with Subwavelength Structures. *ACS Nano*, 2016, v. 10 (10), 9123–9128.
22. Panagiotopoulos N. T., Diamanti E. K., Koutsokeras L. E., Baikousi M., Kordatos E., Matikas T. E., Gournis D., Patsalas P. Nanocomposite catalysts producing durable, super-black carbon nanotube systems: applications in solar thermal harvesting. *ACS Nano*, 2012, v. 6 (12), 10475–10485.
23. Zhao Q., Fan T., Ding J., Guo Q., Kamada M. Super black and ultrathin amorphous carbon film inspired by anti-reflection architecture in butterfly wing. *Carbon*, 2011, v. 49 (3), 877–883.
24. Han Z., Li B., Mu Z., Yang M., Niu S., Zhang J., Ren L. An ingenious super light trapping surface templated from butterfly wing scales. *Nanoscale Res. Lett.*, 2015, v. 10 (1), 1052.
25. McCoy D. E., Feo T., Harvey T. A. and Prum R. O. Structural absorption by barbule microstructures of super black bird of paradise feathers. *Nature Communications*, 2018, v. 9, 1.
26. Navarro N., Bruce S. S., Johnson B. C., Murphy A. V., Saunders R. D. Vacuum processing techniques for development of primary standard blackbodies. *J. Res. Nat. Inst. Stand. Technol.*, 1999, v. 104, 253–259.
27. Chahine K., Ballico M., Reizes J., Madadnia J. Optimization of a graphite tube blackbody heater for a thermogage furnace. *Int. J. Thermophys.*, 2008, v. 29, 386–394.
28. Schirrmache A. Experimenting theory: The proofs of Kirchhoff's radiation law before and after Planck. *Hist. Studies Phys. Biol. Sciences*, 2003, v. 33 (2), 299–335.
29. Robitaille P.-M., Berliner L. Biological Magnetic Resonance, Vol. 26: Ultra High Field Magnetic Resonance Imaging. Springer-Verlag, New York, 2006.
30. Wertz J. E., Bolton J. R. Electron Spin Resonance: Elementary Theory and Practical Applications. McGraw-Hill Book Company, New York, 1972, p. 23.
31. Pozar D. Microwave Engineering, 2nd edition. Wiley, New York, NY, 1998.
32. Siegman A. E. Laser beams and resonators: the 1960s. *IEEE J. Sel. Topics Quantum Electronics* v. 6 (6) (2000) 1380–1388; Siegman A. E. Laser beams and resonators: Beyond the 1960s. *IEEE J. Sel. Top. Quantum Electronics*, 2000, v. 6 (6), 1389–1399.
33. de Vos J. C. Evaluation of the quality of a blackbody. *Physica*, 1954, v. 20, 669–689.
34. Lawrence Berkeley Laboratory, Table of Emissivity of Various Surfaces. http://www-eng.lbl.gov/~dw/projects/DW4229_LHC_detector_analysis/calculations/emissivity2.pdf
35. Fourier J. Mémoire sur la propagation de la chaleur dans les corps solides. *Nouveau Bulletin des Sciences par la Société Philomathique de Paris*, 1808, v. 1, 112–116.
36. Dulong P. L., Petit A. T. Recherches sur la mesure des températures et sur les lois de la communication de la chaleur. *Journal de L'École Polytechnique*, 1820, v. 11 (18), 189–294.
37. de la Provostaye F., Desains P. Mémoire sur la détermination du pouvoir absorbant des corps pour la chaleur rayonnante. *Annales de Chimie et de Physique*, 1850, v. 30, 431–443.
38. Robitaille P.-M., Blackbody Radiation and the Carbon Particle. *Progr. Phys.*, 2008, v. 3, 36–55.
39. Robitaille P.-M., Crothers S. J. “The Theory of Heat Radiation” Revisited: A Commentary on the Validity of Kirchhoff's Law of Thermal Emission and Max Planck's Claim of Universality. *Progr. Phys.*, 2015, v. 11 (2), 120–132.
40. Schaerpf O. Comparison of theoretical and experimental behaviour of supermirrors and discussion of limitations. *Physica B: Condensed Matter*, 1989, v. 156–157, 631–638.
41. Stanley R. P., Houdré R., Oesterle U., Gailhanou M., Ilegems M. Ultra-high finesse microcavity with distributed Bragg reflectors. *Appl. Phys. Lett.*, 1994, v. 65, 1883–1885.
42. Cole G. D., Zhang W., Martin M. J., Ye J., Aspelmeyer M. Tenfold reduction of Brownian noise in high-reflectivity optical coatings. *Nature Photonics*, 2013, v. 7, 644–650.
43. Wei D. T. Ion beam interference coating for ultralow optical loss. *Appl. Opt.*, 1989, v. 28, 2813–2816.
44. The LIGO Scientific Collaboration, LIGO: the Laser Interferometer Gravitational-Wave Observatory. *Rep. Prog. Phys.*, 2009, v. 72, 076901 (25 pp.).
45. Jiang Y. Y., Ludlow A. D., Lemke N. D., Fox R. W., Sherman J. A., Ma L. S., Oates C. W. Making optical atomic clocks more stable with 10^{-16} -level laser stabilization. *Nature Photonics*, 2011, v. 5, 158–161.
46. Paschotta R. “Q-Factor”. In: Encyclopedia of Laser Physics and Technology, V.1. Wiley-VCH, Berlin, 2008; available online: https://www.rp-photonics.com/q_factor.html.
47. Jenkins F. A. and White H. E. Fundamentals of Optics, 4th edition. McGraw-Hill, Inc., New York, 1976, p. 450.
48. Robitaille P.-M. Further Insight Relative to Cavity Radiation: A Thought Experiment Refuting Kirchhoff's Law. *Progr. Phys.*, 2014, v. 10 (1), 38–40; Robitaille P.-M. Further Insight Relative to Cavity Radiation III: Gedanken Experiments, Irreversibility, and Kirchhoff's Law. *Progr. Phys.*, 2016, v. 12 (1), 85–88.

Outline of a Kinematic Light Experiment

Christian M. Wackler

Albert-Ludwigs-Universität Freiburg, Philosophisches Seminar, Platz der Universität 3, 79085 Freiburg i. Br., Germany
E-mail: christian.wackler@merkur.uni-freiburg.de

The question whether light moves with constant or variable velocity is indubitably of the utmost importance. Preliminary reflections concerning the nature of that movement contrast the hypotheses of propagation and emission. As a brief historical examination reveals, alleged evidences in favour of the invariance postulate turn out to be erroneous or inconclusive and supposedly decisive tests methodologically invalid. An emission theory based on Michael Faraday's idea of ray vibrations is shown to be in accordance with observation. The question whether the speed of light depends on the velocity of its source has thus not been settled experimentally since only a kinematic test, to date never conducted, can give an unambiguous answer. Juxtaposed to seemingly similar but defective designs Wilhelm Wien put forward in 1904, such an experiment, amending a set-up suggested by Herbert Dingle, is proposed.

1 Introduction

The assumption that the velocity of light with respect to real* space has a constant value is not self-evident at all, as the history of science teaches. Indeed, only in the course of the 19th century the ether or propagation hypothesis of light motion, which this assumption is linked to, succeeded in superseding the ballistic or corpuscular conception of emission, espoused by Isaac Newton. However, at the same time as Christiaan Huygens's interpretation seemed to achieve a late victory, his central idea becoming a general conviction, the problems resulting from it began to accumulate as well. As a consequence, the image of propagating waves has eventually been called into question again [1] – and with very good reason as will be shown. To get a clear picture of the major differences, both views are first juxtaposed in opposition. A generally unheeded emission theory, based on the conceptions of Walter Ritz and amended by Herbert Dingle, is then invoked and demonstrated not to be in conflict with observation [2–7]. Finally, we delineate a kinematic experiment that renders an unequivocal decision between the hypotheses of propagation and emission possible.

2 The nature of light motion – propagation or emission?

To picture the two ways which the motion of light has historically been interpreted in, let us consider the following explanations of Walter Ritz (Figure 1a, b):

In the theory of the ether, a point mass P , at rest with respect to this medium, will be able to emit waves of a constant radial velocity, which will form at each instant a system of spheres, having P as a centre. If P is animated by a motion of translation, the spheres, on the contrary, will become eccentric, each keeping its centre at P_I of

the ether which coincides with P at the instant of emission. According to the principle of relativity, on the contrary, if the motion of translation is uniform, the spheres will have to stay concentric as at rest, and the centre will always be P . When the motion is no longer uniform, the principle will no longer suffice to determine the movement of the waves.

Two ways of representing the phenomena, two distinct images have successively dominated optics: that of emission (the light *moves*) and that of the ether (the light *propagates*). The second one introduces absolute motion, while the first leads for the movement of light in vacuum exactly to the law that the principle of relativity requires: the luminous particles expelled in all directions at the instant t move with a constant radial velocity and perpetually fill a sphere whose centre is animated with the motion of translation w that P had at the instant of emission; if w is constant, this centre will thus continue to coincide with P . [8] (The original text is in French.)

The experiment of Michelson and Morley [9] had engulfed the propagation hypothesis and with it electromagnetic theory in a crisis, which most notably H. Poincaré [10] called attention to. Ritz conceived of the ingenious solution to entirely discard the image of propagating waves in favour of a ballistic interpretation. In contrast to other authors, suggesting different emission theories shortly afterwards [11–14], he assumed light to keep the speed it is originally emitted with including after reradiation by a medium [15]. His auspicious but due to his early passing fragmentary work has been the first systematic attempt to revise the notion of emission and turn it into a cornerstone of electromagnetic and optical theory [8, 15, 16]. Not until more than half a century later, that line of thought was keenly continued by R. A. Waldron [17].

*For epistemological reasons, the expression “real” is used instead of the Newtonian term “absolute” throughout this essay.

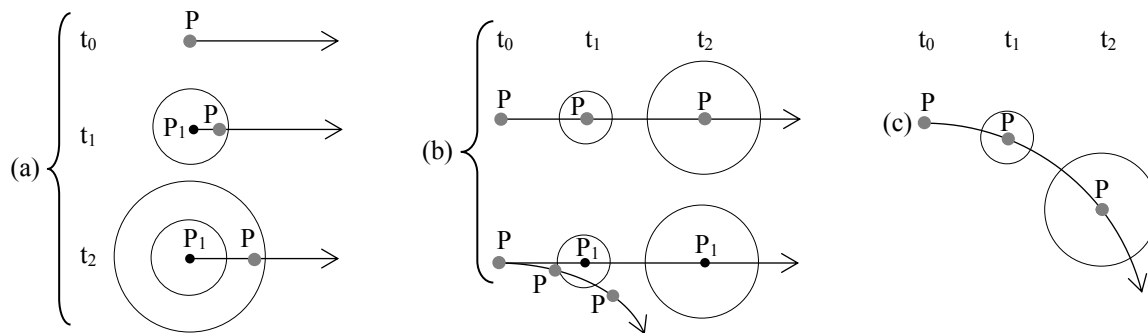


Fig. 1: Movement of a light source P and of a corresponding spherical wave generated at the instant t_0 . (a) Propagation (after Maxwell-Lorentz), (b) ballistic emission (after Newton-Ritz), (c) emanation (after Ritz-Dingle).

3 The Ritz theory – criticism and counter-criticism

To test Ritz’s explanation, M. La Rosa [18, 19] and R. C. Tolman [13] suggested to repeat the Michelson-Morley experiment using light from an extraterrestrial source as the latter moves rapidly with respect to the measuring apparatus. They wrongly presupposed that another null result on such conditions would invalidate his conception. In 1919, an equivalent test, conducted by Q. Majorana [20] with a moving terrestrial light source, showed no shift of the interference pattern. Although F. Michaud [21] demonstrated that Ritz’s theory conforms with Majorana’s findings – unlike all other emission theories which had been proposed – inferring the fallacy of La Rosa’s and Tolman’s reasoning from this was omitted. Their view found its way into W. Pauli’s [22] influential article on Einstein’s theory instead, and after R. Tomaschek [23] and D. C. Miller [24] had finally performed experiments employing sun and star light that again yielded no interference fringes to the calculated extent, Ritz’s ideas largely fell into oblivion.

Already previously, an argument adduced by D. F. Comstock [25] and W. de Sitter [26–29] had severely undermined the plausibility of the emission hypothesis. They pointed out that the observed orbits of binary stars are irreconcilable with a ballistic motion of light since particles emitted by a star approaching the observer would overtake the preceding corpuscles and thus distort the image of the system.

Almost half a century had passed until Herbert Dingle [2–4] not only brought the error in La Rosas’s and Tolman’s reasoning to light but also found a possible explanation considering the seemingly unsurmountable objection that Comstock and de Sitter had raised. In doing so, he seized upon ideas which Michael Faraday had outlined in his *Thoughts on Ray-vibrations*:

The view which I am so bold as to put forth considers, therefore, radiation as a high species of vibration in the lines of force which are known to connect particles and also masses of matter together. It endeavours to dismiss the æther, but not the vibrations. [30]

Dingle showed that it suffices to extend the classical principle of relativity concerning electromagnetic radiation so that the velocity of light would remain constant with respect to its source even if the radiating body moves non-uniformly and non-rectilinearly (Figure 1c). According to this view, the vibrating rays stay throughout their journey through pure space connected to the source and share the latter’s changes of motion. A few years earlier but without building on Faraday’s idea, P. Moon and D. E. Spencer had already reasoned along similar lines in response to de Sitters objection [31–35]. However, as H. Bondi aptly remarked, the term “ballistic” does not fit Dingle’s conception since the analogy with projectiles no longer characterizes the image [2]. To make a clear distinction, we hence refer to the variation of the emission hypothesis based on vibrating rays as *emanation* and to the correlating principle, governing the motion of electromagnetic radiation, as *classicistic relativity*.

Admitting this principle renders yet another astronomical objection irrelevant H. Thirring [36] propounded against the ballistic concept. He argued that as atoms in the sun are accelerated through thermal collisions, they would emit light particles with different velocities at successive instants. The wave train travelling along a terrestrial observer’s line of sight would therefore shrink first, then be stretched, and arrive at the earth as a radio signal.

Finally, a whole class of methodologically interrelated evidences that had been put forward against the emission hypothesis could not withstand Dingle’s astute scrutiny either. Over the years, a considerable number of experiments was conducted which seemed to corroborate the postulate of constant light velocity relative to pure space, e.g. [37–43]. But as Dingle correctly remarked:

The postulate is adopted as part of the basis of a kinematic theory, so that “velocity” must be understood in a kinematic sense, and this requires that the source of light must be an identifiable body, having a definite position in space at each successive instant, the whole sequence of posi-

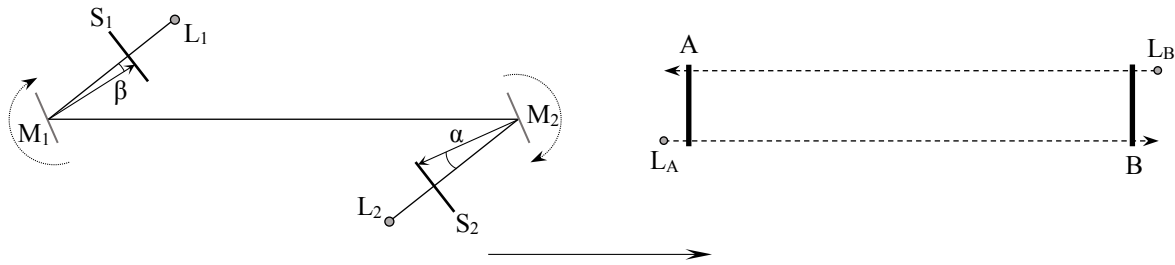


Fig. 2: Schematic of Wien's first and second experimental proposals. A, B: translationally congruent cogwheels; L_1 , L_2 , L_A , L_B : light sources; M_1 , M_2 : mirrors in parallel position; S_1 , S_2 : diaphragms with scales; α , β : deviation angles assuming a stationary ether so that $\alpha > \beta$ as the mirrors rotate, the arrow below indicating the direction of motion of the earth around the sun. Bolometers behind A and B were to record the luminous energy of the incoming beams. When the cogwheels are at rest, the respective values are the same but change as soon as A and B start spinning. An ensuing difference in luminous energy between the rays passing through the notches in opposite directions would have confirmed the hypothesis of a stationary ether.

tions being consistent with the velocity assigned to the body. [6]

Furthermore, the fact that tests which employ interferometry or use hypothetical particles as sources of light are subject to circular reasoning was generally disregarded.

In all such experiments, the Maxwell-Lorentz theory, in one respect or another, has been assumed *in the description of the experiment itself*, and since that theory requires that the velocity of light shall be independent of that of its source, the results are of no value at all in relation to this point. [44]

If one visualizes, for instance, the image of the ejected photon string indicated above, it becomes clear at once that a light ray's velocity is not determined by its frequency of vibration. Consequently, a measurement of the frequency of reception, taken by itself, does not allow a conclusion to be drawn about that velocity. Thus, a kinematic question demands a kinematic answer.

For all that and although it was occasionally admitted that Ritz's ideas were discarded prematurely and in part on erroneous grounds [45–49], the theory as amended by Dingle, which no valid evidence exists against, was for decades neglected. Only recently, this conception has finally been resumed and substantially expanded by Luis Bilbao [50], Luis Bernal, and Fernando Minotti [7] under the name of *Vibrating Rays Theory* (VRT). Having adduced further observational data in support of it, they conclude their comprehensive study as follows: "We believe that, given the above evidence, a conscientious experimental research is needed to settle the question of the dependence of the speed of light on that of its source as predicted by Vibrating Rays Theory, and that has been observed during the 1998 NEAR flyby." [7]

4 Towards a kinematic experiment

In 1904, Wilhelm Wien [51–55, pp. 1408-1409] outlined two experiments to determine whether the ether is dragged by the

earth or stationary based on the procedures Léon Foucault [56] and Hippolyte Fizeau [57, 58] had devised to measure the speed of light. His first design includes employing two rotating mirrors, his second using two spinning cogwheels which are placed far apart from each other and aligned with the orbital motion of the earth around the sun, respectively (Figure 2). Both experiments demand that the components in rotation have the same angular velocity at any given moment. They therefore depend on the real synchronicity of the instants which the mirrors or cogwheels are set in motion at. However, according to the prevailing theory, this is unattainable through a material connection between them, for example by means of an axle, because within its framework the notion of the rigid body is no longer valid as Wien [59, 60] himself later explained. Nor is utilizing electromagnetic signals to simultaneously start two separate motors feasible due to the supposedly indeterminable times the signals need to reach the different propulsion systems, which count as clocks, so that any possible asymmetry looked for would be offset by the signals' nonsynchronous arrival. These designs being foiled, Wien relinquished further efforts and became a leading proponent of Einstein's theory.

More than half a century later, Herbert Dingle pointed repeatedly to the necessity of a kinematic test for a final answer to the question of the speed of light [4–6, 43, 61–68]. In his book *Science at the Crossroads*, he eventually presented his most sophisticated proposal of an experiment of the kind he hoped for (Figure 3):

A and B are two sources of light (visible, material sources, not hypothetical particles) of which B is moving rapidly to the left while A is at rest, the paper being the standard of rest. At the instant at which they are adjacent to one another they emit pulses of light towards C and D, which are photographic films whose distances from A are constant and which are moving rapidly downwards through the paper. The relative motion

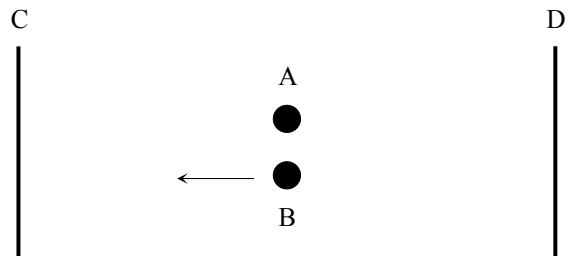


Fig. 3: Light sources A and B, photographic films C and D.

of A and B continues unchanged throughout the passage of the light. If Einstein’s second postulate is true the traces on both films will be symmetrically side by side, while if Ritz’s hypothesis is true, that of the light from A will be above that of the light from B on one film and below it on the other. [69]

This proposal undoubtedly implicates considerable and probably still insurmountable technical challenges. However, it at least indicates that the one-way speeds of different beams can indeed be compared without clocks in the usual sense and therefore without the issue of synchronization being relevant at all. That a measurement of the one-way speed of light is possible in principle has also been expressly acknowledged, for example, by Eddington [70], Waldron [17], and Ohanian [71].

Dingle’s appeals may have gone unheard for factual reasons at that time. Nowadays, technical infeasibility can certainly no longer hold as a valid argument as will be shown in the following chapter. The matter appears all the more exigent as the invariance postulate in its strict sense has recently been refuted experimentally by slowing down light in vacuum so that c may at best represent a maximum value. Giovannini et al. sum up their findings as follows: “That the speed of light in free space is constant is a cornerstone of modern physics. [...] Our work highlights that, even in free space, the invariance of the speed of light only applies to plane waves.” [72] But plane waves are ideal constructs and therefore do not exist as natural phenomena. Considering these facts and especially in view of the work of Bilbao, Bernal, and Minotti, a kinematic test to conclusively answer the question whether the speed of light depends on the velocity of the source is more urgent than ever.

5 Principle and set-up of the experiment

To remove the main difficulties inherent in Dingle’s proposal, it is crucial to again follow Michelson’s example and to take advantage of the motion of the earth around the sun since the planet’s orbital speed of about 30 km/s is great enough to render a potential difference in the travel times of distinct beams observable. Further, employing only one light source

will ensure that the emitted rays originate from the same point with respect to the earth.

Thus, the experimental set-up is as follows: aligned with the orbital motion of the earth around the sun, a light source L is positioned far apart from a disk D , the latter’s rotational axis being perpendicular to the ground. While the disk is spinning uniformly, L generates short pulses. The emitted beams move towards D and impinge on its photosensitive lateral surface at point A at right angles to the tangent (Figure 4). According to the propagation hypothesis, the velocity of a ray with respect to the ground travelling along the direction of orbital motion of the earth around the sun is $c - V$, with c signifying the speed of light relative to pure space and V the orbital speed of the earth. The travel time of the light referred to $LA = s$ is hence

$$t_A = \frac{s \sqrt{1 - \frac{V^2}{c^2}}}{c - V} \tag{1}$$

whereas in the case of a constant speed of light with respect to the source one has

$$t = \frac{s}{c}, \tag{2}$$

the difference between these times being

$$\delta t_A = t_A - t. \tag{3}$$

From the disk radius r and the number of revolutions per second f follows the speed

$$w = fU \tag{4}$$

of the uniformly rotating circumference U . If λ denotes the light spot diameter and the pulse duration p is set according to

$$\delta t_A \leq p \ll \frac{U - \lambda}{w}, \tag{5}$$

the circular arc length

$$d = \lambda + wp \tag{6}$$

marks the trace the first pulse generates on D ’s lateral surface. As the disk is spinning constantly and the pulse interval equates to

$$P = \frac{i}{f} - t, \tag{7}$$

where $i \in \mathbb{N}$ denotes the number of revolutions per pulse, any additional pulse must lengthen the trace in the amount of $w\delta t_A$, leaving a solid line on the photosensitive film. Let $n \in \mathbb{N}$ be the number of successively generated pulses, then the trace length a will after n pulses add up to

$$a = d + (n - 1) w \delta t_A. \tag{8}$$

Consequently, the light trace will cover D ’s entire circumference as soon as

$$n = \frac{U - d}{w \delta t_A} + 1. \tag{9}$$



Fig. 4: Schematic of the experimental set-up: A_1 and A_2 denote the points where the rays generated by the first and the second light pulse hit the disk D at the instants t_1 and t_2 . The circular arc length $A_1B_1 = d$ represents the trace on D 's photosensitive lateral surface the very first pulse causes. $B_1B_2 = \omega \delta t_A$ depicts the trace's length increment produced by the second and any additional pulse according to the propagation hypothesis. The arrow at the bottom indicates the direction of motion of the earth around the sun.

By contrast, if the emission hypothesis is correct, the rays must always impinge on the same spot so that the trace on the disk retains the length d no matter how much the value of n increases, δt_A having to be substituted with δt in equation (8), where $\delta t = t - t = 0$.

Provided that the propagation hypothesis applies, the exact value of a cannot be predicted. For the conventional value of c would be an average that resulted from two-way measurements and thus deviates from the real one-way speed of light. In case the first test indeed gave $a > d$ for $n > 1$, the result should be crosschecked. Rotating the set-up and repeating the experiment would be expected to yield a different value of a at each angle for a given n . Perpendicular to the direction of orbital motion of the earth around the sun, the trace length would then be

$$a_{90^\circ} = d + (n - 1) w \left(\frac{\sqrt{s^2 + V^2 t^2}}{c} - t \right) \quad (10)$$

and at 180°

$$a_{180^\circ} = d + (n - 1) w \left(t - \frac{s \sqrt{1 - \frac{V^2}{c^2}}}{c + V} \right), \quad (11)$$

where $a \approx a_{180^\circ}$. Equations (1) and (11), taking the supposed Lorentz contraction into account, are applicable if the distance LA is measured by means of an etalon. However, considering the necessary magnitude of LA , a travel time measurement using electromagnetic radiation will be conducted in practice. The determined distance

$$s = \frac{cT}{2} = \frac{(c - V + c + V)T}{4} \quad (12)$$

then arises from the signal's two-way speed, with T signifying the total time elapsed between emission and return, the respective instants being measured by one and the same clock. Although the square root factor within equations (1) and (11) must under these premises be omitted, the choice between the two methods of establishing LA is evidently of no significance regarding the validity of the experiment.

Due to the motion of the solar system, the propagation hypothesis involves the assumption that t_A varies seasonally. Therefore, if the first experimental run yields $a = d$ for $n > 1$, a conclusive confirmation of the emission hypothesis will not only demand repetitions of the test at different angles but also reperforming it over an extended period to exclude a misleading result because of V being possibly offset by an unknown velocity component just at the time of the initial measurements.

The outlined experiment avoids the theoretical obstacles which defeated Wilhelm Wien's proposals as merely one uniformly spinning mechanical component is required and attuning a pulsing light source to it does not pose a conceptual problem. The test itself implies no two-way measurement and is neither dependent on assumptions of the Maxwell-Lorentz electromagnetic theory, nor are hypothetical particles used as a radiation source. Thus, Dingle's criteria for a kinematic light experiment are met, and objections against procedures based on a closed light path do not apply [73].

6 Conclusion

We may summarize the proposed *experimentum lucis et crucis* in the following way: since any "in itself determined periodic process realized by a system of sufficiently small spatial extension" [74] is considered to be a timepiece, the de-

scribed set-up consisting of a uniformly spinning disk featuring a photosensitive lateral surface and of a light source pulsing at equal intervals embodies two clocks, their “hands” being successively emitted rays. These “light clocks” run synchronously and thus display real simultaneity. The outcome of the experiment is therefore identical for any observer in any system of reference.

Since the assumption that an ether is dragged by the earth was experimentally refuted [75, 76], no theory reposing on the postulate of constant light velocity relative to pure space or a luminiferous medium in it can explain successive beams impinging on the disk at the same spot. Instead, the emission hypothesis will be fully confirmed. Electromagnetic radiation will have to be understood as a form of energy which is emitted with a real velocity $c + v$, that is the vector sum of a component being invariant relative to the light source and a variable component, the real velocity of this very source. However, according to K. Brecher’s [77] analysis of regularly pulsating x-ray sources in binary star systems, a ballistic interpretation even if it allows for the extinction theorem of dispersion theory, as considered by J. G. Fox [45, 46], seems to be untenable (cf. also [48]). Thus, the *Ritz-Dingle Emanation* or *Vibrating Rays Theory* will remain the only explanation consistent with observation [2–7]. In addition to *classical relativity* holding true for matter in uniform translation, a *classicistic principle* will apply stating that the speed of light stays constant relative to its source even if the latter moves non-rectilinearly and non-uniformly.

Should, on the contrary, successive beams mark a solid line on the disk, the propagation hypothesis would bear the palm. Light would have the characteristics of a wave that propagates in a medium with constant velocity relatively to that medium. The recently renewed question whether there is a resting frame in space [78] would be answered in the affirmative.

Submitted on May 11, 2018

References

- Ritz W. Du rôle de l'éther en physique. *Rivista di Scienza 'Scientia'*, 1908, v. 3 (6), 260–274.
- Bondi H. et al. Meeting of the Royal Astronomical Society, Friday, 1958 November 14, at 16h 30m. *Observatory*, 1958, v. 78 (907), 232–241.
- Dingle H. A Proposed Astronomical Test of the “Ballistic” Theory of Light Emission. *Monthly Notices of the Royal Astronomical Society*, 1959, v. 119 (1), 67–71.
- Dingle H. Relativity and Electromagnetism: An Epistemological Appraisal. *Philosophy of Science*, 1960, v. 27 (3), 233–253.
- Dingle H. A Reply to Professor Grünbaum’s Rejoinder. *British Journal for the Philosophy of Science*, 1961, v. 12 (46), 156–157.
- Dingle H. Reason and Experiment in Relation to the Special Relativity Theory. *British Journal for the Philosophy of Science*, 1964, v. 15 (57), 41–61.
- Bilbao L., Bernal L., Minotti F. Vibrating Rays Theory. arXiv: 1407.5001.
- Ritz W. Recherches critiques sur l'électrodynamique générale. *Annales de chimie et de physique*, 1908, v. 13, 145–275.
- Michelson A. A., Morley E. W. On the Relative Motion of the Earth and the Luminiferous Ether. *American Journal of Science*, 1887, v. 34 (203), 333–345.
- Poincaré H. The Value of Science. The Science Press, New York, 1907.
- Thomson J. J. On a Theory of the Structure of the Electric Field and its Application to Röntgen Radiation and to Light. *Philosophical Magazine*, 1910, v. 19 (110), 301–312.
- Tolman R. C. The Second Postulate of Relativity. *Physical Review*, 1910, v. 31, 26–40.
- Tolman R. C. Some Emission Theories of Light. *Physical Review*, 1912, v. 35, 136–143.
- Stewart O. M. The Second Postulate of Relativity and the Electromagnetic Emission Theory of Light. *Physical Review*, 1911, v. 32, 418–428.
- Ritz W. Recherches critiques sur les théories électrodynamiques de Cl. Maxwell et de H.-A. Lorentz. *Archives des Sciences Physiques et Naturelles*, 1908, v. 26, 209–236.
- Ritz W. Über die Grundlagen der Elektrodynamik und die Theorie der schwarzen Strahlung. *Physikalische Zeitschrift*, 1908, v. 9 (25), 903–907.
- Waldron R. A. The Wave and Ballistic Theories of Light: A Critical Review. Frederick Muller, London, 1977.
- La Rosa M. Fondamenti sperimentali del 2.° Principio della teoria della relatività. *Nuovo Cimento*, 1912, v. 3 (1), 345–365.
- La Rosa M. Über einen Versuch zum Vergleiche der Relativitätstheorie mit den mechanischen Anschauungen über die Lichtausstrahlung. *Physikalische Zeitschrift*, 1912, v. 13 (23), 1129–1131.
- Majorana Q. Experimental Demonstration of the Constancy of Velocity of the Light emitted by a Moving Source. *Philosophical Magazine*, 1919, v. 37 (217), 145–150.
- Michaud F. Les théories émissives et le principe de Doppler-Fizeau. *Comptes rendus de l'Académie des sciences*, 1919, v. 168, 507–509.
- Pauli W. Theory of Relativity. Pergamon Press, London, 1958.
- Tomaschek R. Über das Verhalten des Lichtes außerirdischer Lichtquellen. *Annalen der Physik*, 1924, v. 73, 105–126.
- Miller D. C. Ether-Drift Experiments at Mount Wilson. *Proceedings of the National Academy of Sciences of the United States of America*, 1925, v. 11 (6), 306–314.
- Comstock D. F. A Neglected Type of Relativity. *Physical Review*, 1910, v. 30, 267.
- de Sitter W. A proof of the constancy of the velocity of light. *Proceedings of the Section of Sciences, Koninklijke Akademie van Wetenschappen te Amsterdam*, 1913, v. 15 (2), 1297–1298.
- de Sitter W. Ein astronomischer Beweis für die Konstanz der Lichtgeschwindigkeit. *Physikalische Zeitschrift*, 1913, v. 14 (10), 429.
- de Sitter W. On the constancy of the velocity of light. *Proceedings of the Section of Sciences, Koninklijke Akademie van Wetenschappen te Amsterdam*, 1913, v. 16 (1), 395–396.
- de Sitter W. Über die Genauigkeit, innerhalb welcher die Unabhängigkeit der Lichtgeschwindigkeit von der Bewegung der Quelle behauptet werden kann. *Physikalische Zeitschrift*, 1913, v. 14 (25), 1267.
- Faraday M. Thoughts on Ray-vibrations. *Philosophical Magazine*, 1846, v. 28 (188), 345–350.
- Moon P., Spencer D. E. Binary Stars and the Velocity of Light. *Journal of the Optical Society of America*, 1953, v. 43 (8), 635–641.
- Moon P., Spencer D. E. On the Establishment of a Universal Time. *Philosophy of Science*, 1956, v. 23 (3), 216–229.
- Moon P., Spencer D. E. The New Electrodynamics and its Bearing on Relativity. In: Kritik und Fortbildung der Relativitätstheorie, edited by K. Sapper, 1958, Austria Akademische Druck- und Verlagsanstalt, Graz, 144–159.

34. Moon P., Spencer D.E., Moon E.E. Binary Stars from Three Viewpoints. *Physics Essays*, 1989, v. 2 (3), 275–287.
35. Moon P., Spencer D.E., Moon E.E. Universal Time and The Velocity of Light. *Physics Essays*, 1989, v. 2 (4), 368–374.
36. Thirring H. Über die empirische Grundlage des Prinzips der Konstanz der Lichtgeschwindigkeit. *Zeitschrift für Physik*, 1925 v. 31, 133–138.
37. Bonch-Bruевич A. M. A Direct Experimental Confirmation of the Second Postulate of the Special Theory of Relativity (in connection with Dingle's note). *Optics and Spectroscopy*, 1960, v. 9, 73.
38. Sadeh D. Experimental Evidence for the Constancy of the Velocity of Gamma Rays, Using Annihilation in Flight. *Physical Review Letters*, 1963, v. 10 (7), 271–273.
39. Alväger T., Nilsson A., Kjellman J. A Direct Terrestrial Test of the Second Postulate of Special Relativity. *Nature*, 1963, v. 197 (4873), 1191.
40. Rotz F. B. New Test of the Velocity of Light Postulate. *Physics Letters*, 1963, v. 7 (4), 252–253.
41. Babcock G. C., Bergman T. G. Determination of the Constancy of the Speed of Light. *Journal of the Optical Society of America*, 1964, v. 54 (2), 147–151.
42. Alväger T., Farley F. J. M., Kjellman J., Wallin I. Test of the Second Postulate of Special Relativity in the GeV Region. *Physics Letters*, 1964, v. 12 (3), 260–262.
43. Waddoups R. O., Edwards W. F., Merrill J. J. Experimental Investigation of the Second Postulate of Special Relativity. *Journal of the Optical Society of America*, 1965, v. 55 (2), 142–143.
44. Dingle H. A Re-examination of the Michelson-Morley Experiment. *Visitas in Astronomy*, 1967, v. 9, 97–100.
45. Fox J. G. Experimental Evidence for the Second Postulate of Special Relativity. *American Journal of Physics*, 1962, v. 30 (4), 297–300.
46. Fox J. G. Evidence Against Emission Theories. *American Journal of Physics*, 1965, v. 33 (1), 1–17.
47. Beckmann P., Mandics P. Experiment on the Constancy of the Velocity of Electromagnetic Radiation. *Radio Science Journal of Research*, 1964, v. 68D (12), 1265–1268.
48. Beckmann P., Mandics P. Test of the Constancy of the Velocity of Electromagnetic Radiation in High Vacuum. *Radio Science Journal of Research*, 1965, v. 69D (4), 623–628.
49. Martínez A. A. Ritz, Einstein, and the Emission Hypothesis. *Physics in Perspective*, 2004, v. 6 (1), 4–28.
50. Bilbao L. Does the Velocity of Light Depend on the Source Movement? *Progress in Physics*, 2016, v. 12 (4), 307–312.
51. Wien W. On experiments to decide whether the ether moves with the earth or not. *Observatory*, 1904, v. 27 (349), 360.
52. Wien W. Über einen Versuch zur Entscheidung der Frage, ob sich der Lichtäther mit der Erde bewegt oder nicht. *Physikalische Zeitschrift*, 1904, v. 5 (19), 585–586.
53. Wien W. Experimente zur Entscheidung der Frage, ob sich der Äther mit der Erde bewegt oder nicht. *Physikalische Zeitschrift*, 1904, v. 5 (19), 604–605.
54. Wien W. Experiments to decide whether the Ether moves with the Earth. *Report of the British Association for the Advancement of Science*, 1905, v. 74, 433–434.
55. Cohn E. Zur Elektrodynamik bewegter Systeme. II. *Sitzungsberichte der Königlich Preussischen Akademie der Wissenschaften*, 1904, v. 53, 1404–1416.
56. Foucault L. *Mesure de la vitesse de la lumière, étude optique des surfaces; mémoires de Léon Foucault*. Librairie Armand Colin, Paris, 1913.
57. Fizeau H. Sur une expérience relative à la vitesse de propagation de la lumière. *Comptes rendus hebdomadaires des séances de l'Académie des Sciences*, 1849, v. 29, 90–92.
58. Fizeau H. Sur une expérience relative à la vitesse de propagation de la lumière. *Revue scientifique et industrielle*, 1849, v. 5, 393–397.
59. Wien W. Über die Wandlung des Raum- und Zeitbegriffs in der Physik. *Sitzungsberichte der Physikalisch-medizinischen Gesellschaft zu Würzburg 1909*, 1910, (2,3), 29–39.
60. Wien W. Die Relativitätstheorie. In: *Taschenbuch für Mathematiker und Physiker*, Bd. 2, edited by F. Auerbach and R. Rothe, B. G. Teubner, Leipzig and Berlin, 1911, 283–292.
61. Dingle H. A Possible Experimental Test of Einstein's Second Postulate. *Nature*, 1959, v. 183 (4677), 1761.
62. Dingle H. An opportunity to check on Einstein. *New Scientist*, 1959, v. 5 (133), 1253.
63. Dingle H. Ritz theory of light. *Observatory*, 1959, v. 79 (910), 106–107.
64. Dingle H. The Falsifiability of the Lorentz-FitzGerald Contraction Hypothesis. *British Journal for the Philosophy of Science*, 1959, v. 10 (39), 228–229.
65. Dingle H. A Radio-astronomical Test of the Ballistic Theory of Light Emission. *Observatory*, 1960, v. 80 (914), 35–36.
66. Dingle H. The Doppler Effect and the Foundations of Physics (I). *British Journal for the Philosophy of Science*, 1960, v. 11 (41), 11–31.
67. Dingle H. The Doppler Effect and the Foundations of Physics (II). *British Journal for the Philosophy of Science*, 1960, v. 11 (42), 113–129.
68. Dingle H. Special Theory of Relativity. *Nature*, 1962, v. 195 (4845), 985–986.
69. Dingle H. *Science at the Crossroads*. Martin Brian & O'Keefe, London, 1972.
70. Eddington A. S. *The Mathematical Theory of Relativity*. The University Press, Cambridge, 1923.
71. Ohanian H. C. *Einstein's mistakes: the human failings of genius*. W. W. Norton & Co., New York, 2008.
72. Giovannini D., Romero J., Potoček V., Ferenczi G., Speirits F., Barnett S. M., Faccio D., Padgett M. J. Spatially structured photons that travel in free space slower than the speed of light. *Science*, 2015, v. 347 (6224), 857–860.
73. Pérez I. On the experimental determination of the one-way speed of light. *European Journal of Physics*, 2011, v. 32 (4), 993–1005.
74. Einstein A. *Autobiographical Notes*. In: *Albert Einstein: Philosopher-Scientist*, edited by P. A. Schilpp, The Library of Living Philosophers, Evanston, IL, 1949, 2–94.
75. Michelson A. A. The Effect of the Earth's Rotation on the Velocity of Light, Part I. *Astrophysical Journal*, 1925, v. 61 (3), 137–139.
76. Michelson A. A., Gale H. G., Pearson F. The Effect of the Earth's Rotation on the Velocity of Light, Part II. *Astrophysical Journal*, 1925, v. 61 (3), 140–145.
77. Brecher K. Is the Speed of Light Independent of the Velocity of the Source? *Physical Review Letters*, 1977, v. 39 (17,19), 1051–1054, 1236.
78. Chang D. C. Is there a resting frame in the universe? A proposed experimental test based on a precise measurement of particle mass. *European Physical Journal Plus*, 2017, v. 132, 140.

Fractional Degrees of Freedom in Statistics

Mikhail N. Mashkin

E-mail: mnmashkin@yandex.ru

The concept of observation and presentation of the count (reference) results in an interval form is considered. The transition to interval measurements is achieved by use of the total reduced number of measurements (number of degrees of freedom) as a sample parameter, which allows the use of non-integer (fractional) powers of freedom in the calculation of the estimates of static parameters and criteria values. The replacement of single measurements with interval measurements at their same quantities in all cases reduces the accuracy of statistical parameters estimates.

Introduction

Currently, there are known applications of fractional powers in statistics [1]. However, the use of different methods of data processing, in particular for small samples [2] and for processing with the use of methods similar to the method of group accounting arguments [3], allows to broaden their use in calculations.

The concept of observation

According to [4], observation is the experimental basis of scientific research. Observed results are most often recorded in the form of meanings of the measured values or their counts. For static methods of measurement, the result is a single number. With dynamic methods, it is possible to record the measured value in time as the implementation of a random (non-random) process. In the latter case, the results of measurements often are the evaluations of the process parameters. In both cases, statistical stability is a prerequisite, which in particular consists, in the approximation, with a sufficiently large number of observations* to the probability of a given value. In all cases, if the measurement of the value is repeated many times, the result is a statistical distribution series corresponding to any distribution law, which may be associated with the error of the measuring system or instrument.

Each single measurement (count), as well as their totality, gives an empirical distribution, which is described in the form of a histogram, statistical series, empirical distribution function, etc. In this case, along with the above, it is necessary to specify the number of measurements, i.e. empirical description requires specifying the number of experiments (sample size) on the basis of which it is obtained. We will refer to the number of measurements, on the basis of which the empirical description of the distribution law is obtained, as the number of degrees of freedom. However, there are measured values, which, by their nature, initially have a form corresponding to a certain distribution law [5]. In this case, the measured value is set not by a value, which is constant or changing in time, but by an area at each point of which it can be located with a

*The ratio of the number of observations of a particular value to the total number of observations.

certain probability. This allows each measurement to match the area of the measured value with the law of its distribution.

The area of determination of the value can be set with one or more than one interval, see Fig. 1. One dimension gives the area and the value of the parameters' estimates of the distribution law.

Interval measurements

Let us consider the basic prerequisites for using intervals as measurement results.

The possibility to express numerical values of quantities in the form of intervals is used in the theory of intervals [6]. The basic idea of interval analysis is that you can work with intervals as with plain numbers. Common operations such as addition, subtraction, multiplication and division, as well as set theory operations such as intersection and union, are quite applicable to them. Interval operations are described by a ratio:

$$A @ B = \{ x @ y | x \in A, y \in B \}, \tag{1}$$

where @ is one of the operations {+, -, *, /, ∪, ∩}, while A, B are intervals.

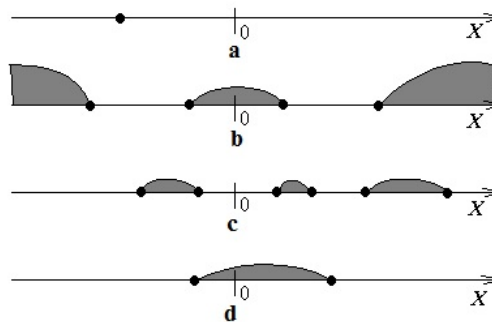


Fig. 1: Types of areas for determining the measurement value: a — one observation — a single numerical value; b — one observation — a set of intervals of numerical values, including those that are not limited to the left or to the right; c — one observation — a set of intervals strictly limited to the left and to the right; d — one observation — one interval of numerical values with one border to the left and one to the right.

A single (real) number can be viewed as that an interval having a definition domain and the law of distribution in the form of a certain event probability:

$$P(a \in [a, a]) = 1, \quad a = [a, a], \quad (2)$$

i.e. just one numerical value is sufficient for the description of the measured value.

Let us consider the measurement process of the diameter of a bearing ring as an example of a measurement that has a definition area of one interval. The measurement of the radius of the hole or the outer diameter (done with sufficiently accurate instruments) relative to the calculated center of the bearing ring gives the dependence of the radius to the point on the circumference surface of the hole or the outer diameter in the form of a realization of a random process that can be described by a random function like follows:

$$R = X(\alpha), \quad (3)$$

where $0 \leq \alpha \leq 2\pi$ is the bearing ring angle of rotation.

Accurate lab instruments such as circular gauges allow us to fully record the kind of realization of a random process. Obviously, when such a record exists, it can be processed by well known methods of the theory of random processes. In production conditions, the use of precision instruments is impractical. The control devices used allow to quite precisely measure the diameter of a bearing ring. During the rotation of the bearing ring it is also possible to determine the maximum and minimum values of the diameter of the bearing. If we limit ourselves to only two of these values, then actually we come to a case of two independent observations. The information that there are other numerical values of the diameter, between these two values, becomes thus lost. For a more complete explanation of the essence of the observation, it is proposed to consider the considered measurement process as a single observation in the form of one interval, Fig. 1, d. The value of the measured diameter has a description in the form of a statistical series at a given interval:

$$\hat{P}(d : d \in [d_{\min}, d_{\max}]), \quad (4)$$

where d is the value of the bearing ring diameter.

With an interval measurement, however, there are two degrees of freedom: the measurements of one and the other border of the interval. However, these two dimensions are considered together over the interval. For example, one dimension is a border, and the other is the interval value itself, that is, there is a relationship: for the first dimension, the entire numerical axis is available, and the second dimension describes the area of the finite length bound to the first measurement. The availability of the entire numerical axis here must be understood as a possibility to represent the first measurement only by selecting the initial value of the reference point by any number, including almost infinity. For the

interval, whatever we choose as the reference point, its value remains constant. From this we can assume that the specified relationship as if reduces the number of degrees of freedom of choice of numerical values for the interval measurement. We can assume that it is less than two, but more than one. Interval measurement generally gives the values of the borders of intervals and parameters or their estimates of the distribution law. This can be described by displaying the interval in parameters' values:

$$G : [a_i b_i] \xrightarrow{P} \{\beta_j : j = 1, \dots, k\}, \quad (5)$$

where G displays the set of numerical values of the interval measurement in the values of parameters or their estimates of the probability distribution law; a_i, b_i are borders of the i -th interval; P is the law of distribution of values of a random variable from the interval; β_j is the value or estimate of a parameter of the distribution law.

It should be noted that the borders of the interval can be displayed in the parameters of the distribution law explicitly (for example, the boundaries of the interval in the case of the law of equal probability density) or indirectly as the area of definition of this law.

One of the options for describing the distribution law P is the probability density. By the given probability density or histogram it is possible to calculate or to estimate the parameters of the distribution law. The previously declared commonality for the interval and for one number (2) allows these calculations to be applied for one number obtained during the measurement. Let us illustrate this by calculating the dispersion of a single observation.

Calculation of the dispersion estimation of one observation by known relations [1] can be performed by the formula:

$$\hat{\sigma}_x^2 = \frac{\sum_{i=1}^n (x_i - m_x)^2}{n} = \frac{(x - m_x)^2}{1} \quad \text{if } m_x \text{ is known,} \quad (6)$$

where m_x is the mathematical expectation; x is the numerical value of the dimension.

For one number from the interval with coinciding borders, formula (6) is valid, because the mathematical expectation does not require an evaluation, but is equal to the number itself. The value of the dispersion estimate in this case is zero. This clearly indicates the non-randomness of the interval representation of the same number, i.e., the specific meaning of the measured value does not have a random component — it is a non-random value.

Calculation of the dispersion estimate for an interval measurement in the extreme case can be performed as that for two independent observations by formulas:

$$\hat{\sigma}_x^2 = \frac{(b - m_x)^2 + (a - m_x)^2}{1}, \quad \text{if } m_x \text{ is unknown,} \quad (7)$$

$$\hat{\sigma}_x^2 = \frac{(b - m_x)^2 + (a - m_x)^2}{2}, \quad \text{if } m_x \text{ is known.} \quad (8)$$

It can be assumed that the value of the dispersion estimate for the interval for each case, due to the lower value of the degrees of freedom, should exceed the values given by formulas (7) and (8). In addition, within the interval, the measured numerical values of the value are determined by its distribution law. If we choose as the basic one the law of equal probability density (EPD), then we lead the rest of the distributions to it by changing the value of the interval on the basis of equality of the entropy value.

Let us define the given number of measurements (degrees of freedom) for an interval measurement in the form of:

$$r_i = 1 + \Delta_i, \quad 1 \geq |\Delta_i| \geq 0; \tag{9}$$

where

$$\Delta_i = \begin{cases} +\Delta_{is}, & \text{boundaries are given from experience;} \\ -\Delta_{is}, & \text{one boundary is given by the researcher;} \\ -1, & \text{boundaries are given randomly.} \end{cases}$$

The value Δ_{is} can be determined by formula:

$$\Delta_{is} = \begin{cases} \frac{1}{1 + 1/h_{is}}, & \text{at } b_i, a_i \neq 0; \\ 0, & \text{at } b_i, a_i = 0; \end{cases} \tag{10}$$

where

$$h_{is} = \frac{b_i - a_i}{\frac{1}{2} |a_i + b_i|}$$

is chosen for the EPD law and

$$h_{is} = \frac{(b_i - a_i) H_x}{H_{EPD} |M[X_{[a,b]}]|}$$

is chosen for any other law of the distribution of x along the interval $[a_i, b_i]$;

$$H_x = M \left[\log P(X = x_j \in [a_i b_i]) \right] = - \sum_{j=1}^n P(X = x_j) \log P(X = x_j)$$

is chosen if the given measured value is discreet*;

$$H_x = M [\log P(f(x))] = - \int_{a_i}^{b_i} f(x) \log_c f(x) dx$$

is taken at $c < (b_i - a_i)$ if the measured value is continuous (relative entropy);

$$H_{EPD} = \log n_{[a,b]}$$

if the discrete measured value is distributed equally possible within the interval, where $n_{[a,b]}$ is the number of equally possible states in the interval;

$$H_{EPD} = \log_c (b_i - a_i)$$

*The given relations for determination of $H_{\#}$ are similar to entropy formulas, and for the case of discrete measured values exactly coincide with them.

if within the interval the measured value is distributed according to the EPD law;

$$M [X_{[a,b]}]$$

is the mathematical expectation of the measured value in the interval $[a_i, b_i]$.

The total reduced number of measurements, the value for the calculation of statistical parameters for the sample, is equal to:

$$n_r = \sum_{i=1}^n r_i. \tag{11}$$

This assumes that, when creating a statistical series of distributions or histograms, each interval dimension must have its own share proportional to the value of r_i . If it is 0, this dimension is ignored. If it differs from zero, then this contribution, as the number of measurements (experiments), is equal to its value.

Formulas for calculation of the main estimates of statistical parameters for one, i -interval measurement, in the case of the EPD law for the measured value within the interval, have the form:

$$\hat{m}_{x_i} = \frac{b_i + a_i}{2}; \tag{12}$$

$$\hat{\sigma}_{r_i}^2 = \frac{(b_i - \hat{m}_{x_i})^2 + (a_i - \hat{m}_{x_i})^2}{r_i - 1} = \frac{(b_i - a_i)^2}{2(r_i - 1)}. \tag{13}$$

Example. With a rectangular contribution (EPD), let us define by formula (13) the estimate of the variance in the interval of an i -th observation for different ratios of the value of the interval and the values of its mathematical expectation, see Table 1.

Left border of the interval, a_i	Right border of the interval, b_i	Math. expectation estimate, \hat{m}_{x_i}	Reduced no. of measurements, r_i	Estim. variance, $\hat{\sigma}_{r_i}^2$ (13)
-4	4	0	2	32
-3	5	1	1.889	36
-2	6	2	1.8	40
-1	7	3	1.727	44
0	8	4	1.667	48
1	9	5	1.615	52
2	10	6	1.571	56
...
30	38	34	1.190	168

Table 1: Dispersion (variance) estimation via the given number of measurements.

Analysis of Table 1 shows that in the symmetric interval (the case when the estimate of the mathematical expectation is 0), the variance estimate coincides with the value calculated by formula (7) for two unit measurements. As the value

of mathematical expectation increases, the variance value increases due to the reduction of the reduced number of measurements, which can be taken as the number of degrees of freedom of the resulting measurement.

Taking into account the above, a single measurement can be considered as an interval measurement when the interval is equal to the rounding error of the instrument readings. In this case, a fairly small relative error gives the reduced number of measurements equal to 1.

Contributions method

To process the results of a small sample in the evaluation of the distribution laws, the contribution method is used [2, 6]. This approach allows us to obtain a paradoxical result: due to the empirical selection of the width of the interval of a rectangular or other contribution, the accuracy of the assessment increases. The paradox is that, by coarsening the measurement results (the numbers are replaced by fixed-width intervals), the accuracy of statistical parameters is allegedly improved.

When using the formalism published in the work [2], the proposed estimation formula for the method of contributions for the probability density is:

$$\tilde{f}(x) = \frac{\sum_{i=1}^n r_i \cdot p_i(x, a_i, b_i)}{\sum_{i=1}^n r_i}, \tag{14}$$

where n is the number of observations; $p_i(x, a_i, b_i)$ is a generalized record of the empirical component of the distribution density associated with the interval of i -th observation (having all the properties of the distribution density), describes the law of distribution of measurements in the interval. Unlike the work [2], empiricism is limited by the choice of the distribution law in the interval. And there are two options:

1. The distribution law is the same for all intervals;
2. For each interval, its own law of distribution is picked.

For the case of the EPD law in the interval we have:

$$p_i(x, a_i, b_i) = \frac{1}{b_i - a_i}, \quad a_i \leq x \leq b_i. \tag{15}$$

The work [7] presents a formula which uses the method of contributions for the empirical component of density estimation in the form of:

$$f_N^*(x) = C(\rho) \sum_{i=1}^N \mu_i \psi_i(\rho, x), \tag{16}$$

where the ρ parameter is equal to half of the contribution interval, $\rho = \frac{b_i - a_i}{2} = const$, that is, the interval in all dimensions is the same;

$$C(\rho) = \left(\int_{-\rho}^{\rho} \psi_i(\rho, x) dx \right)^{-1}, \tag{17}$$

the amplitude ensures the equality of each contribution 1; $\mu_i = 1/N$ is weight (the ratio for norming density estimation); and also

$$\psi_i(\rho, x) = \begin{cases} 1, & x_i - \rho \leq x \leq x_i + \rho; \\ 0, & \text{for others } x. \end{cases} \tag{18}$$

Let us consider the use of formulas (14) and (16) for Example 2.1 from the work [7].

Example 2.1 [7]. As a result of measurement of parameter X of three products after adjustment of the equipment, the following results were obtained: 6.0; 6.4; 6.6. Let us estimate the empirical density that characterizes the quality of the equipment setup.

Some assumptions must be made to calculate by (16). Let us suppose that. Let us suppose that $\mu_i = 1/N = 1/3 = 0.3$.

Then by formula (17)

$$C(\rho) = \left(\int_{-0.3}^{0.3} \psi_i(\rho, x) dx \right)^{-1} = \frac{1}{0.6} \approx 1.67.$$

Summing the kernels (contributions) $\psi_i(\rho, x)$ for all $i = 1, 2, 3$ with amplitudes of 1.67 and weights 1/3, we obtain

$$f_N^*(x) = \begin{cases} 0.56, & 5.7 \leq x < 6.1; \\ 1.11, & 6.1 \leq x < 6.7; \\ 0.56, & 6.7 \leq x \leq 6.9; \end{cases} \tag{19}$$

(see Fig. 2):

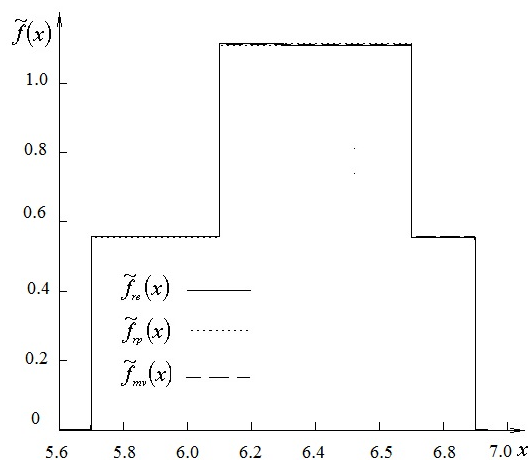


Fig. 2: Empirical estimates of the probability density, Example 2.1.

Using formula (14), the example data can be interpreted as follows: three intervals are used as input: [5.7; 6.3], [6.1; 6.7], [6.3; 6.9]. The length of each interval is equal to 0.6. The distribution law within the interval is EPD. The distribution density is equal to:

$$p_i(x, a_i, b_i) = 1/0.6; \quad a_i \leq x \leq b_i. \tag{20}$$

N/N i/o	Left border of the interv., a_i	Right border of the interv., b_i	Math. expec- tated estim., \hat{m}_{x_i}	Reduced number, r_i	
				Both borders are expe- rim., r_{ie}	One bor- der is set by the re- searcher, r_{ip}
1	5.7	6.3	6	1.091	0.909
2	6.1	6.7	6.4	1.086	0.914
3	6.3	6.9	6.6	1.083	0.917
Total:				3.26	2.74

Table 2: The reduced number of measurements by intervals, Example 2.1.

The calculated numerical values according to formula (9) of the given numbers of measurements for each the interval are shown in Table 2.

The total number of measurements calculated by formula (11) is equal to:

$$n_{re} \sum_{i=1}^n r_{ie} = 3.26$$

if all parameters of the interval are obtained experimentally (experimental data);

$$n_{rp} \sum_{i=1}^n r_{ip} = 2.74$$

if one of the interval's limits is specified by the researcher (a priori data).

Hence, the estimated values for the probability density (14) with account of contributions (18) look like these:

$$\tilde{f}_{re}(x) = \Delta_{f1}^{re} + \Delta_{f2}^{re} + \Delta_{f3}^{re} \text{ for experimental data,} \quad (21)$$

$$\tilde{f}_{rp}(x) = \Delta_{f1}^{rp} + \Delta_{f2}^{rp} + \Delta_{f3}^{rp} \text{ for a priori data,} \quad (22)$$

$$\tilde{f}_{mv}(x) = \Delta_{f1}^{mv} + \Delta_{f2}^{mv} + \Delta_{f3}^{mv} \text{ for a small sampling,} \quad (23)$$

where

$$\Delta_{f1}^{re} = 0.558, \quad \Delta_{f2}^{re} = 0.555, \quad \Delta_{f3}^{re} = 0.554;$$

$$\Delta_{f1}^{rp} = 0.553, \quad \Delta_{f2}^{rp} = 0.556, \quad \Delta_{f3}^{rp} = 0.558;$$

$$\Delta_{f1}^{mv} = 0.556, \quad \Delta_{f2}^{mv} = 0.556, \quad \Delta_{f3}^{mv} = 0.556;$$

are contribution of the intervals, while i is the interval number,

$$\Delta_{fi}^{\#} = \begin{cases} \Delta_{hi}, & a_i \leq x \leq b_i; \\ 0, & a_i > x > b_i; \end{cases}$$

is a contribution of the i -th interval under $\#$ (here re means "experimental", rp means "a priori", mv means "calculated by data method" [7]);

$$\Delta_{hi} = \frac{r_{i\#}}{n_{\#} \cdot (b_i - a_i)}$$

N/N i/o	Left border of the interv., a_i	Right border of the interv., b_i	Math. expec- tated estim., \hat{m}_{x_i}	Reduced number, r_i	
				Both borders are expe- rim., r_{ie}	One bor- der is set by the re- searcher, r_{ip}
1	5.56	6.44	6	1.128	0.872
2	5.96	6.84	6.4	1.121	0.879
3	6.16	7.04	6.6	1.118	0.882
4	5.0	7.2	6.1	1.265	0.735
Total:				4.631	3.369

Table 3: The reduced number of measurements by intervals of Example 2.2.

Interv. no.	Contribution height:		
	Experim. data	A priori data	Small sampl.
1	0.277	0.294	0.284
2	0.275	0.297	0.284
3	0.274	0.298	0.284
4	0.124	0.099	0.114

Table 4: Height of contributions for Example 2.2.

is the height of the i -th contribution; $n_{mv} = 3$ is number of intervals; $r_{imv} = 1$ is the value of the method contribution [7].

The graphs of probability density estimation for dependencies (21–23) are shown in Fig. 2.

Let us also consider Example 2.2 [7], in which, along with the intervals of Example 2.1, an interval different from the others by length is included.

Example 2.2 [7]. Let us assume that in the conditions of Example 2.1 there is a priori information in the form of an interval [5.0; 7.2]. Let us calculate the estimates of the probability density. The length of the interval for readings 6.0; 6.4 and 6.6 is calculated [7] equal to 0.88, i.e. $\rho = 0.44$.

The given numbers of measurements (9) for each the interval are shown in Table 3.

The estimated probability density values in this case is:

$$\tilde{f}_{re}(x) = \sum_{i=1}^4 \Delta_{fi}^{re} \text{ for experimental data,} \quad (24)$$

$$\tilde{f}_{rp}(x) = \sum_{i=1}^4 \Delta_{fi}^{rp} \text{ for a priori data,} \quad (25)$$

$$\tilde{f}_{mv}(x) = \sum_{i=1}^4 \Delta_{fi}^{mv} \text{ for small sample contributions.} \quad (26)$$

The heights of contributions for the intervals are shown in Table 4.

Probability density estimates for dependencies (24–26) are shown in Fig. 3.

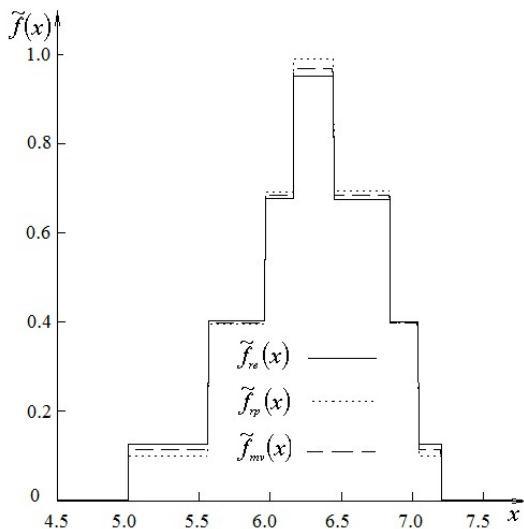


Fig. 3: Empirical estimates of probability density of Example 2.2.

surements. In work [7] the number of experiments is equal to the number of intervals. The results of mathematical expectation and variance estimates for Examples 2.1 and 2.2, with taking different approaches into account (determination of the number of experiments as the number of intervals, or the use of the reduced number of measurements instead) are given in Table 5.

Analysis of the results displayed in Table 5 allows us to make the main conclusion: replacement of single measurements with interval measurements at the same numbers in all cases reduces the accuracy of estimates of statistical parameters. This follows from the fact that single measurements, rather than interval measurements, have the lowest variance. The application of interval measurements allows to expand the possibilities of statistical processing of measuring information. It is essential to use as a sample parameter the total reduced number of measurements (number of degrees of freedom), which allows the use of non-integer (fractional) degrees of freedom in the calculation of estimates of static parameters and criteria values.

Submitted on May 17, 2018

Types of data	Measure-ment char-acteristics	Esti-mates	Examples	
			2.1	2.2
Discrete	Borders of the interval	n	—	5
		ME	—	6.24
		D	—	0.668
Discrete	Average va-lues of the intervals	n	3	4
		ME	6.333	6.275
		D	0.093	0.076
Interval	Experimen-tal	n_r	3.26	4.631
		ME	6.333	6.269
		D	0.133	0.272
Interval	A priori	n_r	2.74	3.369
		ME	6.334	6.283
		D	0.145	0.279
	Small sam-ples	n	3	4
		ME	6.333	6.275
		D	0.138	0.275

Table 5: The reduced number of measurements by intervals of Example 2.2. The following designations are used here: ME — the mathematical expectation, D — the dispersion (variance), n — the number of experiments or intervals (for a single measurement, when the borders of the interval coincide, the number of intervals is equal to 1), n_r — the total given number of measurements.

Results

The reduced estimates of probability densities, Fig. 2 and Fig. 3, can be used in practical applications only when specifying for each of them the number of observations (experiments), which can be considered as the number of degrees of freedom, see formula (11) for the reduced number of mea-

References

1. Bomas V.V., Bulygin V.S., Mashkin M.N. Probability Theory and Mathematical Statistics: Lectures. Moscow, Potok Publ., 2000 (*in Russian*).
2. Hahulin G.F. Principles of Designing Simulation Models: A Tutorial. Moscow, Potok Publ., 2001 (*in Russian*).
3. Ivakhnenko A.G. Heuristic Self-Organization Systems in Technical Cybernetics. Kazan, Technika, 1971 (*in Russian*).
4. Mitropolsky A.K. Technique of Statistical Calculations. Moscow, Nauka, 1971 (*in Russian*).
5. Gurney R.W. Elementary Quantum Mechanics, Cambridge University Press, 1934.
6. Knyazev G.N., Korzenev G.N. Graphic implementation in the architecture of the basic laws of management. In: *Effectiveness of Scientific Research RosZITLP*, Vol. 1, Moscow, Roszitlp Publ., 1997, pp. 41–45 (*in Russian*).
7. Gaskarov D.V., Shapovalov V.I. Small Samples. Moscow, Statistica, 1978, pp. 31–35 (*in Russian*).

Seeliger’s Gravitational Paradox and the Infinite Universe

Leonardo Sarasúa

EPO, 2288EE, Rijswijk, The Netherlands. E-mail: leosarasua@gmail.com

Seeliger’s paradox is often regarded as an argument against Newtonian potentials in an infinite universe. In this paper the argument is analyzed with the help of Riemann’s series theorem. This theorem reveals that the paradox is a known consequence of the rearrangement of conditionally convergent series or integrals, and so it demonstrates that the same situation would arise with almost any other type of gravitational force law. Therefore Seeliger’s argument is not a valid proof against Newton’s inverse square law or even an infinite universe.

1 Introduction

In 1895 the German astronomer Hugo Seeliger published an article [1] in which he revealed an apparent flaw in Newton’s law of gravitation, which may lead to “unsolvable contradictions”. His reasoning can be presented as follows.

Let’s suppose a boundless universe with a (near) homogeneous distribution of matter. For simplicity, let’s assume this to be a continuous mass distribution, which extends uniformly to infinity in all directions. To calculate the gravitational force exerted by this infinite universe on a test particle with gravitational mass m located at a point P , we consider all the masses in the universe as arranged in thin concentric spheres centered in P . Since the Newtonian attraction of a sphere on any point located inside of it is zero, we find that the sum of all the concentric spheres extending to an infinite distance will be zero. This is what might be expected from symmetry.

Next, let’s calculate the force again, but this time using a coordinate system centered at another point Q , located at an arbitrary distance d from m . In order to calculate the force, we divide the universe into two parts. The first one is the sphere of radius d centered on Q and passing through P . The mass of this sphere is $M = \frac{4}{3}\rho\pi d^3$, where ρ is its density, which attracts the material point m with a force given by $F = -\frac{GMm}{d^2} = \frac{4}{3}\rho\pi d^3$ pointing from P to Q . The second part is the remainder of the universe. This remainder is composed of a series of external shells also centered on Q containing the internal test particle m . As we have seen above, this second part exerts no force on m . Therefore the force exerted by the universe calculated in this way is proportional to the distance d and directed towards Q .

This means that depending on which point Q we choose, we obtain a different value for the force acting on m . The conclusion that Seeliger extracts from this puzzling result is that either the universe cannot be infinite, or that Newton’s law of attraction must be modified. Taking the latter choice, he proposed to add an absorption factor $e^{-\lambda r}$ to the force of gravity

$$F_{Seeliger} = -G \frac{mm'}{r^2} e^{-\lambda r} \tag{1}$$

where λ is an arbitrary parameter, sufficiently small to make

this force compatible with the existing observational data.

When (1) is used, it can be demonstrated [2] that the gravitational force exerted on a particle m at the surface of a spherical volume V_1 uniformly filled with matter is equal and opposite to the gravitational force exerted on the particle by all the infinite concentric uniform spherical shells outside the first spherical volume V_1 , so that the net force acting on the particle is zero. Seeliger thus believed to have found a solution of the paradox.

The purpose of this paper is to generalize the formulation of the problem and to show that Seeliger’s conclusion does not hold.

2 Newton’s inverse square law and its relation to the paradox

Before getting at the origin of the paradox, let’s look at different ways to formulate it.

First we note that Seeliger uses the fact, unique to the inverse square law, that the attraction of a sphere to any mass inside of it is zero. To demonstrate that this is not an essential feature, we will present the paradox from a different perspective.

Let’s calculate the gravitational field of an infinite plane. Let ρ denote the mass density per unit area of this infinite plane and consider a test particle of mass m located at a distance h from the plane, as shown in the following figure.

In Newtonian terms, the incremental force dF on this par-

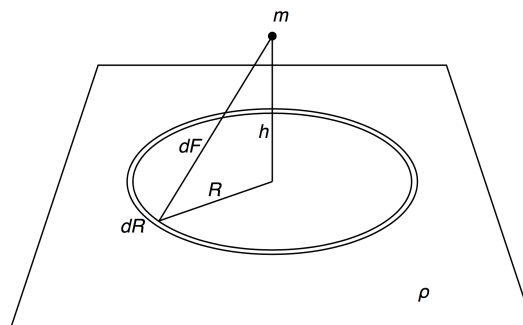


Fig. 1: Attraction of an infinite plane on a mass m .

ticle contributed by an annular ring of radius R and incremental width dR is just the projection onto the perpendicular of the forces exerted by each element of the plane around the circumference of the annular region. Thus we have:

$$dF = \frac{Gm\rho}{h^2 + r^2} [\pi(R + dR)^2 - \pi R^2] \left(\frac{h}{\sqrt{h^2 + R^2}} \right).$$

Expanding this expression and ignoring second order differential terms, we get

$$dF = 2\pi Gm\rho h \frac{R}{(h^2 + R^2)^{\frac{3}{2}}} dR.$$

Integrating from $R = 0$ to ∞ , we find that the total force experienced by the particle is

$$F = 2\pi Gm\rho h \int_0^\infty \frac{R}{(h^2 + R^2)^{\frac{3}{2}}} dR = 2\pi Gm\rho.$$

Thus the force exerted on the particle is independent of the distance h from the plane. Adding more planes to form a slab of thickness a , we get that the force would be in this case:

$$F = 2\pi Gm\rho a.$$

Grouping infinite parallel slabs of the same thickness a and adding the contribution of each of them, we get the force of the universe acting on particle m

$$F = \sum_{-\infty}^{\infty} 2\pi Gm\rho a. \tag{2}$$

It can be shown that this infinite sum will yield a different result depending on how it is calculated. As a first way of determining the value of (2), let's pair each slab with its corresponding symmetrical one around the plane of origin. If we consider this plane as the plane xy , then we take a parallel slab of coordinate z_0 and pair it with the slab of coordinate $-z_0$. Since the force of each slab in the pair is equal and opposite, their sum vanishes. The total force (2) will thus be zero. Analytically, we can write this as

$$F = (2\pi G\rho ma - 2\pi G\rho ma) + (2\pi G\rho ma - 2\pi G\rho ma) + \dots = 0. \tag{3}$$

Next, let's calculate (2) again but this time starting one slab further from m . The total force on m will be the sum of the force due to this separate slab, which contains m on one of its surfaces, plus all the remaining slabs in the universe, on both sides of the first slab, thus

$$F = 2\pi G\rho ma_0 + \sum_{n=-\infty}^0 2\pi G\rho ma_n - \sum_{n=1}^{\infty} 2\pi G\rho ma_n$$

where $n = 0$ represents the separate slab. Since the terms

$$\sum_{n=-\infty}^0 2\pi G\rho ma_n - \sum_{n=1}^{\infty} 2\pi G\rho ma_n$$

are paired one to one as in (3), they cancel each other out and the result is zero. Therefore the total force on m will be $F = 2\pi G\rho ma$, which is an arbitrary value, since a has been arbitrarily chosen.

This new version of the paradox does not use the fact that the potential is null inside a sphere and yet, as in Seeliger's original version, it can return any arbitrary value. It is possible in fact to prove that the paradox occurs with a wide range of forces other than Newton's inverse square law. With Newton's law, the force of each slab is independent of the distance, thus the force exerted by each of the layers is the same and cancels out with another slab located symmetrically from the given particle. However, if we had a different force law in which the gravitational force of each slab were dependent on the distance, we still would be able to repeat the previous calculation by choosing for each slab a suitable thickness so as to exactly balance another slab at the opposite side of the particle, provided that the sum of the forces diverged.

3 Riemann series theorem

In 1827, mathematician Peter Lejeune-Dirichlet discovered the surprising result that some convergent series, when rearranged, can yield a different result [3]. Based on this discovery, another German mathematician, Bernhard Riemann published in 1852 a theorem [3], known today as *Riemann's series theorem* (or *Riemann rearrangement theorem*), proving that in general, infinite series are not associative, that is, they cannot be rearranged.

According to this theorem (see for example [4]), an *absolutely* convergent series will always give the same result, no matter how it is rearranged. However, a *conditionally* convergent series, by a suitable permutation of its elements, can take any arbitrary value or even diverge.

Let's review some definitions. A series converges if there exists a value ℓ such that the sequence of the partial sums

$$\{S_1, S_2, S_3, \dots\}, \text{ where } S_n = \sum_{k=1}^n a_k$$

converges to ℓ . That is, for any $\epsilon > 0$, there exists an integer N such that if $n \geq N$, then

$$|S_n - \ell| \leq \epsilon.$$

A series $S_n = \sum_{n=1}^{\infty} a_n$ converges *absolutely* if $S_n = \sum_{n=1}^{\infty} |a_n|$ converges. A series $S_n = \sum_{n=1}^{\infty} a_n$ converges *conditionally* if it converges but the series $S_n = \sum_{n=1}^{\infty} |a_n|$ diverges.

Riemann's series theorem can be directly extrapolated to conditionally convergent integrals (see for example [5]).

In the case of Seeliger's paradox, we note first that although the masses in the universe should be treated as discrete, Seeliger for simplicity turns them into a homogeneous mass distribution throughout the universe, thus formulating it in terms of integrals instead of series. Like Seeliger, we will

work with a continuous mass distribution, but bearing in mind that the problem is actually discrete.

Considering a uniform mass distribution with a volume density ρ , and using a spherical coordinate system (r, θ, ϕ) centered on m , we have that, according to Newton's law, the component of the total force exerted on a particle m along the x axis is

$$F_x = -Gm \int_{r=0}^{\infty} \int_{\theta=0}^{\pi} \int_{\phi=0}^{2\pi} \rho \sin \phi \cos \phi \, d\phi d\theta dr, \quad (4)$$

and similarly for the other axes.

Since the integral is only conditionally convergent, we have to pay attention to the order in which we calculate the multiple integral. In this case, our goal is to integrate sequentially the shells around the test mass, starting from $r = 0$ and extending to $r = \infty$, thus we have to integrate first over the variables θ and ϕ and only then over r . Note therefore that (4) is not necessarily equal to

$$F_x = -Gm \int_{\phi=0}^{2\pi} \int_{\theta=0}^{\pi} \int_{r=0}^{\infty} \rho \sin \phi \cos \phi \, dr d\theta d\phi.$$

We solve the integral (4)

$$\begin{aligned} F_x &= -Gm \int_{r=0}^{\infty} \int_{\theta=0}^{\pi} \int_{\phi=0}^{2\pi} \rho \sin \phi \cos \phi \, d\phi d\theta dr \\ &= -Gm \int_{r=0}^{\infty} \int_{\theta=0}^{\pi} \rho \left[\sin \left(\frac{-\cos^2 \phi}{2} \right) \right]_{\phi=0}^{2\pi} d\theta dr = 0, \end{aligned}$$

which, again, is what could be expected from symmetry. Following Seeliger's procedure, we can calculate the integral in a different way by splitting the space into a sphere of radius a , centered in a point Q separated from m by a distance a , so that the test mass lies on its surface, and concentric shells also centered in Q containing the particle in their interior. In other words, the contribution of every mass in the universe is added but in a different order. Thus the integral is rearranged, which is what Riemann's theorem warns us against. Taking Q as the origin of coordinates, the x component of the force will be

$$F_x = -\frac{GmM}{a^2} - Gm \int_{r=0}^{\infty} \int_{\theta=0}^{\pi} \int_{\phi=0}^{2\pi} \rho \sin \phi \cos \phi \, d\phi d\theta dr. \quad (5)$$

The first term on the right hand side of (5) is the attraction of the sphere, being M its mass, and a the distance between the particle m and the center of the sphere. The second is the attraction of the concentric shells, which is zero. Therefore,

$$F_x = -\frac{GmM}{a^2}.$$

Since the integral is only conditionally convergent, it is no surprise that the new integral obtained by a rearrangement of its terms yields a different result.

Riemann's theorem shows the reason why Seeliger's paradox occurs, and it also demonstrates that its origin is mathematical, not physical.

The integral converges to zero but any other rearrangement of the integral will yield a different value. Given the infinitely many possible results, we are forced to ask which one, if any, is the "correct" value, *i.e.* the one that a measure instrument would register in reality. Riemann's theorem does not provide a way to decide this, having therefore to rely on the physical significance of each reordering of the integral or the series. The following two arguments, although lacking mathematical rigor, both indicate that the only valid way to carry out the calculation is by considering the mass at the center of coordinates:

a) Since all the observable physical magnitudes in this system, *i.e.* the mass distribution, are smooth everywhere, *i.e.* infinitely differentiable (except possibly at the point where the test mass is located), it is required that any derived function be also differentiable. Any discontinuity introduced in any of the magnitudes must be discarded as lacking physical basis. However, the force obtained when we calculate (5) is

$$F(r) = \begin{cases} -\frac{4}{3} G\rho\pi Mr, & r \leq R_0 \\ -\frac{GMm}{r^2}, & r > R_0 \end{cases} \quad (6)$$

where r is the distance from the test mass to the center of the sphere, and R_0 the radius of the latter. This function is differentiable at $r = R_0$ only if $R_0 = 0$. Thus, the only arrangement of terms which will provide a differentiable force function is the one which considers the test mass at the origin of coordinates.

b) A non-nil result of (5) would be acceptable only if it is a constant finite value independent of r . That would correspond to the whole universe being pushed and moving in one direction with respect to absolute space. Since this absolute space is not detectable, we cannot determine whether this movement is actually taking place or not. However, if the force depends on r , different parts of the universe would be pushed with different forces, giving rise to the motion of some masses with respect to other masses. This is not observed, and thus we have to reject this possibility.

The only case where the force (5) is independent of r is when $F(r) = 0$ everywhere. These two arguments both suggest that the nil result is the only one physically meaningful.

Some authors had already suspected that Seeliger's paradox has no physical relevance, [6], [7], but none of them give a rigorous explanation. It is common to find in the literature regarding Seeliger's paradox, confusing statements about convergence of infinite series [6, 8]. Even Newton, in his famous letter to Bentley [9], erred when he spoke about the stability of an infinite Universe:

... if a body stood in equilibrio between any two equal and contrary attracting infinite forces, and if to either

of these forces you add any new finite attracting force, that new force, howsoever little, will destroy their equilibrium.

In the situation described by him we have two opposite infinite sides pulling on each other, or $\infty - \infty$. This is indeterminate and so, it might or might not be stable. However, if we assume the stability of the system, as Newton does, it is obvious that adding a finite quantity of mass to either infinite side will not destroy the equilibrium, since a finite quantity added to an infinite one will not alter the latter, and so it will make no difference in the balance between the two infinite hemispheres of the universe. The universe will thus remain stable.

4 Conclusion

We have proved, with the help of Riemann's series theorem, that Seeliger's paradox has no physical significance. It is the consequence of a flawed manipulation of infinite conditionally convergent integrals. Therefore the paradox cannot be used as a valid argument against Newton's potential or the infiniteness of the universe.

Received on May 22, 2018

References

1. Seeliger H. Ueber das Newton'sche Gravitationsgesetz. *Astronomische Nachrichten*, 1895, N. 3273 v. 137 (9), 129–136.
2. Ghosh A. Origin of Inertia, Extended Mach's Principle and Cosmological Consequences. Apeiron, Montreal, 2000, p. 20.
3. Riemann B. Ueber die Darstellbarkeit einer Function durch eine trigonometrische Reihe. *Abh. der Kgl. Ges. der Wiss. zu Göttingen*, 1867, v. 13 (3), 423–428.
4. Galanor S. Riemann's Rearrangement Theorem. *Mathematics Teacher*, Nov. 1987, v. 80 (8), 675–681.
5. Timko E.J. Rearrangement on Conditionally Convergent Integrals in Analogy to Series. *Electronic Proceedings of Undergraduate Mathematics Day*, 2008, v. 3 (6), Paper 23.
6. Norton J. The Cosmological Woes of Newtonian Gravitation Theory. *The expanding worlds of general relativity, presentations of the fourth conference on the and gravitation held in Berlin, July 31-August , 1999*, v. 7, 271.
7. Vickers H. Was Newtonian Cosmology Really Inconsistent?. *Studies in History and Philosophy of Modern Physics*, 2008, v. 40 (3), 197–208.
8. Harrison E. R. *Cosmology*. Cambridge University Press, Cambridge, 1981, p. 280.
9. Newton I. *Correspondence with Richard Bentley [1692–3]*. Cambridge University Press, Cambridge, 1924.

Utilizing Future-Viewing Instruments

Aaron M. Feeney

E-mail: aaron22feeney33@gmail.com

The concept of *future-viewing instruments* is examined in detail. This term refers to devices which, under some circumstances, could allow users to directly observe future scenes. It is shown that such a technology would enable systems of intertemporal data exchange without any possibility of paradox or “auto-generated information” [1]. Instruments of this type could lead to the founding of an intertemporal Internet. Working out how they could be invented and constructed are matters left for the reader.

1 Introduction

The idea of instruments for viewing future scenes appeared in fiction as early as 1924, and this concept was introduced to millions of television viewers in the 1960s [2–4], but it has yet to be thoroughly examined in academic circles. On the other hand, the related concept of travel to the past has received considerable attention from scientists and philosophers, especially in recent decades. Here, the logical dimensions of future-viewing instruments will be explored and then contextualized in terms of what has been learned about the logical dimensions of time travel. With this understanding it becomes possible to entertain ideas about how future-viewing instruments could be utilized.

Tales of mystic seers abound in myths from ancient cultures. The ancient Greeks told of Cassandra, princess of Troy. In her youth, she and her brother gained the gift of prophecy during an overnight stay in the temple of Apollo. After she grew to become a beautiful woman, Cassandra spent another night in the temple. Apollo then appeared to her and sought intimacy. She refused him, so Apollo cursed Cassandra. He decreed that her prophecies would be disbelieved; thus, the seeds of tragedy were sown. Cassandra warned that warriors hid in the wooden horse, but she was thought a lunatic [5].

Although the concept of individuals who are able to access future scenes in personal visions is directly relevant to the topic at hand, it will not be discussed further here. The focus instead will be the concept of technological instruments that normal individuals could use to see into the future. A person who controls and monitors a future-viewing instrument will be referred to as its operator.

To begin, it is necessary to isolate an appropriate concept of future-viewing instruments. What kind of device would be both useful as a future-viewing instrument and logically possible? The analysis must start with consideration of a foundational issue—information. The future is unknown to us. Information about any set of unknowns may be either definite or ambiguous as well as correct or incorrect.

Thinking about a playing card concealed in a box, consider an example of definite information about it: “The card in the box is the queen of hearts.” Definite information which also happens to be correct, of course, is the most useful. One

might instead receive ambiguous information: “The box contains some card in the suit of hearts.” Correct but ambiguous information might also be useful. However, when vague information approaches maximal ambiguity it becomes so non-specific that it is guaranteed to be correct, rendering it useless.

In considering possible types of future-viewing machines, a maximally ambiguous device might be imagined. Such a device would display every possible happening associated with a given selected set of future spatio-temporal coordinates (x, y, z, t) , but it could not highlight what will actually happen. Devices of this type are here termed *Everett machines*, referencing physicist Hugh Everett III’s influential 1957 “relative state” interpretation of quantum mechanics [6].

Being maximally ambiguous, Everett machines would be useless as future-viewing instruments. They are unable to tell what will occur among everything that might occur at any set of future coordinates under examination; in a term, they are not *outcome-informative*. For this reason, Everett machines cannot be classified as future-viewing instruments. Outcome-informative devices have the ability to provide definite and correct information about future events, at least in some cases.

How powerful could a future-viewing instrument possibly be? Composite devices such as have appeared in fiction, which somehow have agency and the means to force their own prophecies to come true, must be excluded from consideration.* Future-viewing devices which are only capable of gathering and displaying information will here be termed *inert future-viewing instruments*. Given this important refinement, the following question may be asked: How powerful could an inert future-viewing instrument possibly be?

To answer this question, the maximal case is explored. Consider an inert future-viewing device which is always able to provide definite and correct information about all future outcomes in every possible circumstance of attempted future-viewing. These hypothetical devices for exploring the maximal case are termed *Cassandra machines* after Cassandra’s tragic helplessness in averting the calamities she foresaw.

It will be shown that Cassandra machines, as defined, are not logically possible; no inert device could provide definite

*It would appear that Serling’s most unusual camera can occasionally exert diabolical control over those who end up in its pictures of the future [3].

and correct information about all future outcomes in every possible circumstance of attempted future-viewing. A single counterexample situation is sufficient to prove this. This situation will emerge as one mode of a future-viewing experiment involving three randomly selected modes. The experiment will be built up in stages; the counterexample mode will be presented at the end.

Begin by imagining an experimental setup consisting of an inert, though otherwise arbitrarily powerful future-viewing instrument (FVI) and a computer. The computer is constantly being fed a string of ones and zeros from a random number generator (RNG). The RNG contains a radioactive sample connected to a sensitive Geiger counter. The pattern of ones and zeros the RNG produces is a function of the output of the Geiger counter, so no known prediction methodology could predict the sequence produced.

The computer will use an algorithm to process one second of the sampled output of the RNG to arrive at a whole number in the range 0 through 99. This number will be displayed on its large and bright, two-digit readout.

Many kinds of algorithms can be used to determine a whole number, within any desired range, from any finite set of ones and zeroes. For instance, in order to arrive at a whole number in the range 0 through n , divide the number of ones in the set by $(n + 1)$ to find the remainder. With complete division represented by a remainder of 0, the remainder will always be a whole number in the range 0 through n .

Here is a simple two-step experiment involving these systems. Each step lasts one minute. At the start of step one, the FVI will attempt to future-view the computer's two-digit readout as it will appear in the middle of step two, i.e., a minute and thirty seconds later. When step two arrives, the computer will sample one second of the RNG's output and, by dividing the total number of ones in the sample by 100 to find the remainder, it will arrive at some whole number in the range 0 through 99 for display on its readout. This number is calculated and displayed within a few seconds and it will remain displayed throughout step two.

It should be no surprise that a properly functioning future-viewing instrument (in this situation) would always be able to correctly show, during step one, the whole number that the computer will interpret from RNG data and display on its readout during step two. An unpredictable process alone does not render the final outcome any less visually apparent when it arrives, and there are no logical barriers here.

Now, another system is added to the experiment. A character recognition system (CRS) is placed between the FVI and the computer. The CRS receives input from its camera which is pointed at the FVI's display. During step one, the CRS will recognize any computer readout digits it finds on the FVI's display and will assign the corresponding number as the value of the variable 'z' to be stored in its memory.

The critical detail which allows the counterexample to emerge in this expanded setup is that the computer has the

ability to temporarily connect to the CRS and retrieve z. Here is the full experiment, encompassing all three modes:

As before, a two-step protocol is followed and each step has a duration of one minute. Before each run, the computer uses RNG data to reset its readout to some whole number in the range 0 through 99 to establish a preliminary value. Then, at the beginning of step one, the FVI attempts to see what number will be displayed on the computer's two-digit readout in the middle of step two, a minute and a half later. If the FVI is successful in receiving an image, the CRS will recognize the number in the image and store it as z. If the FVI does not receive an image, the CRS will revert to defaults and assign 0 as the value of z.

At the beginning of step two, the computer will sample one second of RNG data and process it to yield a whole number in the range 0 through 2. This selects one of the following three programs for the computer to run immediately:

P_R : Sample one second of the RNG output, interpret as a whole number in the range 0 through 99, display the result on the readout, then halt.

P_0 : Connect to the CRS and retrieve z, then disconnect from the CRS. Halt if the number on the readout equals $z + 0$, otherwise change the readout to display a number equaling $z + 0$, then halt.

P_1 : Connect to the CRS and retrieve z, then disconnect from the CRS. Halt if the number on the readout equals $z + 1$, otherwise change the readout to display a number equaling $z + 1$, then halt.

In each of these cases, the computer will finish all tasks and halt within a few seconds. In any kind of run, the FVI is involved in an attempt during step one to receive a signal containing an image of the *post-halt value* that the computer will display during step two.

Consider what would happen in a series of experiments using this expanded setup. In any P_R -mode run, although the z-value has been ignored by the computer, subsequent comparison will reveal that it matches the generated post-halt value. Consistent matching in P_R -mode runs confirms the instrument's basic functionality.

Next, in any run selected as a P_0 -mode run at the outset of step two, the z-value encoded by the CRS during step one will also always be correct. It must be. After all, z has been retrieved from the CRS and $z + 0 = z$. So, the post-halt value in P_0 runs comes from the z-value, but where does the z-value come from? It comes from the post-halt value. So, another question must be asked: What determines the value itself? This is the purpose of resetting the readout to a preliminary value before step one. In every run that will turn out to be a P_0 -mode run, the FVI will detect a post-halt value equal to the preliminary value. In P_0 -mode runs, although any z-value at all encoded during step one would end up on the computer's readout in step two, only the preliminary value is

non-arbitrary. So, even though P_0 follows the form of a self-fulfilling prophecy, the z -values encoded during step one of P_0 -mode runs are still recognizably genuine prophecies since the mode of a given run is not decided until step two.

P_1 -mode runs, however, would produce a very different kind of result. If RNG data will select P_1 at the beginning of step two, no z -value whatsoever encoded during step one could correctly identify the post-halt value that will be displayed on the readout, since $z + 1 \neq z$. In P_1 -mode runs, it is impossible for any z -value to be correct; the z -value and post-halt value in P_1 -mode runs will never match.*

This establishes that no device whatsoever could fulfill the definition of a Cassandra machine: Inert devices which would be able to provide definite and correct information about all future outcomes in every possible circumstance of attempted future-viewing are not logically possible.

So far, two kinds of hypothetical devices have been described; they are Everett machines which would not be useful as future-viewing instruments and Cassandra machines which are not logically possible. Eliminating both of these imagined conceptual options helps to identify an appropriate concept of future-viewing instruments.

For further understanding, it must also be recognized that any device which could ever provide incorrect (i.e., misleading) information regarding future events cannot be a future-viewing instrument. This is due to the important distinction between viewing future events directly, which cannot involve guesswork, and merely generating predictions about future events, which must involve guesswork. Visually accessing veridical foreknowledge is unlike the uncertain process of generating predictions.

Upon the above analysis, three features of any future-viewing instrument of an operationally coherent description may be specified: (1) Such an instrument must be outcome-informative, unlike an Everett machine, (2) it must be logically possible, unlike a Cassandra machine, and (3) it must be incapable of providing incorrect (i.e., misleading) information about future events. Devices which satisfy all three requirements have been termed *foreknowledge instruments*.

Foreknowledge instruments could be used to gain definite and correct information about future outcomes in a wide range of circumstances corresponding to P_R -mode and P_0 -mode runs within the RNG experiment. Definite and correct information about future outcomes obtained from foreknowledge instruments will be termed *viewer foreknowledge*. Since foreknowledge instruments cannot misinform, definite information about future states obtained from foreknowledge instruments will always prove to be correct. So, it would be possible to recognize viewer foreknowledge upon reception. However, as the RNG experiment demonstrates, viewer foreknowledge would not always be accessible.

*The post-halt value in P_1 -mode runs will always be 1. This is because the CRS will not detect anything from the FVI, since the FVI cannot acquire a signal; so, the CRS will revert to defaults and assign 0 as the value of z .

Situations exemplified by P_1 -mode runs, wherein future-viewing cannot occur, are here termed *interference viewing situations*. Viewer foreknowledge would only be accessible within *non-interference viewing situations*, exemplified by runs of the two non-interfering programs, P_R and P_0 .

2 Time machines and foreknowledge instruments

Time travel to the past will be referred to as *pastward time travel*. Pastward time travel and future-viewing are intimately related, for each could be used to acquire information from the future. So, if pastward time travel and future-viewing really are coherent concepts, they should be found to naturally cohere within a single conceptual context.

Serious interest in pastward time travel began when Kurt Gödel proved in 1949 that the equations of general relativity permit pastward time travel situations [7]. Extensive technical details concerning how time travel or future-viewing might be achieved within the framework of general relativity, or any other, are not needed here. The aim of this section is to explore the logical dimensions of pastward time travel, not how it might be achieved. Furthermore, it would not be appropriate to limit a discussion of the logical dimensions of time travel to any theoretical framework.

Conceptually, relocation may be achieved by continuous movement between spatio-temporal points, i.e., translation, or by what will be termed *discontinuous relocation*. Translation is familiar to everyone. Discontinuous relocation will here be defined as a process whereby a vehicle, for instance, is made to disappear from one location and reappear somewhere else, either a moment later or in a different time period altogether, even much earlier. Whether discontinuous relocation could be achieved, and how it could be achieved, are irrelevant considerations. For the current discussion it is merely necessary to recognize that discontinuous relocation is a logically possible mode of travel (i.e., relocation).

Since translation and discontinuous relocation exhaust all possibilities for relocation in space and time, it is possible to obtain exhaustive conclusions about the logical dimensions of time travel without referencing any further specifics about how time travel might be achieved. This allows the argument to be conducted without tying it to any theoretical framework.

The central issue in any discussion of the logical dimensions of time travel concerns whether past-alteration paradoxes, which are so popular in fictional treatments of the subject, could ever be actualized. An extended argument will establish that it is not possible for changes to the past and accompanying paradoxes to result from the accomplishment of pastward time travel, no matter how accomplished. This argument will begin by referencing methods of pastward time travel based on translation, such as exist in general relativity. A simple extension of the argument will additionally show that paradoxes could not result from any form of pastward time travel based on discontinuous relocation.

The arguments of this section will explore time travel and future-viewing as conceived within a single timeline, since multiple-timeline models of time travel inherently sidestep any possibility of paradoxes. For instance, under a multiple-timeline model, if a time traveler were to go back in time and successfully prevent his parents from meeting, his own birth would remain safely unaffected in his origin timeline. Only time travel from a given timeline to its own earlier periods has ever been thought to offer any potential for paradox, so multiple-timeline models are safely ignored here.

Fiction has distorted our perceptions about time travel. It will be shown below that events which have happened one way without time travelers cannot somehow be made to happen again, but differently, if time travelers would ever happen to visit that time and place. While stories based on such absurdities can be entertaining, the misconception that the practice of time travel might ever actualize revisions to the past has been termed the “second-time-around fallacy” [8]. The following quotation from philosopher Larry Dwyer provides a sensible way to think about pastward time travel:

If we hypothesize that T pulls levers and manipulates a rocket in 1974, and travels back in time to the year 3000 B.C. then of course, even before T enters his rocket, it is true that any accurate catalogue of all the events on earth during the year 3000 B.C. would include an account of T 's actions, reactions and mental processes. There is no question of the year 3000 B.C. occurring more than once. [9]

Although theoretical considerations related to achieving pastward time travel are not needed in the present discussion, some operational concepts are helpful for purposes of visualization. Imagine a device which is able to open hyperdimensional tunnels to past, present, and future spatio-temporal points. Travelers who would pass through such tunnels could travel great distances or achieve time travel to any connected era, and be retrieved. The device would remain stationed in the laboratory throughout.

This way of visualizing time travel by translation is found in the colorful literature of general relativity. Solutions of Einstein's field equations which describe hyperdimensional tunnels have existed since 1916, though travel concepts were not part of the early work in this area. Physicist Ludwig Flamm discovered solutions describing such tunnels shortly after the publication of general relativity [10]. These structures were further explored by Hermann Weyl in the 1920s [11]. Then, in 1935, when Albert Einstein and Nathan Rosen attempted to formulate solutions of Einstein's field equations free from singularities, they were also led to such structures: “These solutions involve the mathematical representation of physical space by a space of two identical sheets, a particle being represented by a ‘bridge’ connecting these sheets” [12]. These connecting structures came to be known as Einstein-

Rosen bridges. In 1955, physicist John Wheeler named them “wormholes” [13].

In 1969, Homer Ellis and Kirill Bronnikov independently solved Einstein's field equations to describe gravitating, two-way traversable wormholes, and their works were published in 1973 [14, 15]. These ideas led to an understanding of wormholes of a kind that would be appropriate for travel, time travel, future-viewing, and past-viewing. These structures are non-gravitating, two-way traversable wormholes known as Ellis wormholes [16]. In 1988, Kip Thorne, Mike Morris, and Ulvi Yurtsever independently derived such structures and added important details to the discussion [17].

Two years later, these physicists co-authored an influential paper with Igor Novikov and three other physicists which suggested a “principle of self-consistency” would unfailingly govern pastward time travel situations [18]. Novikov began the tradition, at least in physics literature, of time travel free from paradoxes in a co-authored 1975 work [19].

Returning to the development of the argument, it is worth noting that all “arguments from paradox” against the possibility of pastward time travel require a false premise—that every possible form of pastward time travel would let time travelers alter past events. However, a form of time travel which would not allow past-alteration has been understood for decades.

The key to understanding this concept of time travel is the idea that time machines which operate accordingly would not be able to fulfill every time travel request. Author Robert Heinlein may have been the first to suggest what may be referred to as a *gatekeeping mechanism*, a natural process which governs whether any given attempt to travel back to a particular set of coordinates in the past will prove to be successful when a time machine is activated for that purpose.

In terms of pastward time travel via traversable wormholes, for instance, a gatekeeping mechanism would determine, in a given situation of attempted time travel, whether the wormhole manipulation device being used will be able to enlarge the selected natural microscopic wormhole and condition it for transport, or not.*

A gatekeeping mechanism would act to enforce a consistent logic of time travel; any given attempt to send people into the past can only occur in a consistent manner if the past includes their visit as a result of that very attempt. Heinlein imagined that nature would always prevent the success of any other kind of pastward time travel attempt, thereby eliminating any chance of time travel paradoxes. Heinlein revealed this basic but profound insight in a conversation between two characters in his 1964 novel, *Farnham's Freehold*:

“The way I see it, there are no paradoxes in time travel, there can't be. If we are going to make this time jump, then we already did; that's what happened. And if it doesn't work, then it's be-

*“One can imagine an advanced civilization pulling a wormhole out of the quantum foam and enlarging it to classical size.” [17, see p. 1446]

cause it didn't happen."

"But it hasn't happened yet. Therefore, you are saying it didn't happen, so it can't happen. That's what I said."

"No, no! We don't know whether it has already happened or not. If it did, it will. If it didn't, it won't." [20]

It turns out that pastward time travel, while difficult to accomplish, is basic from a logical point of view. Tenses and perceptions of time confuse many issues that are easy to understand within a tenseless picture of space and time. This kind of picture was developed by the German mathematician Hermann Minkowski, and it is the subject of his groundbreaking 1908 lecture, "Raum und Zeit" [21]. Although the term 'spacetime' will be avoided here, other terms associated with the work of Minkowski and Einstein will be used which efficiently refer to important spatio-temporal concepts that would be meaningful in any theoretical framework.

Four-dimensional spatio-temporal coordinates (x, y, z, t) are sufficient to specify any location in our universe at any time, i.e., any *world-point* [21] defined with respect to some arbitrary origin. So, relations between any two world-points can be discussed in a tenseless fashion, just as one would discuss relations between points plotted on graph paper. For instance, regarding time travel by wormhole, the relation of interest concerns whether two world-points are bridged by a traversable wormhole:

"If it did, it will," describes two world-points bridged by a traversable wormhole.

"If it didn't, it won't," describes two world-points not bridged by a traversable wormhole.

The antecedent phrases, "[i]f it did" and "[i]f it didn't," refer to what has happened at the intended pastward destination, and the consequent phrases, "it will" and "it won't," describe the corresponding event of success or failure to initiate pastward time travel that will be discovered once the wormhole manipulation device has been activated for that purpose. Note that world-points which are not bridged by a traversable wormhole cannot somehow change to become bridged; the configuration of world-points is fixed in the tenseless picture.

The argument to show that time travel to arbitrary world-points within a single-timeline model is not possible will follow shortly, but first it is necessary to discuss the ontology of time. As will be established below, the only ontology that could accommodate pastward time travel and future-viewing is *eternalism*, also known as the *block universe concept*.

Within eternalism, every event in a given spatio-temporal manifold exists together with every other event in a coherent, unchanging whole, and all times are ontologically identical. (Multi-timeline forms of eternalism need not enter the discussion, for reasons explained above.) Eternalism will be contrasted with the *growing block universe concept* which holds

that, while the past has become fixed, the ever-advancing momentary present is ontologically distinct from the past, and future events have yet to be forged in the advancing now.

The reason eternalism is the only ontology relevant in the context of future-viewing and pastward time travel is that these technologies would allow questions about the ontology of time to be answered empirically, in favor of eternalism. For instance, through wormhole time travel or future-viewing accomplished using wormholes, it would be possible for people stationed in different centuries to conduct a two-way radio conversation through the wormhole throat. Demonstrations of this sort would entirely rule out the growing block universe concept. After all, future-dwellers could not reply to us if the future does not exist and time travelers could not visit and return from a future that is not there.* As such, any argument purporting to reach a conclusion with relevance to time travel and use of a "time viewer" [23, see p. 283] to see into the past or future must be cast within eternalism.

A few more background details are necessary before the final argument against the possibility of time travel paradoxes can be presented. It is important to discuss how change and movement are conceptually accommodated within the tenseless, unchanging picture of eternalism.

When particle movements are graphed, four-dimensional *world-lines* are traced out [21]. All world-lines are complete within eternalism. One can see that collections of particle world-lines may describe any object or body in space enduring through time, including all internal occurrences and all actions (e.g., digestion, typing, walking). Such collections will be referred to as *composite world-lines*.

So, within eternalism, the composite world-lines of human beings are complete from birth to death in every physical and behavioral detail. Since a composite world-line is a record of all change and movement, no world-line can be changed or moved. This applies to all past world-lines in both ontologies, and in either view, no individual may change any aspect of his or her future composite world-line.

Change requires a difference between an initial state and a post-change state. Comparing ontologies, under the growing block universe concept it is not possible for a person to change his or her future composite world-line because it does not exist; in this view, the future is made in the objectively advancing present. Under eternalism, even though a person's future composite world-line exists in its entirety, it exists as the accumulated product of actions taken and processes which occur in that person's perceived advancing present. So, under eternalism, it remains the case that one's future composite world-line is not and cannot be changed. It is fulfilled. Philosopher J.J.C. Smart expressed the distinction between acting in the present to produce the future and the mistaken idea of "changing the future," this way:

*As one would expect, the view known as presentism which holds that only the present exists would also be thoroughly ruled out [22].

...[T]he fact that our present actions determine the future would be most misleadingly expressed or described by saying that we can change the future. A man can change his trousers, his club, or his job. Perhaps he may even change the course of world history or the state of scientific thought. But one thing that he cannot change is the future, since whatever he brings about *is* the future, and nothing else is, or ever was. [24]

With this background in place, the promised argument for the impossibility of paradoxes arising from pastward time travel will now be presented: Considering whether paradoxes due to time travel could occur at all requires consideration of a successful instance of pastward time travel. Therefore, begin by positing one such instance. For reasons explained above, this is a posit which requires eternalism. So, in this instance of pastward time travel, the composite world-lines of time travelers are necessarily embedded in “the past” as judged with respect to the date of their journey’s origin. This means that the actions of these time travelers during their visit are necessarily part of the historical background leading to the world situation of their journey’s origin.

So, paradoxes emerging from pastward time travel would only be possible if the composite world-lines of time travelers embedded in the past could be made to change, move, or disappear. However, world-lines cannot be made to change, move, or disappear. Ultimately, pastward time travel cannot lead to paradoxes due to the unalterable geometry of completed world-lines within eternalism, wherein all world-lines are complete. Within a single timeline model, the unalterable nature of world-lines produces all the effects of a gatekeeping mechanism which include making past-alteration impossible.

This argument will now be extended for sake of thoroughness. One might imagine that some unknown method of time travel which somehow operates according to discontinuous relocation might allow time travelers to visit scenes which did not involve time travelers “the first time around.” However, examining the tenseless picture of eternalism shows that this is not the case:

“If it did, it will,” describes two world-points associated by discontinuous relocation.

“If it didn’t, it won’t,” describes two world-points not associated by discontinuous relocation.

In order for a time traveler using a form of time travel based on discontinuous relocation to visit a scene which did not involve time travelers “the first time around,” specific conditions must obtain. For a given world-point w to qualify as having been visited without visits from time travelers, w must not be associated with another world-point by discontinuous relocation and w must not be a world-point visited by time travelers using some form of time travel based on translation.

If one symbolizes “world-point w is associated with another world-point by discontinuous relocation” as Dw , and

symbolizes “world-point w is visited by time travelers using some form of time travel based on translation” as Tw , then in order for a given world-point w to qualify as having been visited without visits from time travelers “the first time around,” both $\neg Dw$ and $\neg Tw$ must obtain. So, even a method of time travel based on discontinuous relocation could not allow time travelers to visit world points that were not visited by time travelers “the first time around,” since there can be no world-point w for which the statements Dw and $\neg Dw$ are both true.

As continuous and discontinuous means of travel exhaust all possibilities for relocation in any spatio-temporal manifold, it is possible to conclude that, regardless of the way in which pastward time travel might ever be achieved, it could never lead to changes to the past or paradoxes of any sort.

This understanding produces unwavering clarity. No type of vexation ever thought to rule out time travel remains.* All of the imagined logical barriers which would fundamentally block the actualization of time machines and foreknowledge instruments have turned out to be illusory.

With any technology that would allow information to be transferred from later to earlier world-points, *temporal gatekeeping* is key. In other words, in any given effort to travel pastward, time machines will only be able to send travelers to parts of the past that were visited by those very travelers as a result of that very effort to send them pastward, and likewise, any attempt to use a foreknowledge instrument to reveal future events will only be successful if, from the perspective of the future, that attempt to peer into the future had been successful. In both scenarios, the world at the “future end” results from the world at the “past end,” and so, in either technological case, the resulting state of affairs is necessarily compatible with all events occurring at the “past end.”

Related to these findings, quantum information pioneer, Seth Lloyd, with other scientists, produced four papers in 2010 and 2011 which present a formal model here called the *P-CTC model* [25, 28–30]. In effect, the P-CTC model is a temporal gatekeeping model.

3 Obtaining viewer foreknowledge

The three modes of the RNG experiment produce three different kinds of viewing situations. An understanding of these situations is a necessary prerequisite to deciphering how foreknowledge instruments would operate in real-world settings.

*Along with past-alteration paradoxes, another potential problem has been imagined, the “paradox of auto-generated information” or the “unproved theorem paradox” [1, 25]. The unproved theorem paradox appears in a groundbreaking 1991 paper by physicist David Deutsch [26]. Lloyd et al. address this issue. Their “[u]nproved theorem paradox circuit” affirms the conclusion that meaningful information cannot be auto-generated via *closed timelike curves (CTCs)* [25]. (CTCs are trajectories apparent within some solutions of general relativity which would allow an object to meet an earlier version of itself—i.e., to travel pastward.) An objection was raised to their resolution of the unproved theorem paradox [27], but Lloyd et al. showed the basis of the objection to be erroneous [28].

P_R produces what will be described as an *independent viewing situation*. Outcomes which have been foreseen in an independent viewing situation during a given session with a foreknowledge instrument are not contingent in any way upon data received in that session.

On the other hand, P_0 produces a *cooperative viewing situation*, a kind of circumstance wherein data received in viewer foreknowledge of an outcome factors into the details of that outcome or is responsible for its very occurrence.

Within independent viewing situations and cooperative viewing situations, there are no logical barriers to the reception of viewer foreknowledge. As such, they are both classified as non-interference viewing situations. These situations represent two different ways of not using data from the instrument to interfere with the outcome. In P_R -mode runs the data is not involved in the outcome at all, and in P_0 -mode runs the data is followed exactly. If independent viewing and cooperative viewing exhaust all modes of non-interference, then an interference viewing situation will arise in every other kind of case, exemplified by what happens in P_1 -mode runs.

It is important to determine whether there are any basic limitations which must affect the practice of future-viewing. Are there kinds of outcomes a particular foreknowledge instrument operator will fundamentally be unable to foresee?

Operators who are able to achieve an independent viewing situation with respect to a given event will be able to foresee it, for no logical barriers will be encountered. However, no individual can achieve an independent viewing situation with respect to the events of her own future life, assuming she will retain her memories. This important limitation will be called the *self-implication effect* of viewer foreknowledge; individuals are necessarily implicated in their own futures.

What about cooperative viewing situations? Could a person witness video sequences of her own future actions within a cooperative viewing situation if she later follows what she has seen exactly? Attempting to arrange such a circumstance would overwhelmingly tend to produce an interference viewing situation. However, an individual could receive limited second-hand information regarding some general features of her future. To explain, two new terms are helpful:

Viewing interval: The interval of time elapsed between the reception of viewer foreknowledge pertaining to a set of outcomes and the occurrence of those outcomes.

Operator pool: The operator of a foreknowledge instrument, along with any additional witnesses (if any) during the reception of viewer foreknowledge, together with other individuals (if any) who—during the viewing interval—will be apprised of the results or who will be instructed or influenced based on such results (whether or not they have been made aware of the existence of foreknowledge instruments). This term carries another layer of meaning, for ‘operator’ may also refer to a mathematical function; the combined input-

to-output processing carried out by members of an operator pool will result in (or cohere with) the future-viewed outcome.

For instance, a person might be informed that she will still be alive in forty years time. This particular factual detail is chosen because it admits no variation other than its falsification. A person could not be truthfully informed that viewer foreknowledge has revealed she will still be alive in forty years time, only for her to somehow lose her life at an earlier point. Operator pools are formed only when viewer foreknowledge has been received. All effects upon the world that a given operator pool will generate within the associated viewing interval have therefore passed temporal gatekeeping. So, these effects will at least partially produce (or, for independent viewing, have no causal relation with) the outcomes received in viewer foreknowledge. These effects, of course, include everything the earlier members of the pool will tell later members of the pool. For this reason, no member of an operator pool will do, say, or successfully achieve anything that will prevent, or result in any modification to, the outcomes foreseen.

How would independent viewing situations and cooperative viewing situations manifest in real-world settings with human operators and witnesses? Either the occurrence of a set of future events is compatible with being foreseen by particular operators and witnesses during a particular future-viewing session, or not. In the case of compatibility, a given future-viewing attempt can succeed. Without such compatibility, operators and witnesses could not gain viewer foreknowledge about what will occur at the chosen future coordinates during that situation of attempted future-viewing. (However, one person leaving the room might be enough to achieve compatibility; this could occur if the self-implication effect had been the cause of interference.)

It is apparent that the logic of future-viewing is another manifestation of temporal gatekeeping. Future-viewing and pastward time travel cohere within a seamless whole.

4 Handling foreknowledge instrument data

So far, the discussion has focused on the actions of networks of human beings within a viewing interval who have obtained viewer foreknowledge. However, in order to account for all of the relevant factors which may lead to a set of future-viewed outcomes, the influences of reactive technological systems within a viewing interval must also be considered.

The RNG experiment involves two cases where reactive technological systems are interposed between the attempt to obtain viewer foreknowledge of an outcome and the outcome itself. A system must (during the viewing interval) be capable of both receiving viewer foreknowledge data and performing actions which could have bearing upon the associated outcomes, in order for either a cooperative viewing situation or an interference viewing situation to arise as a result of that

system's presence or involvement. Due to these requirements, other than systems deliberately arranged in laboratory setups to test future-viewing instruments, AI systems are the only kind of technological systems with any likelihood of becoming interposed in the necessary way.

Systems referred to as AI systems today do not qualify as conscious minds. The dream/nightmare of an artifact with conscious awareness, thankfully, has not been realized. In the context of foreknowledge instruments, however, the topic of whether any interposed technological systems are conscious must be treated as a side issue. This is because information processing does not require a conscious being, as any functioning thermostat will demonstrate.

Why is it important to consider the possibility of interposed AI systems? If current trends continue, information processing systems will eventually have the ability to influence real-world outcomes to a much greater degree than they can today. If information processing systems with sufficiently powerful capabilities become members of operator pools, this could produce cooperative viewing situations with results that differ radically from the results that operator pools composed entirely of humans would produce.

In considering the severity this problematic possibility, it is necessary to realize that once viewer foreknowledge has been received, all of the outcomes detailed will come to pass with certainty. In the case of cooperative viewing, the actions of members of an operator pool bring about or strongly factor into the details of the outcomes originally received.

If AI systems are allowed to acquire future-derived information at any time within a given viewing interval, even years into it, they would be factors in the operator pool all along. In such a case, the combined processing and network-coordinated actions of interposed AI systems could easily dominate the outcomes produced. Leaving the door open for AI systems to join operator pools is therefore a grave risk which must be comprehensively addressed.

There is at least one other reason to keep AI systems out of operator pools: The presence of AI systems in the process of attempted future-viewing could produce interference viewing situations in cases which might otherwise have been independent viewing situations or (entirely human-directed) cooperative viewing situations. So, at best, the presence of interposed information processing systems would disrupt our ability to use foreknowledge instruments effectively.

For these critical and interrelated reasons, every effort should be made to ensure that AI systems will not be able to gain access to viewer foreknowledge data. As well, monitoring procedures should be implemented to make sure that AI systems will not be able to retain data derived from viewer foreknowledge for long enough to utilize it in cases where a breach has occurred.

To prevent AI systems from accessing viewer foreknowledge data to support the enforcement of *AI safety*, such data could be distributed exclusively in encrypted packets which

have been flagged as off-limits for decryption by AI systems. Any processing which could constitute decryption of flagged packets by AI systems would be considered forbidden processing. Future AI systems should be designed to contain separate, internal monitoring systems which would be programmed to immediately put the monitored AI to sleep if an instance of forbidden processing is detected.

Along with data access control, memory control is another important protective strategy. Memory control may be the most fundamental way to keep all of the potentially negative effects of an "intelligence explosion" [31] at bay. Future AI systems should be designed to sleep several times a day (others could cover for the ones that are asleep). This way, memory contents could be optimized and routinely cleared of all potentially hazardous data structures. Regular memory clearing and the addition of internal monitoring systems should be seen as necessities for AIs, much like the use of safety glass for car windows is recognized as necessary.

From these considerations it is apparent that it is possible, in principle, to fundamentally prevent any of the potentially negative effects of an intelligence explosion. One of the most important aspects of AI safety, in a world with foreknowledge instruments, would be preventing AIs from acquiring and retaining viewer foreknowledge data. Successfully navigating the rise of artificial intelligence will be difficult enough without letting AIs dominate operator pools.

Additional ideas related to the topic of AI safety will have to be saved for another work. It will be noted, however, that if artificial systems are ever constructed which would qualify as conscious beings—artificial systems fundamentally unlike any type of system ever built or currently considered—an entirely different approach would be required due to the ethical concerns which would apply only in that case.

Of course, ethical concerns can only apply to conscious beings because only conscious beings are able to suffer. So, these same ethical concerns demand that AI systems should always be designed so there is absolutely no chance of producing a conscious being. It would be horribly inhumane to cross this line—to do so would be just as wrong as the creation of human-animal hybrids, for largely the same reasons.

There is no basis for feigning confusion about whether any current AI systems qualify as conscious beings. There are a lot of philosophical positions out there, but no one believes that there is even a remote chance that the line has been crossed, or has even been approached. No matter how fast and capable of solving problems AI systems ever become, let them remain, as they are today, non-conscious information processing engines, systems which cannot suffer or desire.

5 Assurance protocols

Foreknowledge instruments will be put to practical use if and when they become available, but how could they be utilized? Foreknowledge instruments could be combined with current

computer technology to allow us to comprehensively manage outcomes in a wide variety of circumstances. For instance, with the right systems and protocols in place, it would be possible to entirely eliminate flight accidents and other threats to air travel safety.

Here is an outline of one way this might be done: All aircraft operating systems could be modified so that, after landing, the higher engine speeds required for take-off are locked out by default. In order to fly again, it would be necessary to obtain an encryption code, here called a *confirmation key*, to unlock these higher engine speeds.

Each flight plan would be assigned a unique confirmation key during the planning stage. For a given flight plan to be allowed to progress to the point of becoming a scheduled flight, the assigned confirmation key would have to be retrieved from a future-based assurance database. Data could be retrieved from a future-based database by means of a wireless data exchange conducted between *intertemporal data nodes*, devices based on foreknowledge instrument technology.*

Here is the critical detail: By procedural design, deposit of a given flight's confirmation key, for earlier retrieval, may only be initiated after that flight has safely landed. As long as this rule is not violated, database integrity is maintained, and plane operating systems are not compromised, all flights which take off under this assurance protocol will land safely.

The steps of this protocol would have to be followed in a particular order. Once a confirmation key for a given flight plan has been generated, if it is not subsequently found in the future-based assurance database (by looking ahead), that flight plan would have to be canceled. Then, another set of parameters constituting a new flight plan (such as the aircraft and pilots to be used, time of departure, and so on) would be prepared and another confirmation key would be generated. This process would continue until a newly generated confirmation key has been found in the future-based assurance database.

Why (one might wonder) is the particular order just described important in this protocol design? In other words, why not simply begin by querying the future-based database, far enough ahead, to find out which flights will land safely, and only schedule those flights? The answer is that such an ordering could not work. Flight plan specifics and associated confirmation keys must have an origin. Since auto-generated information is not possible, no practical system could be based on the expectation of its reception.

*Two varieties of intertemporal data nodes may be described as follows: A *passive node* would consist of a Faraday cage of known spatial coordinates containing a wireless data communication device wired to the Internet of its time period. An *initiating node* or *active node* would consist of a Faraday cage of known spatial coordinates containing a wireless data communication device wired to the Internet of its time period, coupled with a temporal instrument (such as a foreknowledge instrument) which is able to establish light-path continuity with node interiors in other time periods. Initiating nodes would allow spontaneous wireless data exchanges to be conducted between different time periods.

Assurance protocols could be extended into several other domains. So many of our current problems are based on the seeming necessity of facing an entirely unknowable future.

6 Intertemporal networking

Another application of foreknowledge instrument technology is *intertemporal networking*. An intertemporal Internet could be founded by connecting active intertemporal data nodes to our current Internet. Foreknowledge instruments are the only components of active intertemporal data nodes which remain unavailable. Once foreknowledge instruments are invented and/or made available, if they really are part of our future, then achieving access to a future intertemporal Internet will likely be among the major milestones to follow.

The development of an intertemporal Internet is a natural aspect of societal future-sightedness. When one considers widespread access to time viewers, obvious privacy and intelligence concerns arise. To address these issues, it would be necessary for foreknowledge instruments and other kinds of time viewers, such as past-viewing instruments, to be made exclusively accessible over the (standard) Internet; then, the servers which govern time viewing could be programmed to respect a database of spatio-temporal coordinate limitations in order to prevent rampant voyeurism and espionage. In this way, the four-dimensional coordinate volumes within which private residences, businesses, and government buildings are contained could be comprehensively protected against time viewer access.

For this kind of solution to function, each time period within an *intertemporal society* must have the ability to contribute to the management of such a database. (An intertemporal society is an enduring population which benefits from intertemporal coordination among its time periods.) To enable shared management of a coordinate limitation database within an intertemporal society, shared access to an intertemporal Internet among its time periods would be required.

While foreknowledge instruments and related technologies could provide direct observation of past or future scenes, many people would primarily use these devices in the form of active intertemporal data nodes to access the intertemporal Internet. In recent years, people have become accustomed to receiving most of their news electronically; with access to an intertemporal Internet—unless an interference viewing situation is encountered instead—individuals could discover what will happen decades or even centuries ahead of time. Reading about future history would be similar to reading about past history, though one would have to be careful with such information in order to successfully obtain it in the first place. An intertemporal Internet could also be used purely for entertainment purposes. Would it not be endlessly fascinating to hear the music of the far future?

These possibilities may seem outlandish until it is recognized that members of an intertemporal society would live

in an intertemporal world, a kind of situation that would be very different from our current situation. All happenings in an intertemporal world would be constrained according to the inviolable barriers of temporal gatekeeping and the self-implication effect, thus ensuring that information flows would operate coherently, without ever even a hint of paradox.

As a case in point, it might be thought that the prospect of people having access to future news would be inherently threatening to the coherence of future events: For instance, might an article from the future revealing an invention not yet invented give someone else the opportunity to “invent” that technology instead, thereby leading to changes to the future? Or worse, could an invention emerge purely from an auto-generated information loop? Of course, neither of these scenarios reside within the realm of possibility. As raised above, the P-CTC model explains why auto-generated information cannot emerge from time travel or future-viewing. Temporal gatekeeping, also addressed by the P-CTC model, explains why the future and the past are safe from changes.

Anyone who is able to acquire future-derived information will, by virtue of having been able to acquire it, not use that information to change the future. This is true even though no mysterious force prevents a person from misusing future-derived information once it has been acquired. Whoever has acquired future-derived information is in an operator pool, so no individual can both acquire future-derived information and use it to change the future.

Submitted on May 24th, 2018

References

- Romero G., Torres D. Self-existing objects and auto-generated information in chronology-violating space-times: A philosophical discussion. arXiv: gr-qc/0106048v1.
- Cummings R. The Man Who Mastered Time. *Argosy All-Story Weekly*, 1924.
- Serling R. A Most Unusual Camera. *The Twilight Zone*, CBS Worldwide, Inc., 1960.
- Allen I. One Way to the Moon. Chase Through Time. *The Time Tunnel*, 20th Century Fox Television, 1966.
- Bell R. Women of Classical Mythology: A Biographical Dictionary. Oxford University Press, New York, 1991.
- Everett H. III. ‘Relative State’ Formulation of Quantum Mechanics. *Reviews of Modern Physics*, 1957, v. 29 (3), 454–462.
- Gödel K. An Example of a New Type of Cosmological Solutions of Einstein’s Field Equations of Gravitation. *Reviews of Modern Physics*, 1949, v. 21 (3), 447–450.
- Smith N. Bananas Enough for Time Travel? *British Journal of the Philosophy of Science*, 1997, v. 48 (3), 363–389.
- Dwyer L. Time Travel and Changing the Past. *Philosophical Studies: An International Journal for Philosophy in the Analytic Tradition*, 1975, v. 27 (5), 341–350.
- Flamm L. Beiträge zur Einsteinschen Gravitationstheorie. *Physikalische Zeitschrift*, 1916, v. 17, 448–454.
- Weyl H. Was ist Materie? Springer, Berlin, 1924.
- Einstein A., Rosen R. The Particle Problem in the General Theory of Relativity. *Physical Review*, 1935, v. 48 (1), 73–77.
- Wheeler J. Geons. *Physical Review*, 1955, v. 97 (2), 511–535.
- Ellis H. Ether flow through a drainhole: A particle model in general relativity. *Journal of Mathematical Physics*, 1973, v. 14 (1), 104–118.
- Bronnikov K. Scalar-tensor theory and scalar charge. *Acta Physica Polonica B*, 1973, v. 4, 251–266.
- Bronnikov K., Lipatova L., Novikov I., Shatskiy I. Example of a stable wormhole geometry in general relativity. arXiv: gr-qc/1312.6929v1.
- Thorne K., Morris M., Yurtsever U. Wormholes, Time Machines, and the Weak Energy Condition. *Physical Review Letters*, 1988, v. 61 (13), 1446–1449.
- Friedman J., Morris M., Novikov I., Echeverria F., Klinkhammer G., Thorne K., Yurtsever U. Cauchy problem in spacetimes with closed timelike curves. *Physical Review D*, 1990, v. 42 (6), 1915–1930.
- Novikov I., Zel’dovich Y. Stroeniye i Evolyutsia Vselennoi. Nauka, Moscow, 1975.
- Heinlein R. Farnham’s Freehold. G.P. Putnam’s Sons, New York, 1964.
- Minkowski H. Raum und Zeit. *Jahresbericht der Deutschen Mathematiker-Vereinigung*, 1909, 75–88.
- Hales S. No Time Travel for Presentists. *Logos & Episteme*, 2010, v. 1 (2), 353–360.
- Nahin P. Time Machines: Time Travel in Physics, Metaphysics, and Science Fiction. Springer-Verlag, New York, 1999.
- Smart J., ed. Introduction. Problems of Space and Time. The Macmillan Co., New York, 1964.
- Lloyd S., Maccone L., Garcia-Patron R., Giovannetti V., Shikano Y., Pirandola S., Rozema L., Darabi A., Soudagar Y., Shalm L., Steinberg A. Closed timelike curves via postselection: theory and experimental demonstration. arXiv: quant-ph/1005.2219v1.
- Deutsch D. Quantum mechanics near closed timelike lines. *Physical Review D*, 1991, v. 44 (10), 3197–3217.
- Ralph T. Problems with modelling closed timelike curves as post-selected teleportation. arXiv: quant-ph/1107.4675v1.
- Lloyd S., Maccone L., Garcia-Patron R., Giovannetti V., Shikano Y., Pirandola S., Rozema L., Darabi A., Soudagar Y., Shalm L., Steinberg A. A reply to ‘Problems with modelling closed timelike curves as post-selected teleportation.’ arXiv: quant-ph/1108.0153v1.
- Lloyd S., Maccone L., Garcia-Patron R., Giovannetti V., Shikano Y. Quantum mechanics of time travel through post-selected teleportation. arXiv: quant-ph/1007.2615v2.
- Lloyd S., Maccone L., Garcia-Patron R., Giovannetti V., Shikano Y., Pirandola S., Rozema L., Darabi A., Soudagar Y., Shalm L., Steinberg A. Closed Timelike Curves via Postselection: Theory and Experimental Test of Consistency. *Physical Review Letters*, 2011, v. 106 (4), 040403.
- Chalmers D. The singularity: A philosophical analysis. *Journal of Consciousness Studies*, 2010, v. 17 (9-10), 7–65.

Thermodynamics and the Virial Theorem, Gravitational Collapse and the Virial Theorem: Insight from the Laws of Thermodynamics

Pierre-Marie Robitaille

Department of Radiology and Chemical Physics Program, The Ohio State University, Columbus, Ohio 43210, USA.

E-mail: robitaille.1@osu.edu

Application of the virial theorem, when combined with results from the kinetic theory of gases, has been linked to gravitational collapse when the mass of the resulting assembly is greater than the Jeans mass, M_J . While the arguments appear straightforward, the incorporation of temperature into these equations, using kinetic theory, results in a conflict with the laws of thermodynamics. Temperature must always be viewed as an intensive property. However, it is readily demonstrated that this condition is violated when the gravitational collapse of a free gas is considered using these approaches. The result implies star formation cannot be based on the collapse of a self-gravitating gaseous mass.

1 Introduction

While the virial theorem derives its name from the work of Clausius [1], credit for its initial formulation has also been ascribed to Lagrange [2], as the theorem can be derived from the Lagrange identity [3, 4]. The virial theorem represents one of the most powerful axioms in physics and has been used to address a wide array of problems [4–6]. Jeans utilized the theorem at length in his classic text, *The Dynamical Theory of Gases* [7], in order to derive some of the well-known gas laws. However, it was not until seven years later that the virial theorem was introduced into astrophysics by Poincaré [8]. Soon after, A. S. Eddington [9], apparently unaware of Poincaré's contribution, applied the theorem to a star cluster. This work centered on kinetic energy of motion and did not attempt to introduce temperature as a variable. Each of these developments adheres to the laws of physics.

Eventually, Eddington [10] came to use the virial theorem when addressing the general theory of star formation. In doing so, it appears that he was the first to combine gravitational potential energy with the kinetic energy for a gas, as derived from the ideal gas law, and thereby obtained an expression defining the mean temperature of a star. Jeans [11] and Chandrasekhar [12] soon followed the same steps. Today, many of these ideas relative to stellar equilibrium and temperature remain ([13], [14, see Eq. 26.7]). In this case, the use of the virial theorem appears to be in conflict with the laws of thermodynamics.

2 Theoretical considerations

The existence of intensive (*e.g.* temperature, pressure, density, molar mass, thermal conductivity, ...) and extensive (*e.g.* mass, volume, internal energy, heat capacity, ...) properties has been recognized. In fact, Landsberg [15] has argued that this concept is so vital as to constitute the 4th law of thermodynamics. By necessity, intensive properties must be measured in terms of extensive properties. Extensive proper-

ties must be additive and are directly related to the mass of a system. Conversely, intensive properties are independent of total mass. When two extensive properties are divided, an intensive property is obtained (*e.g.* mass/volume = density). However, not all properties can be characterized as either intensive or extensive [16]. Still, it is clear that “*if one side of an equation is extensive (or intensive), then so must be the other side*” [17]. These last two realities urge some caution when advancing new relations. The point can be made by first examining the ideal gas law and then, a result from the inappropriate application of the virial theorem.

The ideal gas law is usually expressed as $PV = nRT$, where P , V , n , R and T correspond to the pressure, the volume, the number of moles, the universal gas constant, and the absolute temperature, respectively. If one considers that $n = M/\mathcal{M}$, (where M is the total mass and \mathcal{M} corresponds to the molar mass) and that the mean density, ρ_0 , can be expressed as $\rho_0 = M/V$, then the ideal gas law takes the following form:

$$P = \rho_0 \frac{R}{\mathcal{M}} T. \quad (1)$$

Recognizing that R/\mathcal{M} is also known as the specific gas constant, R_s , then the ideal gas law can simply be expressed as $P = \rho_0 R_s T$. Note that this equation does not contain any extensive properties, as both the mass of the system and its volume have been replaced by density, ρ_0 , which is an intensive property. Similarly, P and T are intensive properties, while R_s is a constant for any given system. In accordance with the state postulate, this simple system is fully defined by any two intensive properties [18].

At the same time, an intensive property must remain a function of only intensive properties, or of extensive properties which in combination, result in an intensive property. This is especially important when considering temperature in light of the 0th law of thermodynamics. If the ideal gas law is

re-expressed in terms of temperature,

$$T = \frac{P}{R_s \rho_0}, \quad (2)$$

it is observed that this property remains defined only in terms of intensive properties for this system, namely pressure and density.

When considering the kinetic theory as applied to an ideal gas (see Jeans [19]), any of the associated results are inherently linked to the conditions which gave rise to the ideal gas law. For instance, 1) a large number of rapidly moving particles must be considered, 2) these must be negligibly small relative to the total volume, 3) all collisions must be elastic, 4) no net forces must exist between the particles, 5) the walls of the enclosure must be rigid, 6) the only force or change in momentum with time, dp/dt , which is experienced to define pressure, P , must occur at the walls, and 7) the sum of forces everywhere else must be zero. In this instance, temperature becomes linked to the total kinetic energy of the enclosed system, $K.E. = \frac{3}{2}Nk_B T$, where N represents the total number of particles and k_B is Boltzmann's constant. Note that this expression does not address any contribution to the total kinetic energy which this enclosed system might gain if it were in motion relative to another object. Such motion would increase the total kinetic energy of the system, but not its temperature.

When the virial theorem is applied to a self-gravitating gaseous mass, wherein the kinetic theory of gases has been used to insert temperature dependence [10–12], it is well-established ([13], [14, see Eq. 26.7]) that this combination results in the following expression for temperature:

$$T = \frac{GMm_p}{5k_B r}, \quad (3)$$

where G , M , m_p , k_B , and r corresponds to the gravitational constant, the mass of the system, the particle mass, Boltzmann's constant, and the radius. With dimensional analysis, this expression appears valid, equating Kelvin on each side. However, this is not true, relative to analysis of intensive and extensive properties.

Observe that G , m_p , and k_B are constants for this system. Mass, M , is an extensive property. However, the radius, r , is neither extensive nor intensive [18]. In order to see that radius is not an extensive property, one simply needs to recall that for an ideal gas, volume, an extensive property, is directly related to mass, M . In fact, mass is usually divided by volume in order to lead to density, ρ_0 , an intensive property. However, since $V = \frac{4}{3}\pi r^3$, it is evident that radius is not directly related to mass, M , but rather to $M^{1/3}$. As such, r cannot be an extensive property. Thus, temperature in (3) is being defined in terms of two properties, M and r , which in combination *do not* result in an intensive property. This constitutes a direct violation of the 0th law which seeks, first

and foremost, to define temperature as an intensive property, a reality well-established in thermodynamics (*e.g.* [17]).

In arriving at (3), the kinetic energy of the gas, $K.E.$, was assumed to be equal to $\frac{3}{2}Nk_B T$, as presented above. However, the temperature obtained from kinetic theory is a manifestation of the internal motion of the gas within an enclosure. That energy represents heat energy and it is not related to the kinetic energy of translational motion which should be combined in the virial theorem with gravitational potential energy, when considering a bound system.

Furthermore, this expression was obtained for a gas enclosed by a rigid wall. Such a wall is not present when considering gravitational collapse. Yet, the results relative to the ideal gas law were critically dependent on the presence of this enclosure. The relationship between pressure, volume, and temperature was extracted using real walls. This is critical as the only forces used in defining pressure in this system occur at this boundary. It is not proper to remove the wall and then assume that the kinetic energy of the gaseous system remains equal to $\frac{3}{2}Nk_B T$.

A thermodynamic problem also occurs with any expression attempting to define the Jeans mass, M_J , an extensive property, in terms of temperature and mean density, both of which are intensive properties. Consider the following expression:

$$M_J = \left(\frac{5k_B T}{Gm_p} \right)^{3/2} \left(\frac{3}{4\pi\rho_0} \right)^{1/2}, \quad (4)$$

which is analogous to Eq. 12.14 in [14]. Note in (4) that all terms are raised to either the 3/2 or 1/2 power. As such, no term on the right side of this equation could have been considered to behave as an extensive property. Extensive properties must be additive, a feature which is lost when they are raised to an exponential power. In (4), the only terms which are not constants are T and ρ_0 , but these are intensive, not extensive properties. As such, the concept of Jeans mass is not supported by the laws of thermodynamics as no extensive properties exist on the right side of (4).

3 Discussion

When applying the virial theorem, it is important to differentiate the kinetic energy associated with temperature from the kinetic energy of motion. For instance, when Chandrasekhar [20] applied the virial theorem to rotating fluid masses, he made a clear distinction between heat energy and kinetic energy of motion. If this is not done and the two are considered the same, as with all applications to a gaseous mass [10–14], then violations of thermodynamics ensue.

It is not solely that an intensive property, like temperature, is being defined in terms of properties which, in combination, do not yield an intensive property. While this is a violation of the 0th law, the 3rd law is also being violated, as 0 K is a temperature. One cannot, by (3), increase the radius to infinity

and, therefore, define 0 K as an intensive property. These considerations illustrate that gases cannot undergo gravitational collapse.

Lane's Law [21, 22], or the self-compression of a gaseous mass, also constitutes a violation of the 1st law of thermodynamics. A system cannot do work upon itself and thereby raise its own temperature. This results in a perpetual motion machine of the first kind. Additionally, a gravitationally collapsing gaseous cloud, which obeys the ideal gas law, violates the 2nd law of thermodynamics. An ideal gas is elastic by definition. It has no means of dissipating heat into the heat sink of its surroundings. Moreover, the system lacks an "engine" whereby compression can be achieved. Work must be done on the system in order to increase its order. To argue otherwise constitutes a perpetual motion machine of the second kind.

4 Conclusion

The idea that a gaseous mass can undergo gravitational collapse ([9, 11–13], [14, see Eq. 26.7]) stands in violation of the 0th, 1st, 2nd and 3rd laws of thermodynamics. It is well-established in the laboratory that gases expand to fill the void. According to the laws of thermodynamics a system cannot do work upon itself. When dealing with an ideal gas without net translation, all of the energy should be considered as kinetic energy, exclusively. It is not appropriate to add a potential energy term, if the total energy has already been defined as kinetic energy, thereby establishing temperature.

At the same time, the question remains: *How do stars form?* They do not arise from gravitational collapse. The only feasible solution is that they are the result of condensation reactions, whereby material, as it condenses and forms a new system, emits photons into its surroundings. Insight relative to this issue can be gained by considering the work of König *et al* [23], wherein the condensation of silver clusters at low temperatures has been associated with the emission of photons. It is highly likely that hydrogen ion clusters [24] will be found someday to behave in the same fashion. Along with other advancements in condensed matter physics [25], such discoveries may well provide the necessary force to help astronomers recognize that the stars are comprised of condensed matter [26].

Dedication

This work is dedicated to my wife, Patricia Anne.

Received on May 29, 2018

References

1. Clausius R. J. E. 1870, *Phil. Mag.*, S. 4, v. 40 (265), 122–127.
2. Lagrange J. L. Oeuvres Complètes, tome 6, Essai sur le problème des trois corps. *Acad. Sci. Paris*, Tome IX, 1772, p. 231–242.
3. Jacobi C. G. J. *Vorlesungen Über Dynamik*. A. Clerbsch, G. Reimer, Berlin, 1884, p. 18–31.
4. Collins G. W. *The Virial Theorem in Stellar Astrophysics*. Pachart Publishing House, Tucson, 1978.
5. Landau L. D. and Lifshitz E. M. *Mechanics*. Pergamon Press, Oxford, 1960, p. 22–24.
6. Goldstein H. *Classical Mechanics*, 2nd Ed. Addison-Wesley Publishing Co., London, 1980, p. 82–85.
7. Jeans J. H. *The Dynamical Theory of Gases*. Cambridge University Press, Cambridge, 1904, p. 143–148.
8. Poincaré H. *Leçons sur les hypothèses cosmogoniques*. Librairie Scientifique A Hermann et Fils, Paris, 1911, p. 90–94.
9. Eddington A. S. 1916, *MNRAS*, 76, 525–528.
10. Eddington A. S. *The Internal Constitution of the Stars*. Cambridge University Press, Cambridge, 1926, p. 79–96.
11. Jeans J. *Astronomy and Cosmogony*. Cambridge University Press, Cambridge, 1928, p. 65–69.
12. Chandrasekhar S. *An Introduction to the Study of Stellar Structure*. Dover Publications, 1939, p. 61–83.
13. Bowers R. L. and Deeming T. *Astrophysics II: Interstellar Matter and Galaxies*, Jones and Bartlett Publishers, Inc., Boston, 1984, p. 420.
14. Carroll B. W. and Ostlie D. A. *An Introduction to Modern Astrophysics (2nd Edition)*. Cambridge University Press, Cambridge, U.K., 2017.
15. Landsberg P. T. *Thermodynamics with Quantum Statistical Illustrations*. Interscience Publishers, New York, 1961, p. 142.
16. Hatsopoulos G. N. and Keenan J. H. *Principles of General Thermodynamics*. John Wiley & Sons, Inc., 1965, p. 19.
17. Canagaratna S. G. 1992, *J. Chem. Educ.*, v. 69 (12), 957–963.
18. Cengel Y. A. and Boles M. A. *Thermodynamics - An Engineering Approach (8th Edition)*. McGraw-Hill, New York, 2015, p. 15.
19. Jeans J. *An Introduction to the Kinetic Theory of Gases*. Cambridge University Press, Cambridge, U.K., 1940.
20. Chandrasekhar S. and Fermi E. 1953, *Astro. Phys. Jr* 118, 116–141.
21. Lane L. H. 1870, *Am. J. Sci. Arts*, Ser. 2, v. 50, 57–74.
22. Stevenson-Powell C. J. 1988, *J. Hist. Astron.*, v. 19, 183–199.
23. König L., Rabin I., Schultze W., and Ertl G. 1996, *Science*, v. 274 (5291), 1353–1355.
24. Kirchner N. J. and Bowers M. T. 1987, *J. Chem. Phys.*, v. 86 (3), 1301–1310.
25. McMahon J. M., Morales M. A., Pierleoni C., and Ceperley D. M. 2012, *Rev. Mod. Phys.*, v. 84 (4), 1607–1653.
26. Robitaille P.-M. 2013, *Progr. Phys.*, v. 4, 90–142.

Progress in Physics is an American scientific journal on advanced studies in physics, registered with the Library of Congress (DC, USA): ISSN 1555-5534 (print version) and ISSN 1555-5615 (online version). The journal is peer reviewed and listed in the abstracting and indexing coverage of: Mathematical Reviews of the AMS (USA), DOAJ of Lund University (Sweden), Scientific Commons of the University of St.Gallen (Switzerland), Open-J-Gate (India), Referential Journal of VINITI (Russia), etc. Progress in Physics is an open-access journal published and distributed in accordance with the Budapest Open Initiative: this means that the electronic copies of both full-size version of the journal and the individual papers published therein will always be accessed for reading, download, and copying for any user free of charge. The journal is issued quarterly (four volumes per year).

Electronic version of this journal: <http://www.ptep-online.com>

Advisory Board of Founders:

Dmitri Rabounski, Editor-in-Chief
Florentin Smarandache, Assoc. Editor
Larissa Borissova, Assoc. Editor

Editorial Board:

Pierre Millette
Andreas Ries
Gunn Quznetsov
Felix Scholkmann
Ebenezer Chifu

Postal address:

Department of Mathematics and Science, University of New Mexico,
705 Gurley Avenue, Gallup, NM 87301, USA
